UNIVERSITY OF ALBERTA

STUDIES OF AN END-ON INDUCTIVELY COUPLED PLASMA ATOMIC EMISSION SPECTROMETER (ICP-AES) AND A DIRECT SAMPLE INSERTION INDUCTIVELY COUPLED PLASMA ATOMIC EMISSION SPECTROMETER (DSI-ICP-AES)

by

Guangcheng Chen ©

A thesis submitted to the Faculty of Graduate Studies and Research in partial fulfillment of the requirements for the degree of Master of Science.

DEPARTMENT OF CHEMISTRY

Edmonton, Alberta

Spring 1999

National Library of Canada
Acquisitions and Bibliographic Services
395 Wellington Street
Ottawa ON K1A 0N4
Canada

Bibliothèque nationale du Canada
Acquisitions et services bibliographiques
395, rue Wellington
Ottawa ON K1A 0N4
Canada

Your file Votre référence

Our file Notre référence

The author has granted a non-exclusive licence allowing the National Library of Canada to reproduce, loan, distribute or sell copies of this thesis in microform, paper or electronic formats.

L'auteur a accordé une licence non exclusive permettant à la Bibliothèque nationale du Canada de reproduire, prêter, distribuer ou vendre des copies de cette thèse sous la forme de microfiche/film, de reproduction sur papier ou sur format électronique.

The author retains ownership of the copyright in this thesis. Neither the thesis nor substantial extracts from it may be printed or otherwise reproduced without the author's permission.

L'auteur conserve la propriété du droit d'auteur qui protège cette thèse. Ni la thèse ni des extraits substantiels de celle-ci ne doivent être imprimés ou autrement reproduits sans son autorisation.

0-612-40036-0

Canada

UNIVERSITY OF ALBERTA

LIBRARY RELEASE FORM

NAME OF AUTHOR: Guangcheng Chen

TITLE OF THESIS: **Studies of an end-on inductively coupled plasma atomic emission spectrometer (ICP-AES) and a direct sample insertion inductively coupled plasma atomic emission spectrometer (DSI-ICP-AES)**

DEGREE: Master of Science

YEAR THIS DEGREE GRANTED: 1999

Permission is hereby granted to the University of Alberta Library to reproduce single copies of this thesis and to lend or sell such copies for private, scholarly or scientific research purposes only.

The author reserves all other publication rights in association with the copyright in the thesis, and excepts as hereinbefore provided neither thesis nor any substantial portion thereof may be printed or otherwise reproduced in any material form whatever without the author's prior written permission.

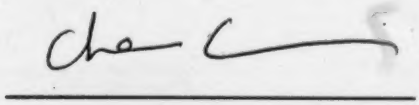

11308-50 Avenue
Edmonton, Alberta
Canada T6H 0J3

Date: April 09, 1999

UNIVERSITY OF ALBERTA

FACULTY OF GRADUATE STUDIES AND RESEARCH

The undersigned certify that they have read, and recommend to the Faculty of Graduate Studies and Research for acceptance, a thesis entitled **"Studies of an end-on inductively coupled plasma atomic emission spectrometer (ICP-AES) and a direct sample insertion inductively coupled plasma atomic emission spectrometer (DSI-ICP-AES)"** submitted by Guangcheng Chen in partial fulfillment of the requirements for the degree of Master of Science.

Gary Horlick

Dr. G. Horlick, Supervisor

Mark T. McDermott

Dr. M. T. McDermott

Daniel W. Smith

Dr. D. W. Smith

Date: March 31, 1999

To Dale and Hongrui

ABSTRACT

The studies undertaken in this thesis are the effect of plasma operating parameters on analyte signals in Inductively Coupled Plasma Atomic Emission Spectrometry (ICP-AES) with axial viewing plasma and Direct Sample Insertion Inductively Coupled Plasma Atomic Emission Spectrometry (DSI-ICP-AES), the effect of the addition of oxygen into the coolant flows of DSI-ICP-AES and the application of ICP-AES to the analysis of rock samples.

An Optima 3000 XL (Perkin-Elmer) was used to study the effects of plasma operating parameters (nebulizer flow rate and RF power) on analyte signals in ICP-AES. Optimum parameter values for rock sample analyses were selected and detection limits were obtained.

The spectral interferences of Ca, Mg on analyte signals and K matrix effects were investigated.

Detection limits were obtained for both DSI-ICP-AES and mixed gas DSI-ICP-AES in pg range. The calibration curves were set up for Pb, Cd and Zn in solution residue (dynamic range is 0.001 to 1.0 ppm for Pb, 0.01 to 1.0 ppm for both Zn and Cd).

Acknowledgements

I would like to thank my supervisor, Professor Gary Horlick for his invaluable advice, guidance and patience throughout this work. I would also like to thank Youbin Shao, Lishi Ying and all other members of the research group for their assistance and thoughtful discussions.

Finally, I would like to thank the Department of Chemistry for financial support.

TABLE OF CONTENTS

		page
Chapter 1		
INTRODUCTION		1
1.1	General Introduction	1
1.2	Instrumentation	4
1.2.1	Inductively Coupled Plasma-Atomic Emission Spectrometry	4
1.2.2	ICP Torch	5
1.2.3	Direct Sample Insertion (DSI)	7
1.3	Overview of Thesis	9
REFERENCES		10
Chapter 2		
EXPERIMENTAL		12
2.1	Experimental Setup	12
2.2	Operating Conditions	20
2.3	Sample Descriptions	24
REFERENCES		25
Chapter 3		
ICP-AES MEASUREMENTS		26
3.1	Introduction	26
3.2	Results and Discussions	28
3.2.1	Effect of Nebulizer Flow Rate on Analyte Signals	30
3.2.2	Effect of RF Power on Analyte Signals	51

3.2.3 Ca and Mg Interferences and K Matrix Effect on Analyte Signals (with Xinbang Feng) 58
3.2.4 The Analysis of NIST SRM 88a (dolomitic limestone) and Rock Samples 68
REFERENCES 73

Chapter 4
DIRECT SAMPLE INSERTION MEASUREMENTS 75
4.1 Introduction 75
4.2 Results 82
4.2.1 Operating Parameter Studies 82
4.2.2 Figures of Merit 90
4.3 Introduction of Oxygen into the Plasma 96
4.3.1 Introduction 96
4.3.2 Results 98
4.4 Conclusions 101
REFERENCES 102

Chapter 5
SUMMARY AND FUTURE WORK 104
REFERENCES 106

LIST OF FIGURES

FIGURE	DESCRIPTION	PAGE
1.1	A schematic diagram of the Inductively Coupled Plasma (ICP) torch	6
1.2	A schematic diagram of a direct sample insertion (DSI) device	8
2.1	A block diagram of experimental set up used in this work	13
2.2	Layout of the optical system	14
2.3	Axial viewing of ICP with sheer gas	18
2.4	A diagram of the direct sample insertion system	19
2.5	A schematic diagram of the graphite sample probes	20
3.1	Intensity vs nebulizer flow rate plots for As and Be at different power	31
3.2	Intensity vs nebulizer flow rate plots for Be and Ca at different power	32
3.3	Intensity vs nebulizer flow rate plots for Cd and Co at different power	33
3.4	Intensity vs nebulizer flow rate plots for Co and Cr at different power	34
3.5	Intensity vs nebulizer flow rate plots for Cu and Fe at different power	35
3.6	Intensity vs nebulizer flow rate plots for Fe and Mg at different power	36

3.7 Intensity vs nebulizer flow rate plots for Mn and Mo at different power 37
3.8 Intensity vs nebulizer flow rate plots for Mo and Ni at different power 38
3.9 Intensity vs nebulizer flow rate plots for Ni and Pb at different power 39
3.10 Intensity vs nebulizer flow rate plots for Sb and Se at different power 40
3.11 Intensity vs nebulizer flow rate plots for Se and Tl at different power 41
3.12 Intensity vs nebulizer flow rate plots for V and Zn at different power 42
3.13 Intensity vs nebulizer flow rate plots for Zn at different Power 43
3.14 Intensity vs nebulizer flow rate plots for As, Be, Ca and Cd at 1000 W 45
3.15 Intensity vs nebulizer flow rate plots for Co, Cr, Cu and Fe at 1000 W 46
3.16 Intensity vs nebulizer flow rate plots for Mo, Mg and Ni at 1000 W 47
3.17 Intensity vs nebulizer flow rate plots for Mn, Pb, Sb and Se at 1000 W 48
3.18 Intensity vs nebulizer flow rate plots for Tl, V and Zn at 1000 W 49
3.19 Normalized intensity vs nebulizer flow rate plots for Cu, Be and Zn at 1000 W 50

3.20	Intensity vs power plots for As, Be, Ca and Cd	53
3.21	Intensity vs power plots for Co, Cr, Cu and Fe	54
3.22	Intensity vs power plots for Mg, Mn, Mo and Ni	55
3.23	Intensity vs power plots for Pb, Sb, Se and Tl	56
3.24	Intensity vs power plots for V and Zn	57
3.25	Mg and Ca interference on SI 180.669 nm	62
3.26	K matrix effects on Mg	64
3.27	K matrix effects on Cd	65
3.28	K matrix effects on Cu	66
3.29	K matrix effects on Na	67
4.1	Three-dimensional view of the DSI device	78
4.2	The diagram of side door used in this work	79
4.3	Diagram of modified torch for DSI-ICP-AES	81
4.4	Diagram of heating chamber	83
4.5	Diagram of time relationship used in Chapter 4	85
4.6	Calibration curves of Pb solution residue	93
4.7	Calibration curves of Cd solution residue	94
4.8	Calibration curves of Zn solution residue	95
4.9	Spectra of Au (I) 242.795 nm.	100

LIST OF TABLES

TABLE	DESCRIPTION	PAGE
2.1	Optical component specifications	16
2.2	Hardware specifications	22
2.3	Operating conditions	24
3.1	Operating conditions used in chapter 3	29
3.2	Wavelengths, excitation potentials and ionization potentials for the elements studied in chapter 3	52
3.3	Interference of Ca on analyte signal	59
3.4	Interference of Mg on analyte signal	60
3.5	Calibration standards used in this section	68
3.6	Analytical results of ICP-AES	70
3.7	Analytical results of ICP-AES and ICP-MS	72
4.1	Plasma operating parameters used in chapter 4	77
4.2	Optimization of sample ashing time	86
4.3	Optimization of insertion position of sample probe	87
4.4	Optimization of integration time and read delay time	89
4.5	Blank intensities of Pb, Cd and Zn	90
4.6	Reproducibility of Pb, Cd and Zn (10µl, 1.0 ppm)	91
4.7	Detection limits for solution residues of Pb, Cd and Zn	92
4.8	Detection limits for solution residue samples (mixed gas) ..	99

CHAPTER 1

INTRODUCTION

1.1 General Introduction

The inductively coupled plasma atomic emission spectrometry (ICP-AES) is widely accepted as a standard elemental analytical technique and has been applied to a wide variety of sample types. The method is used in the detection of trace elements in a wide variety of environmental and biological samples, including soils and sediments, natural waters, wastewaters and biological solids and liquids.

There are several features of inductively coupled plasma - atomic emission spectrometry (ICP-AES) which have lead to its widespread use in many areas, including low detection limits, wide linear dynamic range, relative freedom from interference effects, acceptable accuracy and good precision, and an inherent capability for simultaneous determinations [1]. Although the capabilities of the ICP are not unlimited, its characteristics approach those of an ideal atomic spectroscopy source.

An ideal source for atomic spectroscopy should have the following characteristics:

- Can convert any sample into gas phase atomic vapor with little or no sample pretreatment.
- Do so for all elements at all concentrations.
- Have identical operating conditions for all elements and samples.

- Have a simple function between analytical signal and the concentration of the individual elements, i.e. no interferences, no matrix effects.
- Be characterized and understood at a fundamental level.
- Be accurate and precise.
- Have low initial cost, low maintenance and running costs.
- Be simple to operate and reliable.

It has been over 30 years since the inductively coupled plasma was first introduced to analytical chemistry by Greenfield [2] and Fassel [3]. It is a very good source for generating atomic vapor from a sample for atomic emission, atomic absorption, atomic fluorescence and mass spectrometry. It meets almost all of the above criteria for an ideal source but the first one, sample introduction. Sample introduction by pneumatic nebulization is a key sub-system in most plasma-based instrumentation, but it is also the weakest link [1, 4], because of two major limitations: low sampling efficiency (typically less than 3%) [1] and lack of flexibility with sample form (the requirement for solution samples and volumes greater than 1 ml) plus nebulizer blockage at high salt concentrations and drift [4, 5].

Pneumatic nebulization of liquid samples does have its special features: including relatively good stability; simplicity in design and operation; and with the exception of ultrasonic nebulization, rapid change over and minimal memory effect [1]. However, the limitations of solution sample introduction stated above are obvious and serious and poor efficiency is perhaps the most important shortcoming of pneumatic nebulization. The consequences are that large sample volumes are required during analysis and the absolute sensitivity is limited.

Because many samples in the real world are soils, powders or alloys, they must be converted into solution forms before they can analyzed by ICP spectrometry. Many concerns can arise as a consequence of the sample conversion process [6].

1. Loss of speciation and phase distribution information.
2. Loss of homogeneity/heterogeneity information.
3. Loss of analyte through formation of volatile compounds and precipitates.
4. Pneumatic nebulization system usually needs at least 1 to 2 ml of samples.
5. Samples are destroyed.
6. Digestion always led to dilution of sample.
7. Risk of contamination is increased by adding chemical reagents into samples.
8. The cost of ultra-pure reagents may be a problem for some laboratories.

So direct sample analysis by ICP spectrometry without pretreatment is extremely desirable.

Several attempts to minimize or eliminate some of the limitations of pneumatic nebulization have been made [5, 7-10]. In 1979, Salin and Horlick developed a technique known as direct sample insertion (DSI) [11] in this laboratory, and later, Shao and Horlick made significant changes to the mechanical system [12]. Karanassios and Horlick have reviewed and summarized direct sample insertion devices, instrumentation, analytical figures of merit, etc [1].

The advantages of DSI for inductively coupled plasma atomic emission spectrometry (ICP-AES) include increased sample introduction efficiency and an ability to handle small volumes of liquids (μl) and small amounts of powdered or solid samples (mg) with little or no sample pretreatment. Limitations of DSI include a low vaporization temperature (~2000 K) [13-16], which results in selective volatilization, an inability to vaporize refractory materials (such as W, Mo and Zr), and carbide formation (such as V, Ba and Ca). The basic instrumentation for DSI-ICP-AES will now be outlined.

1.2 Instrumentation

1.2.1 Inductively Coupled Plasma-Atomic Emission Spectrometry

An Optima 3000XL inductively coupled plasma-atomic emission spectrometer (Perkin-Elmer) with axial viewing (end-on) of the plasma was used in this study. Axial viewing of the plasma relative to side-on viewing increases the sensitivity of ICP measurements, has a higher optical throughput and can reduce detection limits. The signal-to-background ratios are also better compared to side-on viewing ICP-AES.

There are two special features associated with this instrument [17, 18]. First, a new type of solid-state detector has been used. The device is based on charged coupled devices (CCDs) with unique features for optical emission spectroscopy. The main advantage, relative to photomultiplier tubes (PMTs), is the large increase in spectral coverage, which can be used for simultaneously detecting many emission lines together with their

spectral backgrounds. The other advantages include high quantum efficiency in the UV, low noise, wide dynamic range, rapid readout and broad spectral coverage.

Second, an echelle polychromator was used with the multichannel solid-state detector described above. The optical system has separate output sections for the UV and visible wavelength ranges, which permit high spectral resolution and high optical throughput while covering the spectral range from 167 to 782 nm. The total spectrum is divided into two output regions, UV and visible, which are optimized independently for resolution and throughput. Each region has its own cross-dispersion, focal length, and multichannel solid-state detector. A Schmidt spherical reflector in the UV section corrects for spherical aberration, and then substantially improves resolution while providing high optical throughput. The optical system will be illustrated in the next chapter.

1.2.2 ICP Torch

A schematic diagram of the ICP torch is shown in Figure 1.1. The plasma is generated by wrapping an induction coil about a quartz tube containing an argon flow. A Tesla discharge gives a seed of free electrons in the tube. The induction coil is connected to an RF generator whose oscillating current generates an oscillating magnetic field perpendicular to the load coil, which in turn induces an eddy current of free electrons which circulate in closed annular paths inside the quartz tube. These electrons meet with resistance and heating occurs which ionizes the argon, to form a plasma.

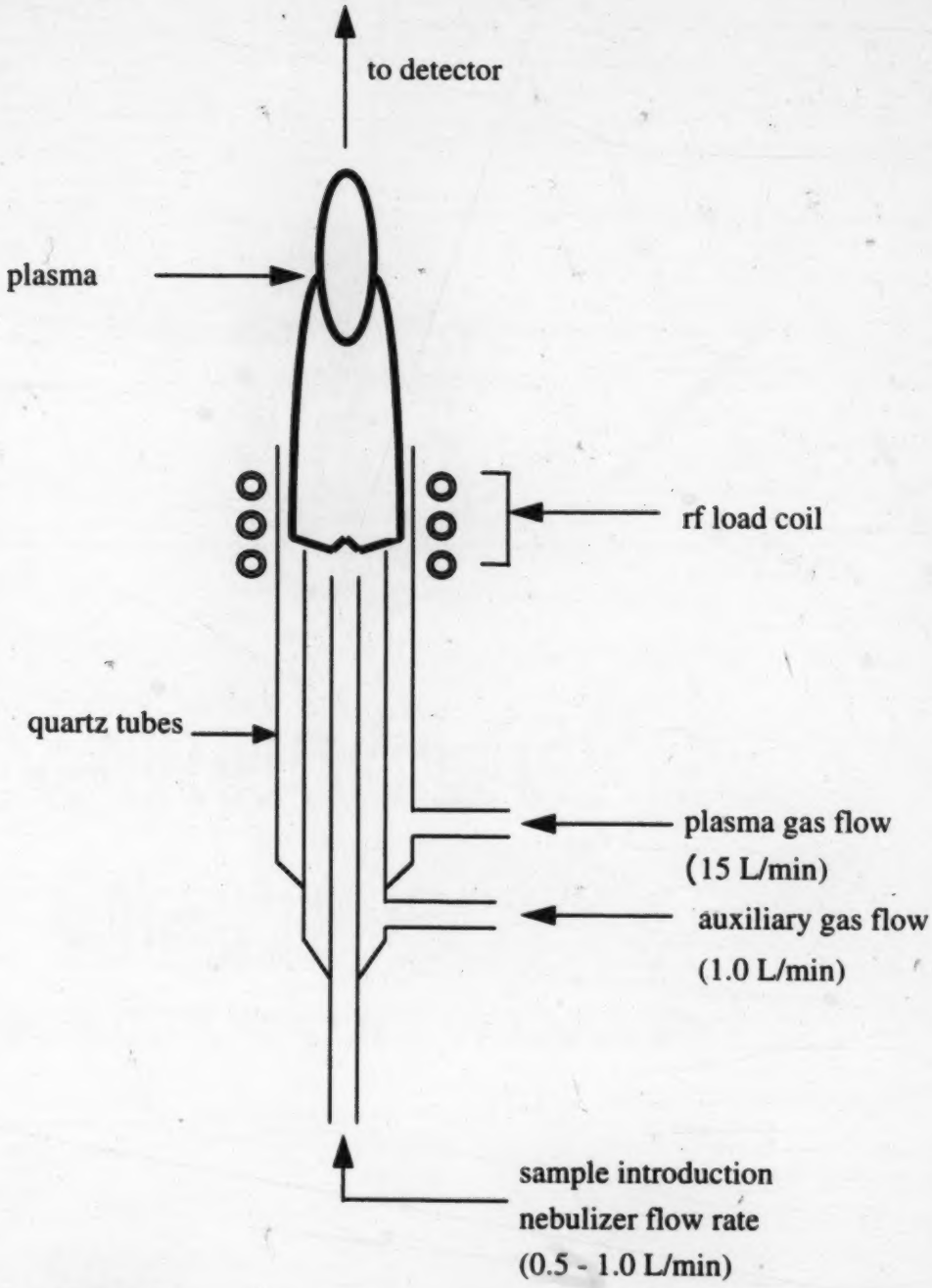

Figure 1.1

A schematic diagram of the inductively coupled plasma (ICP) torch.

The plasma is formed from the plasma gas, which flows axially through the outer tube of the torch. The auxiliary gas flow lifts the plasma 1 to 2 mm above the inner quartz tube. Nebulizer flow carries the sample in solution into the nebulizer and spray chamber, then aerosol is carried into the plasma. The sample aerosol is desolvated, vaporized, dissociated, excited, and ionized by the ICP.

1.2.3 Direct Sample Insertion

A schematic diagram of a direct sample insertion (DSI) device is given in Figure 1.2. A sample (μl's of solution or mg's of solid sample) is placed to a sample probe (graphite cup in this thesis), and the sample probe is introduced into the plasma by an insertion mechanism through the central tube of the torch. The sample is then vaporized, atomized, excited and ionized.

Karanassios and Horlick [1] presented an extensive review of DSI devices and they have built and characterized a DSI system for ICP-AES [19-21] and ICP-MS [22-24]. The DSI device used in this work is similar to the one Karanassios and Horlick described in reference 22. The device was connected to the ICP torch of the Optima 3000XL through a specially designed side door (there is a description of the side door in Chapter 4) and the software which controls the device was rewritten by Lishi Ying. The torch used here is a modified torch with a big central tube that guides the sample probe into the plasma. The torch was designed by Youbin Shao.

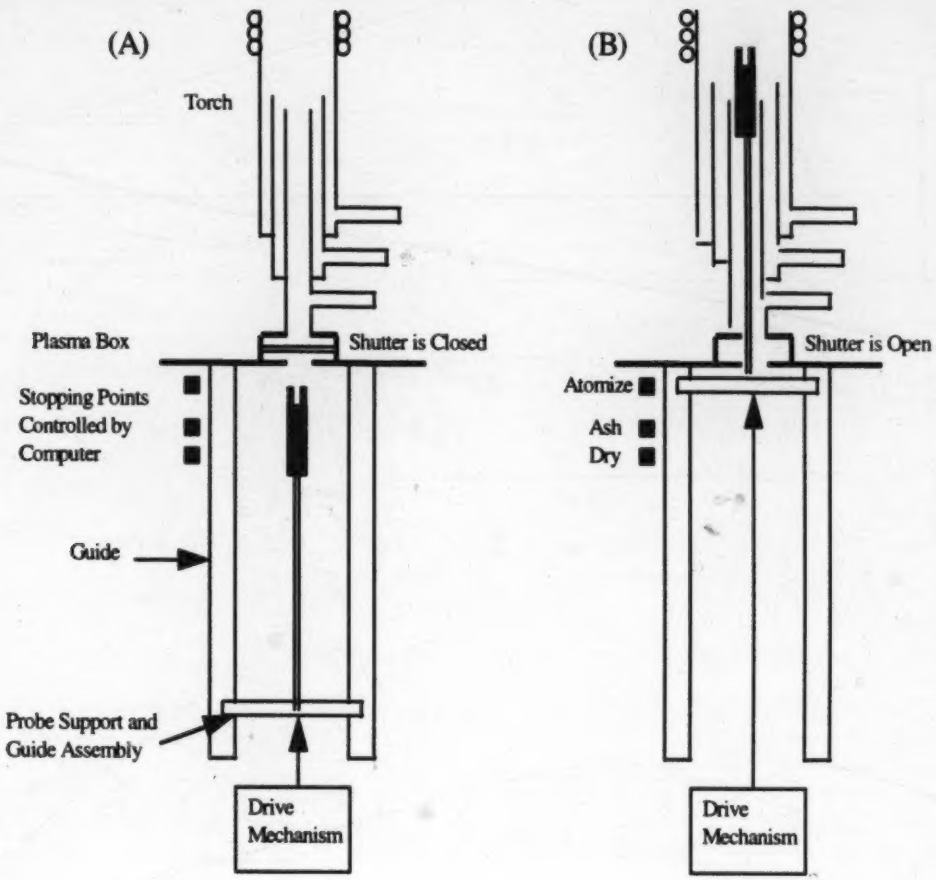

Figure 1.2
A schematic diagram of a direct sample insertion (DSI) device.

1.3 Overview of Thesis

Almost all DSI-ICP-AES measurements have been carried out with DSI into a side-on viewed ICP system. The basic goal of this work was to couple a DSI system to the end-on viewed Optima spectrometer available in the laboratory.

In the next Chapter, a description of the instrument used in this work will be given. The instrumental operating conditions and sample descriptions are also presented in Chapter 2.

Chapter 3 of this thesis is focused on studies of the effect of nebulizer flow rate and plasma power on analyte signals and a study of Ca, Mg interference effects on some elements. The analysis of NBS Standard Reference Material 88a (SRM 88a), Dolomitic Limestone, and real rock samples will be given and discussed. Finally detection limits are presented for some elements. This study was to provide in with the basic performance data of the end-on viewed ICP.

Chapter 4 presents the DSI results including the introduction of oxygen into the plasma. Calibration curves of Pb, Zn and Cd in solution residue samples by DSI-ICP-AES will be given, and detection limits of Pb, Zn and Cd for both DSI-ICP-AES and mixed gas DSI-ICP-AES will be presented.

REFERENCES

1. V. Karanassios and G. Horlick, *Spectrochim. Acta Rev.* **13,** 89 (1990).
2. S. Greenfield, I. L. Jones and C. T. Berry, *Analyst*, **89,** 713 (1964).
3. R. H. Wendt and V. A. Fassel, *Anal. Chem.* **37,** 920 (1965).
4. A. G. T. Gustavson, Liquid sample introduction into plasmas, in: *Inductively Coupled Plasmas in Analytical Atomic Spectroscopy,* Eds. A. Montaser and G. W. Golightly, 399, VCH Publishers, Inc. (1987).
5. R. F. Browner and A. W. Boorn, *Anal. Chem.* **56,** 787A (1984).
6. X. R. Liu, Ph.D. Thesis, University of Alberta (1994).
7. J. C. Van Loon, *Anal. Chem.* **52,** 955A (1980).
8. R. F. Browner and A. W. Boorn, *Anal. Chem.* **56,** 875A (1984).
9. M. W. Routh and M. W. Tikkanen, Introduction of solids into plasmas, in: *Inductively Coupled Plasmas in Analytical Atomic Spectroscopy,* Eds. A. Montaser and G. W. Golightly, 431, VCH Publishers, Inc. (1987).
10. H. Matusiewicz, *J. Anal. At. Spectrom.* **1,** 171 (1986).
11. E. D. Salin and G. Horlick, *Anal. Chem.* **51,** 2284 (1979).
12. Y. B. Shao and G. Horlick, *Appl. Spectrosc.* **40**, 386 (1986).
13. E. R. Prack and G. J. Bastiaans, *Anal. Chem.* **55,** 1654 (1983).
14. N. W. Barnett, M. J. Cope, G. F. Kirkbright and A. A. H. Taobi, *Spectrochim. Acta,* **39B,** 343 (1984).
15. A. G. Page, S. V. Godbole, K. H. Madraswala, M. J. Kulkapni, V. S. Mallapurkar and B. D. Joshi, *Spectrochim. Acta,* **39B,** 551 (1984).
16. A. Lorbe and Z. Goldbart, *Analyst,* **110,** 155 (1985).

17. T. Barnard, M. Crockett, J. Ivalda and P. Lundberg, *Anal. Chem.* **65,** 1225 (1993).

18. T. Barnard, M. Crockett, J. Ivalda, P. Lundberg, D. Yates, P. Levine and D. Sauer, *Anal. Chem.* **65,** 1231 (1993).

19. V. Karanassios and G. Horlick, *Spectrochim. Acta* **45B,** 85 (1990).

20. V. Karanassios, G. Horlick and M. Abdullah, *Spectrochim. Acta* **45B,** 105 (1990).

21. V. Karanassios, M. Abdullah and G. Horlick, *Spectrochim. Acta* **45B,** 119 (1990).

22. V. Karanassios and G. Horlick, *Spectrochim. Acta* **44B,** 1345 (1989).

23. V. Karanassios and G. Horlick, *Spectrochim. Acta* **44B,** 1361 (1989).

24. V. Karanassios and G. Horlick, *Spectrochim. Acta* **44B,** 1387 (1989).

25. J. A. C. Broekaert, F. Leis, B. Raeymaekers and G. Zaray, *Spectrochim. Acta* **43B,** 339 (1988).

CHAPTER 2

EXPERIMENTAL AND SAMPLES

2.1 Experimental Setup

All experiments were carried out on a commercially available Perkin-Elmer Optima 3000-XL inductively coupled plasma atomic emission spectrometer (ICP-AES). A block diagram of the experimental set-up used in this work is shown in Figure 2.1. An echelle polychromator for inductively coupled plasma atomic emission spectroscopy (ICP-AES) is coupled to a multichannel solid-state detector, providing high quantum efficiency in the UV, low noise, wide dynamic range, rapid readout, broad spectral coverage, and high spectral resolution.

The detector is based on charged coupled devices (CCDs) with unique features for optical emission spectroscopy. The main advantage, relative to photomultiplier tubes (PMTs) is the large increase in spectral coverage which can be used for simultaneously detecting many emission lines together with their spectral backgrounds. The spectral coverage is from 167 to 782 nm with 224 linear photodetector arrays. These arrays are targeted on three to four primary analytical lines for each of 72 elements and cover over 5000 ICP emission lines.

The optical system has separate output sections for the UV and visible wavelength ranges, which permit high spectral resolution and high optical throughput while covering the spectral range from 167 to 782 nm. The layout of the optical system is shown in Figure 2.2.

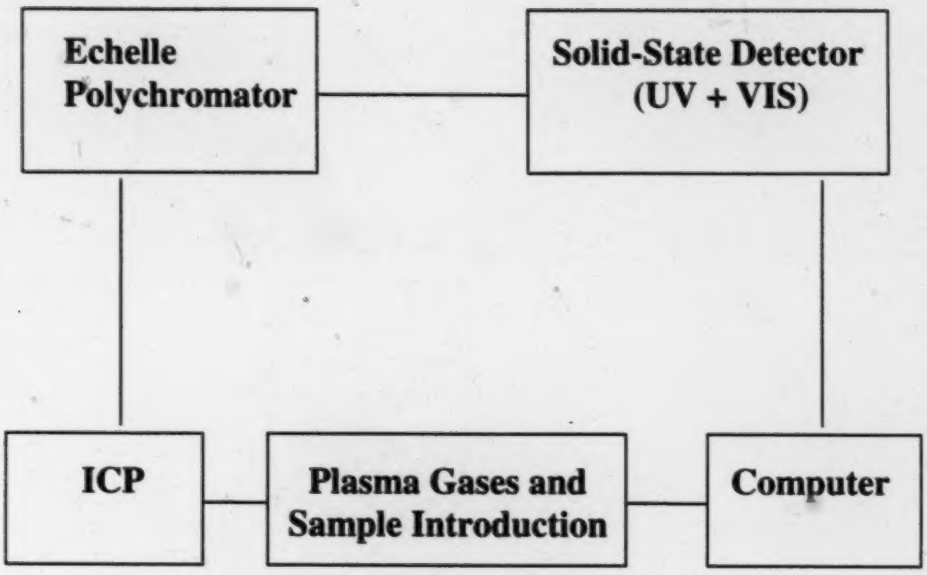

Figure 2.1
A block diagram of experimental set up used in this work.

This Figure was removed due to copyright.

Figure 2.2
Layout of the optical system (ref. 1).

Echelle spectrometers with two-dimensional, multichannel solid-state detectors offer high flexibility in the choice of emission lines and can monitor spectral backgrounds simultaneously. This optical system has two distinguish features: first, the total spectrum is divided into two output regions, UV and visible, which are optimized independently for resolution and throughput. Each region has its own cross-dispersion, focal length and multichannel solid-state detector. Second, a Schmidt spherical reflector in the UV section corrects for spherical aberration, and then substantially improves resolution while providing high optical throughput. Table 2.1 gives the specifications of key optical components. The design of this echelle grating optical system and solid-state detector are described by Barnard *et. al.* [1, 2] in detail.

In contrast to the layout shown in Figure 2.2, our Optima system was configured for axial viewing (i.e. end-on) of the plasma. Advantages of this configuration include improved sensitivity, lower detection limits and better signal-to-background ratios [3-8]. The system is equipped with a sheer gas to eliminate the tail plume zone. This removes cooler absorbing atoms in the tail plume of the plasma, which might exhibit self-absorption and thereby reduce the attainable dynamic range [5, 7]. Axial viewing of an ICP with a sheer gas is shown in Figure 2.3.

The inductively coupled plasma used in this work consisted of a four-turn silver-plated copper tubing load coil and demountable design quartz torch, mounted horizontally, and operated at a power 0.75 to 1.5 kW at 40 MHz generated by a free-running radio frequency generator which allowed the use of a wide range of solvents from aqueous to organic.

Table 2.1 Optical Component Specifications

entrance slits	
height	250 μm
widths	31 μm, 62 μm, 185 μm
collimator	
optical figure	10-deg off-axis parabola
focal length	503.8 mm
aperture diameter	75 mm
echelle grating	
groove frequency	79.0 lines/mm
blaze angle	63.4^0
size	80 x 160 mm
UV Schmidt cross-disperser	
aberration correction	for 400 mm radius sphere
groove frequency	374 lines/mm
blaze angle	2.7^0
size	90 x 90 mm with 30-mm-diameter central hole
UV camera mirror	
figure	spherical
focal length	209 mm
size	140-mm diameter
UV pixel/exit slits	
heights	120 to 180 μm
widths	12.5 and 25 μm
visible prism cross-disperser	
apex angle	60^0 nominal
material	fused quartz (F-2 NH1)

Table 2.1 Optical Component Specifications (continued)

visible compound lens	
effective focal length	100 mm nominal
aperture diameter	30 mm
visible pixel/exit slits	
heights	75 to 100 μm
width	12.5 μm

Aqueous sample was introduced into the ICP by a peristaltic pump (Perkin-Elmer) at a constant rate of 1.0 ml per minute. This solution stream was nebulized into a Scott type spray chamber by a cross-flow nebulizer and then introduced into the plasma. Argon was used as the nebulizing gas. The cross-flow nebulizer was constructed with chemically resistant GemTips on it and the spray chamber was manufactured from Ryton corrosion-resistant material for complete corrosion resistance to most acids, including HF.

The ICP was always ignited using one hundred percent argon, although a mixed gas of argon and oxygen was introduced into one of the gas flow inlets in some work. This could be done after the Ar plasma was ignited and stabilized. Oxygen then was gradually added into the argon flow. The plasma could be extinguished if oxygen was added too fast [9].

The direct sample insertion device was used to introduce sample into the plasma for direct sample insertion inductively coupled plasma atomic emission spectrometry (DSI-ICP-AES) analysis. The specific DSI sub-system used was the horizontal drive system developed by Karanassios and Horlick [10]. A schematic of the system is shown in Figure 2.4. In this

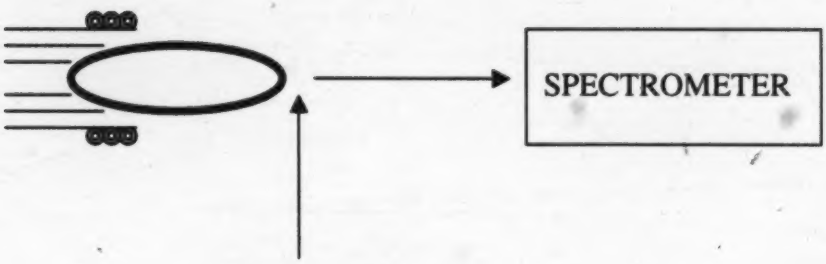

Figure 2.3
Axial viewing of ICP with sheer (cut-off) gas.

This Figure was removed due to copyright.

Figure 2.4 A diagram of the Direct Sample Insertion System.

system, a sample is placed into a probe and the probe is then inserted into the plasma. The probe is a standard d.c. arc graphite electrode which is inserted into the central channel of the plasma. The only modification to the probe was to drill out the bottom of the electrode so that it could be mounted on the quartz rod of the DSI system (see Figure 2.5 and Table 2.2 for details. The stepper motor driving the DSI probe is controlled by an IBM PC. The hardware components are listed in Table 2.2.

The system computer is a 486DX/33 MHz computer with 24 MB RAM and Windows 95, which is used for data acquisition and data reprocessing. The software used to control the Optima 3000 XL is Perkin-Elmer Winlab (version 1.06). The resultant intensities (spectrum) were transferred from the 486 computer to a Pentium 100. The data were manipulated using commercially available software (Microsoft Excel 7.0).

2.2 Operating Conditions

The operating conditions were close to those recommended by the manufacturer. The software sets and controls the gases and power as well as the observation position and the alignment of torch on the optical axis.

During a normal analysis, the plasma flow rate was kept at 15 l/min, the auxiliary flow rate at 1.0 l/min and the nebulizer flow rate at 0.6 l/min. The power of RF generator was 1300 W. Operating conditions are summered in Table 2.3.

Reported net signal values (net intensities) are background subtracted and corrected intensities are blank subtracted from net intensities.

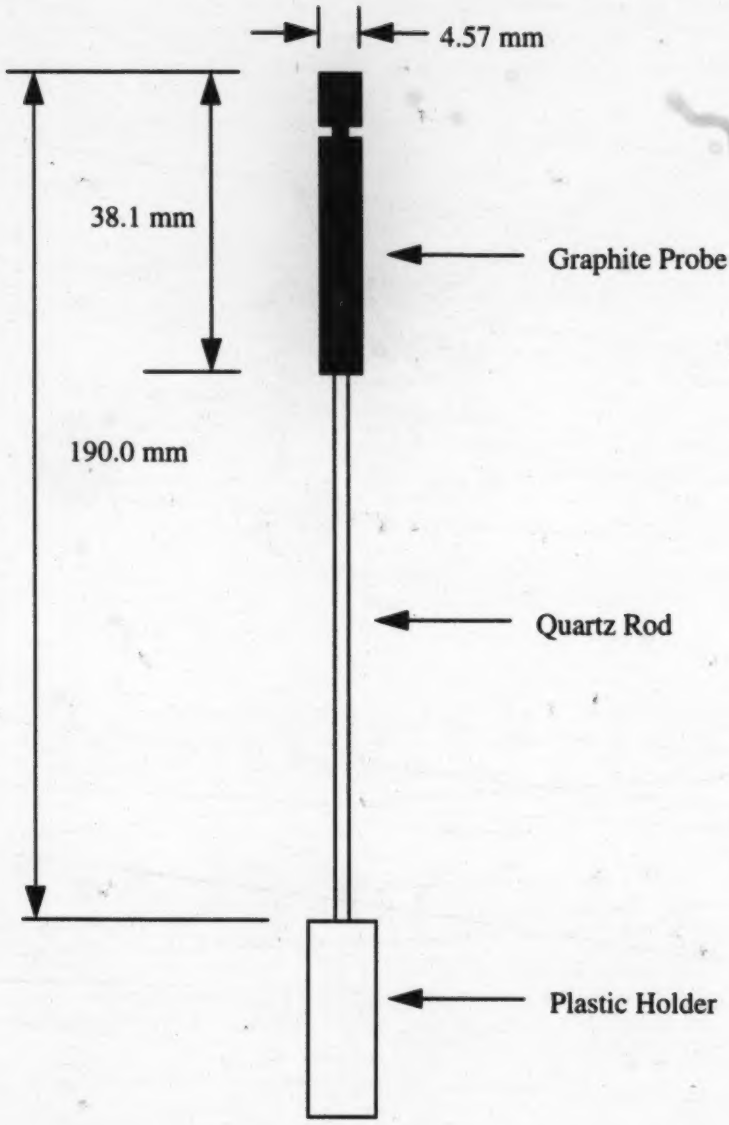

Figure 2.5
A schematic diagram of the graphite sample probes.

Table 2.2 Hardware Specifications

ICP system	
frequency	40 MHz, free-running
plasma power	adjustable from 750 to 1500 W
coil	4-turn 1/8 inch silver-plated copper tubing
argon flow controls	
plasma argon flow	binary-scaled solenoid valves are computer controlled within the range of 5 to 20 l/min
auxiliary argon flow	binary-scaled solenoid valves are computer controlled within the range of 0 to 2.0 l/min
nebulizer argon flow	mass flow controller is computer controlled within the range of 0 to 2.0 l/min
sample introduction system	
torch	standard torch, demountable design
spray chamber	Scott design and constructed of Ryton
nebulizer	cross-flow design with chemically resistant GemTips
peristaltic pump	Perkin-Elmer, computer controlled pump
spectrometer	
polychromator	Perkin-Elmer design, high energy echelle based polychromator which utilizes two detector focal planes and two cross dispersers.

Table 2.2 Hardware Specifications (continued)

detector	Perkin-Elmer Segmented-array Charge-coupled-device Detector (SCD)
system controller	
computer	DECpc 433dx
processor	33 MHz industry standard 486DX
memory	24 MB RAM (70 ns)
hard disk drive	426 MB, SCSI
floppy disk drive	3.5 inch (1.44 MB capacity)
interfaces	1-IEEE-488 communication interface 2-RS232C serial interface 1-Centronics parallel interface
graphics	SVGA with 512 KB video memory
printer	apple laser printer 360
operating system	SCO/UNIX ODT, MS-DOS and Microsoft Windows
software	Perkin-Elmer Winlab 1.06 for Optima 3000
DSI system	
DSI probe	undercut standard graphite electrodes, Spex Industries, Edison, NJ, USA
Stepper motor control board	PCMotion (Ragers Labs, Santa Ana, CA, USA) for IBM-PC

Table 2.3 Operating Conditions

Forward power	0.75 to 1.50 kW, 1.30 kW for most measurement
Gas flow rate	
plasma flow rate	15 l/min
auxiliary flow rate	0.5 l/min
Nebulizer flow rate	0.35 to 1.20 l/min, 0.8 l/min for most measurement

Signal intensity is measured as ion counts per second. Detection limits were evaluated as three times the standard deviation of the base line noise.

2.3 Sample Descriptions

All multi-element analyte solutions were prepared from 1000 parts per million (ppm) stock solutions (Spex industries Inc. Edison, NJ, USA) and diluted to different concentration standard solutions in two percent reagent grade nitric acid in deionized distilled water (DDW). Solutions containing two percent reagent grade nitric acid in distilled deionized water were used as blanks.

The standard rock samples of NIST and all other samples were prepared in our laboratory. About 0.10 g Samples were dissolved and digested in concentrated hydrochloric acid, evaporated to almost dry and diluted in two percent reagent grade nitric acid with deionized distilled water to 100 ml.

REFERENCES

1. T. Barnard, M. Crockett, J. Ivalda and P. Lundberg, *Anal. Chem.* **65,** 1225 (1993).
2. T. Barnard, M. Crockett, J. Ivalda, P. Lundberg, D. Yates, P. Levine and D. Sauer, *Anal. Chem.* **65,** 1231 (1993).
3. M. H. Abdallah, R. Diemiaszonek, J. J. Jarosz, J. M. Mermet, J. Robin and C. Trassy, *Anal. Chim. Acta,* **84,** 271 (1976).
4. F. E. Lichte and S. R. Koirtyohann, *FACSS Meeting,* Philadelphia, PA (1976), **paper No. 26.**
5. *Fourier Transform and Polychromator Studies of the Inductively Coupled Plasma,* Los Alamos National Laboratory, Los Alamos, New Mexico.
6. J. C. Ivaldi and J. F. Tyson, *Spectrochim. Acta.* **50B,** 1207 (1995).
7. C. Dubuisson, E. Poussel and J-M. Mermet, *J. Anal. At. Spectrom.* **12,** 281 (1997).
8. C. D. Skinner and E. D. Salin, *J. Anal. At. Spectrom.* **12,** 725 (1997).
9. X. R. Liu and G. Horlick, *J. Anal. At. Spectrom.* **9,** 833 (1994).
10. V. Karanassios and G. Horlick, *Spectrochim. Acta Rev.* **13,** 89 (1990).

CHAPTER 3

ICP-AES MEASUREMENTS

3.1 Introduction

The establishment of inductively coupled plasma atomic emission spectrometry (ICP-AES) as a simultaneous multi-element analysis method has required finding a set of conditions for operation of the associated instrumentation [1-4]. A large number of variables affect the measured signal intensity in ICP-AES. When analyte is introduced into the plasma, the observed emission intensities are mainly subject to the following parameters:

1. RF power coupled into the plasma.
2. Nebulizer flow rate.

The way in which the variation of these parameters affects net emission intensity was investigated by Boumans and DeBoer [1, 2] in order to establish conditions for simultaneous multi-element analysis.

In 1976, Lichte and Koirtyohann [5] suggested that there might be analytical performance advantages in viewing the plasma along the length of the vertical axis in an "end-on" configuration (Fig. 2.3). This was accomplished by laying the torch assembly over horizontally, so that the central orifice of the torch pointed directly toward the entrance slit of the spectrometer. The advantages of "end-on" plasma are:

- Increased analyte line intensity.
- Reduced background.

- Reduced molecular band intensity.
- Increased simultaneous multielement performance.
- Decreased influence of gas flow rates.

The disadvantages are:

- Decreased dynamic range.
- Increased observed interferences.

In 1979, Demers [6] evaluated the "end-on" viewing configuration and the study reported improved detection limits by factors of five to ten or greater for aqueous solution samples.

The "end-on" viewing configuration was further evaluated in an extensive study by Ivaldi and Tyson [7] who compared analytical results for the "side-on" and "end-on" configurations using an Optima 3000XL. This study reported improved detection limits by factors of five, reduced background, decreased dynamic range, increased matrix effects and increased molecular emission intensity from OH. There are also several papers [8-11, 16, 17] regarding matrix effects with the "end-on" plasma configuration.

As well, with most end-on system, a sheer gas is used to cut off the tip of the plasma. This removes cooler absorbing atoms in the tail plume of the plasma, that might exhibit self-absorption and thereby reduce the attainable dynamic range [5, 9, 12] and protect the optics from thermal damage.

In this section, data on the effects of nebulizer flow rate and RF power on the measured signal intensity will be presented. This allows us to find the relationship between the various parameters studied and their

effects on signal intensity, to select compromise conditions for ICP-AES analysis.

All solutions were made up using reagent grade chemicals (Spex Company) and in house deionized distilled water. All dilutions were performed using laboratory pipettes and volumetric flasks. A 0.1 ppm multielement stock solution of As, Be, Ca, Cd, Co, Cr, Cu, Fe, Mg, Mn, Mo, Ni, Pb, Sb, Se, Tl, V, and Zn was used in the experiment and data were collected for increments of 0.05 l/min. increase in nebulizer flow, and 0.10 kW increments increase in power.

3.2 Results and Discussion

The operating conditions were very close to those recommended by the manufacturer and summarized in Table 3.1. The software sets and controls the gas flow rate and power as well as the observation height and the alignment of the torch on the optical axis.

In most analytical methods and in particular, inductively coupled plasma-atomic emission spectrometry, the concentration is not directly measured. A spectral intensity is first measured and then the signal is related to a concentration via a calibration graph. In ICP-AES, the experimental spectral intensity is a gross signal (S+B), which consists of the sum of the line intensity S plus the background B. Then, the net signal is obtained by subtracting the value of the background B (with the use of the standard automatic background correction software). The value of B is obtained via an off-peak or on peak measurement. The corrected intensity is obtained by subtracting the blank intensity from the net signal.

Table 3.1 Operating Conditions Used in This Chapter

Plasma power	1100 to 1300 W
Plasma gas flow rate	15 l/min
Auxiliary gas flow rate	0.5 to 1.0 l/min
Nebulizer gas flow rate	0.5 to 1.0 l/min
Sample uptake rate	1.0 ml/min
Viewing height	15 mm
Integration time	1.0 s
Number of replicates	3
Scan	Off
Measurement mode	Area

The most easily adjusted variable operating parameters, which most affect signal intensity, are nebulizer gas flow rate and forward power. For the ICP, the plasma gas flow is 15.0 l/min, the auxiliary gas flow is 0.5 l/min, the nebulizer gas flow rate is varied throughout the experiments. The key variable in this study is the nebulizer flow rate and much of the data reported here were acquired as functions of nebulizer flow rate.

In this work, the features of an argon only plasma and its dependence upon various operating parameters will be described. The experimental set-up was shown in Figure 2.1. A number of plots of signal intensity versus nebulizer flow at different plasma powers are shown in this section.

3.2.1 Effect of Nebulizer Flow Rate on Analyte Signals

Usually, the plot of signal vs. nebulizer flow rate is the most informative. Berman and McLaren [4] noted that as the nebulizer flow rate is increased, signal reaches a maximum, and then decreases over the range 0.7 to 1.0 l/min. They also observed that for both Cr atom and Cr ion emission, net line intensity passed through a maximum as power was varied from 1.0 to 1.8 kW, although atom lines peaked at a lower power than ion lines.

In 1976, Lichte and Koirtyohann [5] reported increased signal intensity, decreased influence of gas flow rates and reduced background intensity and noise, with decreased dynamic range and more interference for "end-on" viewing ICP (self-absorption was increased for low energy atomic species, hence the dynamic range was also decreased).

In this section, intensive studies of the influence of gas flow rates on analyte signal intensity are presented. The analyte count is plotted vs. nebulizer flow rate and then on the same set of axes, a family of such curves is plotted representing the nebulizer flow rate behavior at different plasma power.

The plots for all the elements studied are shown in Figure 3.1-3.13. The plots clearly show that the spectral line intensities of all the elements studied pass through a maximum when the nebulizer flow rate is increased. Lichte and Koirtyohann [5] stated that there was decreased influence of gas flow rate when "end-on" plasma was used, but our observation shows there is still a large influence of nebulizer gas flow rate on signal intensity. And

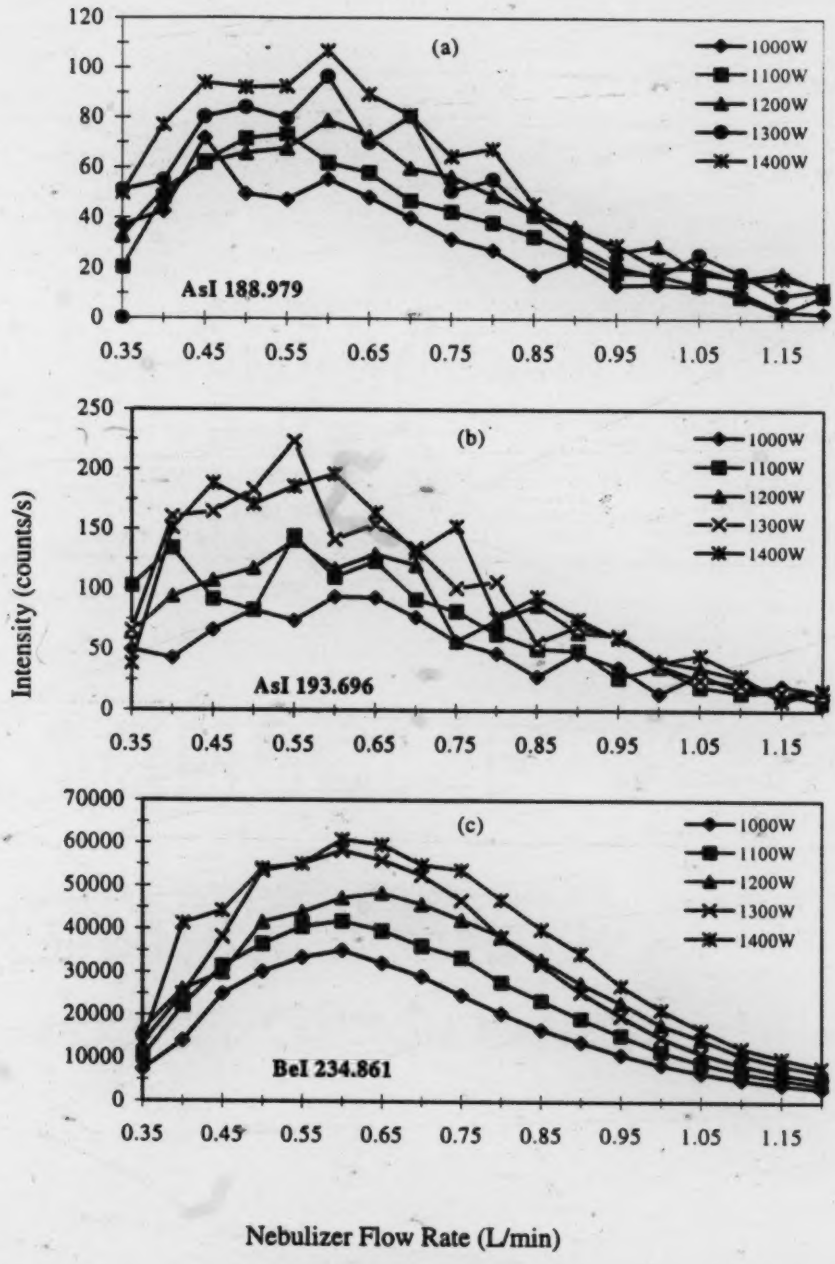

Figure 3.1 Intensity vs Nebulizer Flow Rate Plots for As (a, b) and Be (c) at different Power.

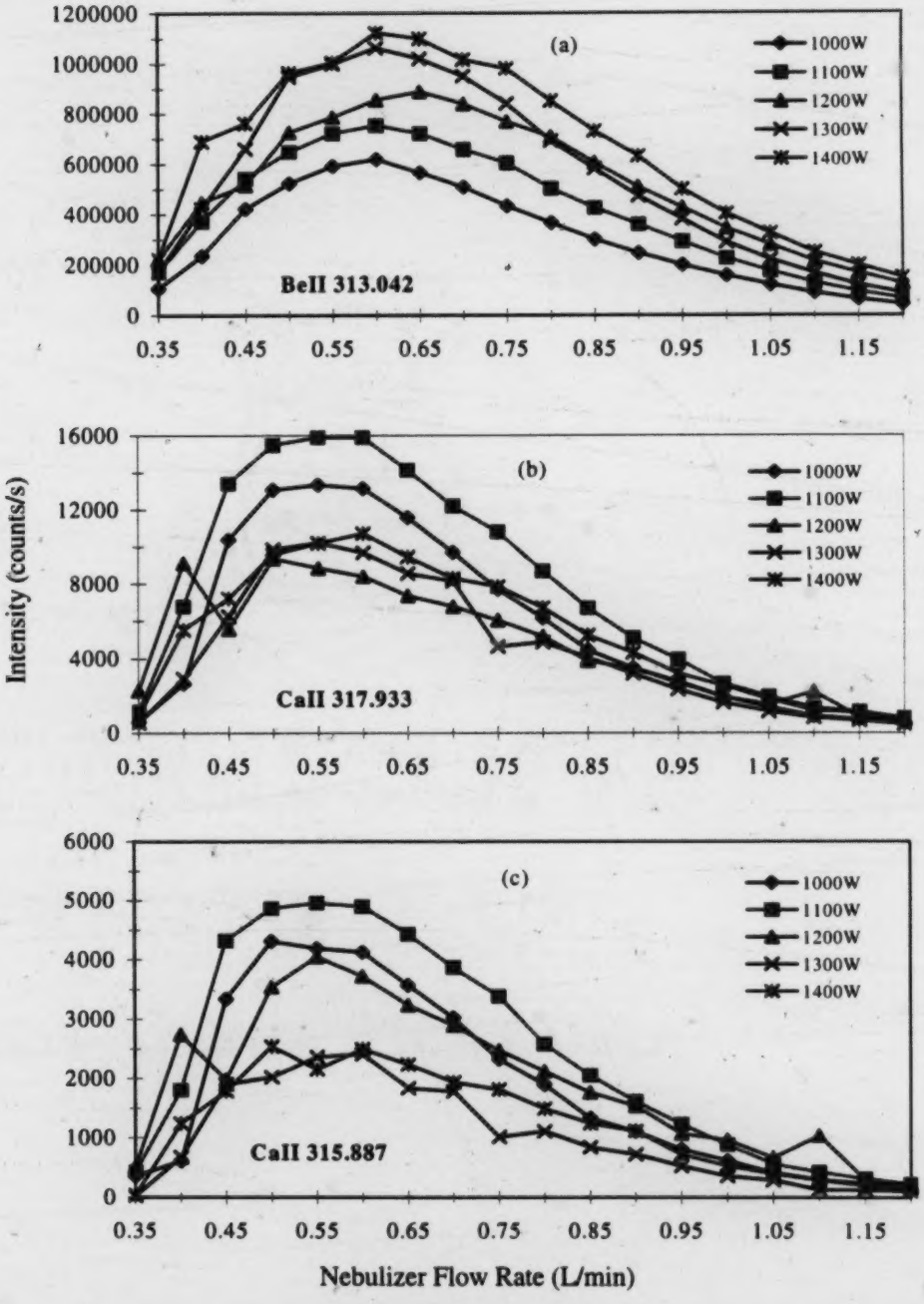

Figure 3.2 Intensity vs Nebulizer Flow Rate Plots for Be (a) and Ca (b, c) at different Power.

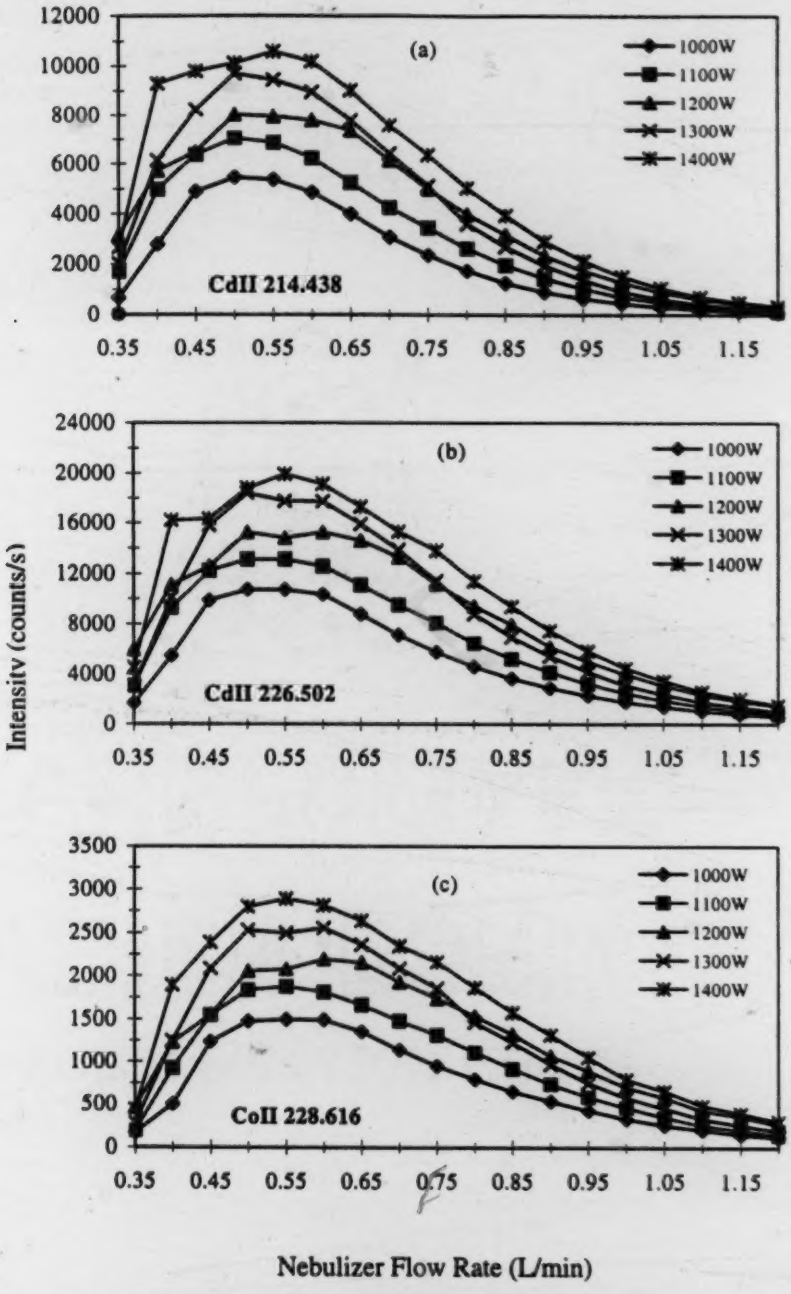

Figure 3.3 Intensity vs Nebulizer Flow Rate Plots for Cd (a, b) and Co (c) at different Power.

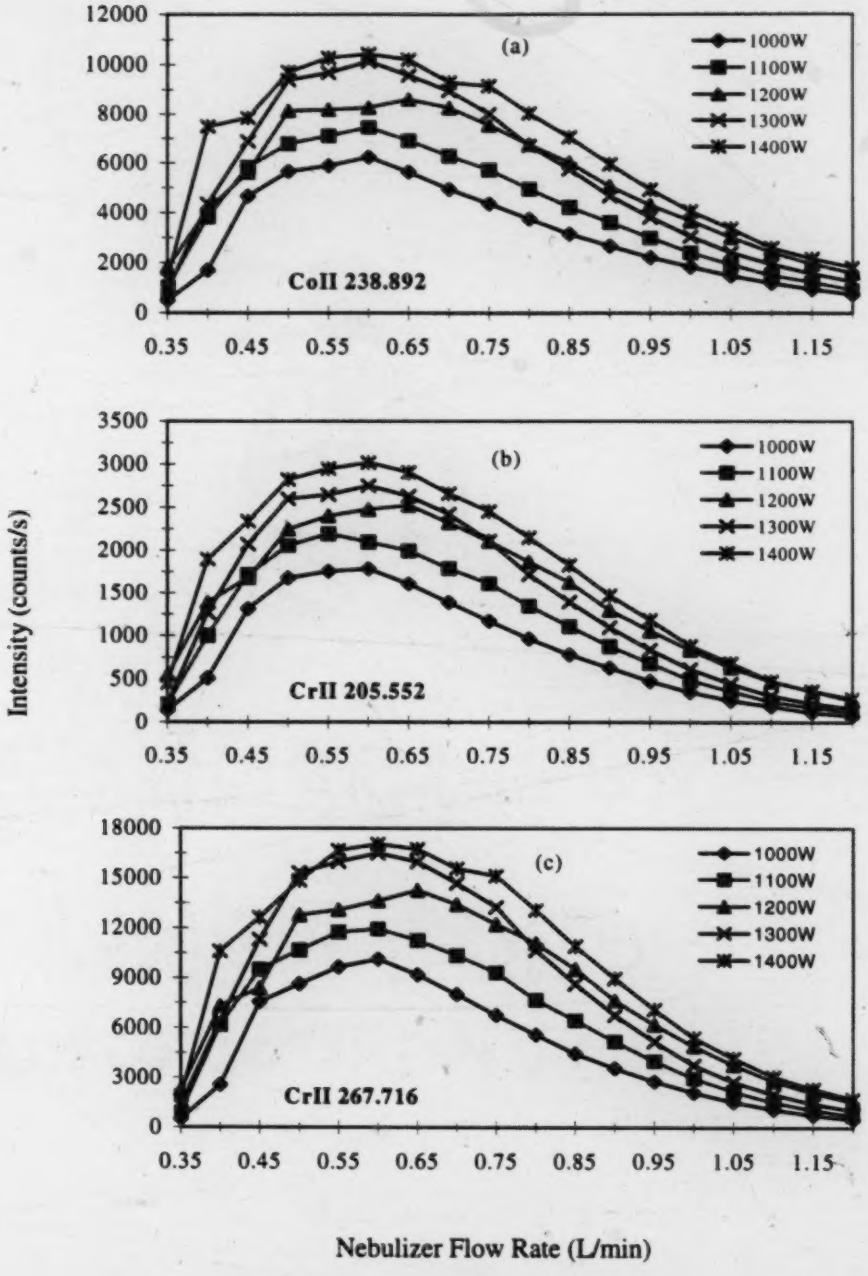

Figure 3.4 Intensity vs Nebulizer Flow Rate Plots for Co (a) and Cr (b, c) at different Power.

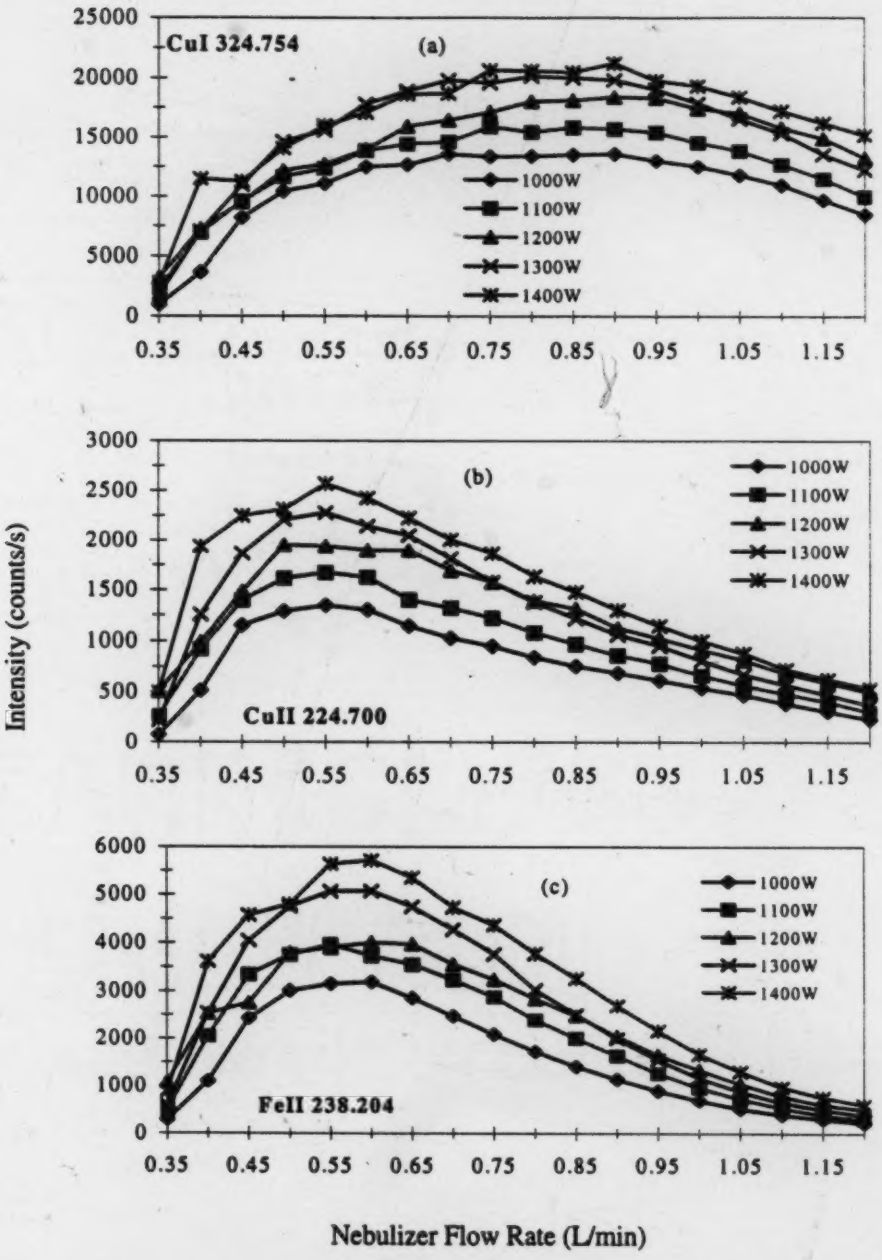

Figure 3.5 Intensity vs Nebulizer Flow Rate Plots for Cu (a, b) and Fe (c) at different Power.

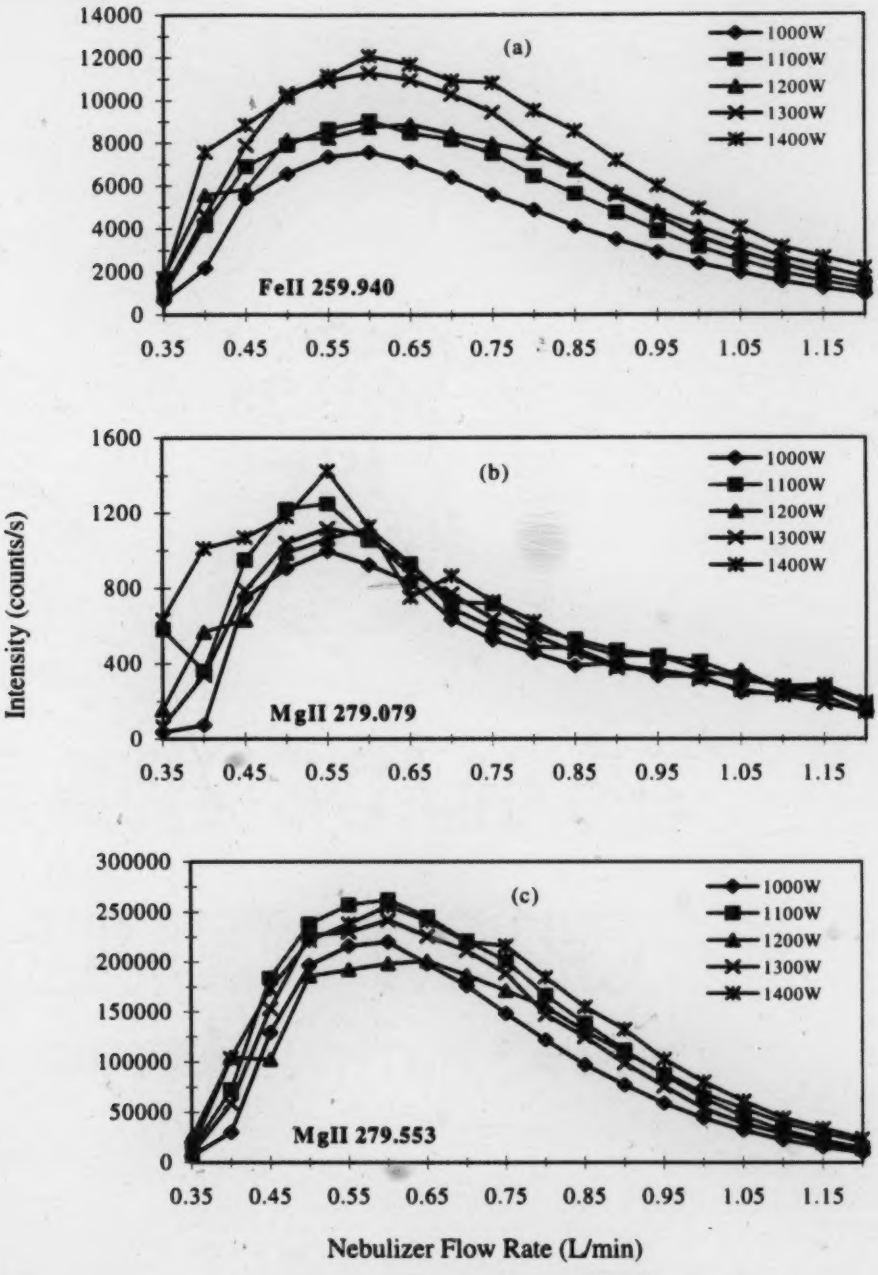

Figure 3.6 Intensity vs Nebulizer Flow Rate Plots for Fe (a) and Mg (b, c) at different Power.

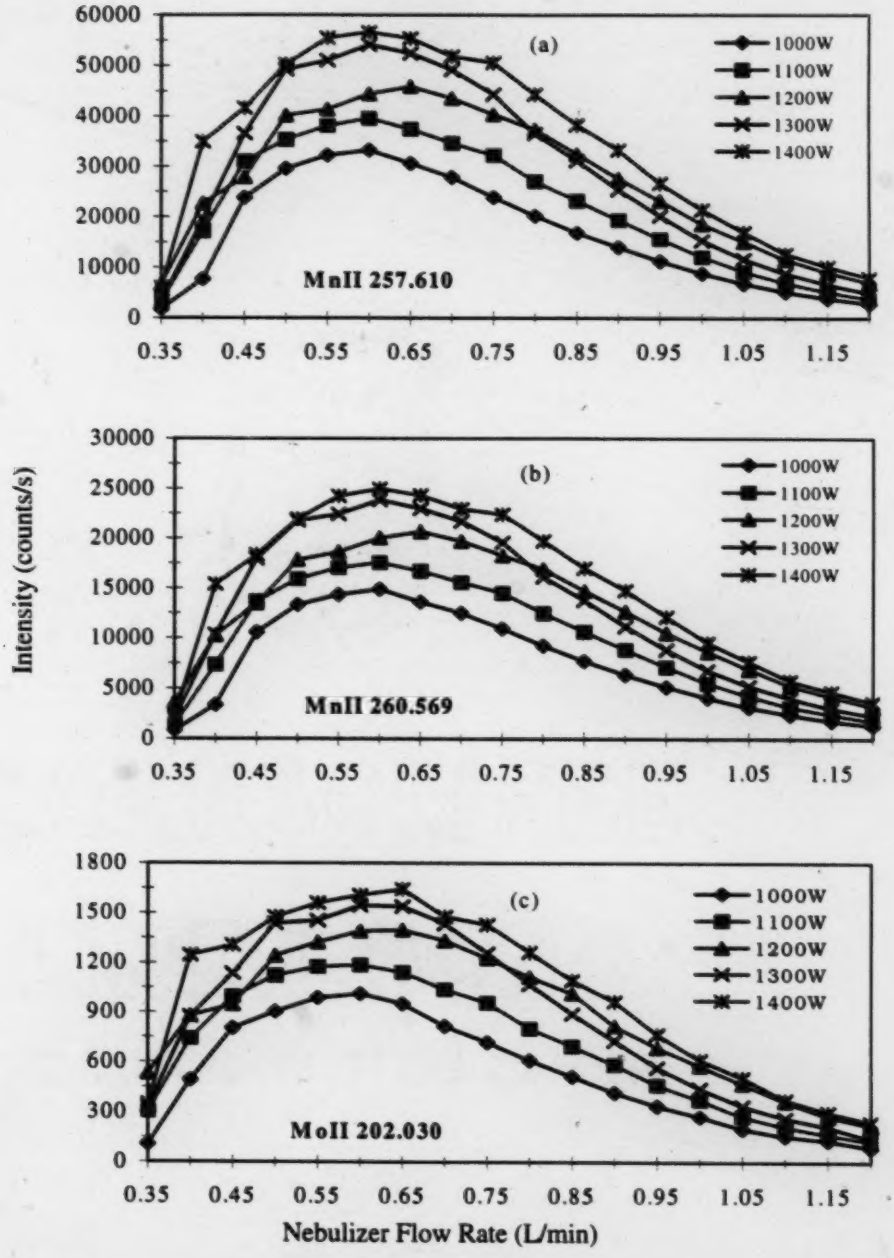

Figure 3.7 Intensity vs Nebulizer Flow Rate Plots for Mn (a, b) and Mo (c) at different Power.

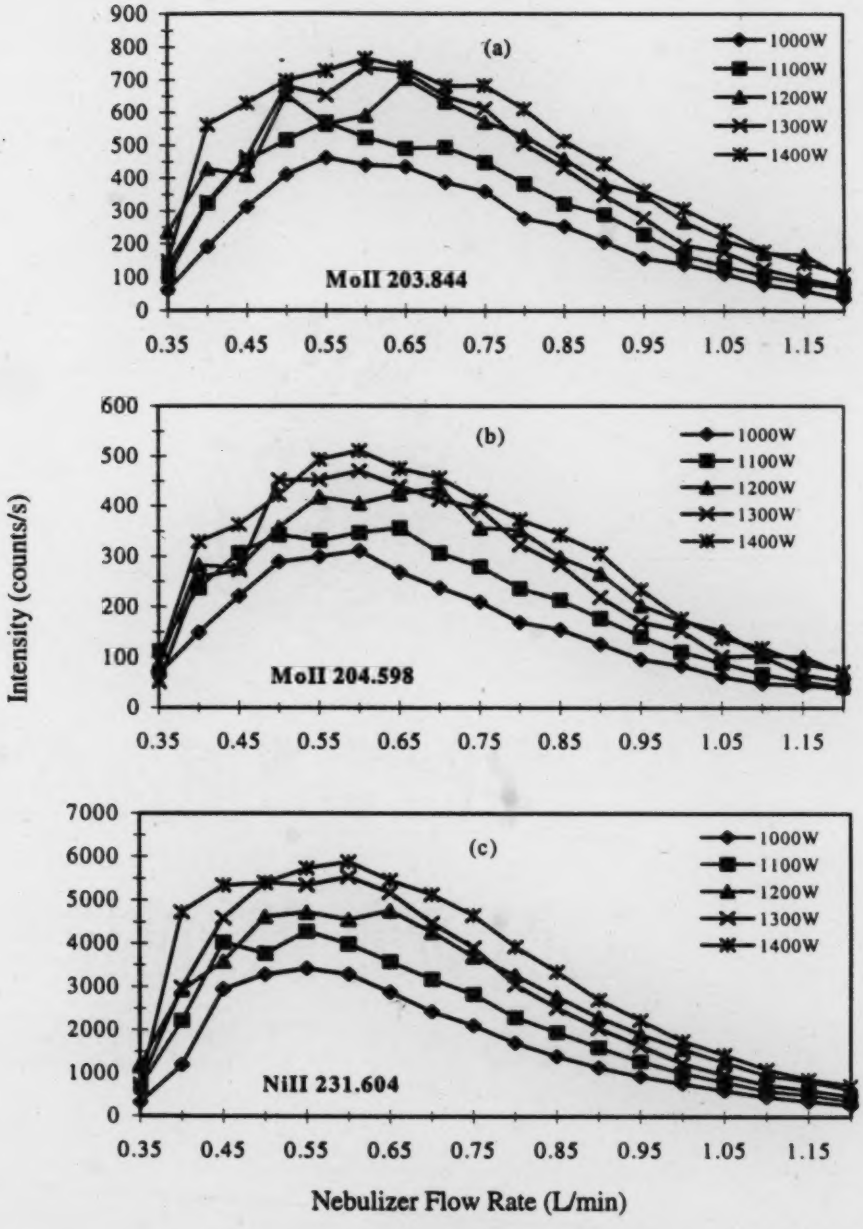

Figure 3.8 Intensity vs Nebulizer Flow Rate Plots for Mo (a, b) and Ni (c) at different Power.

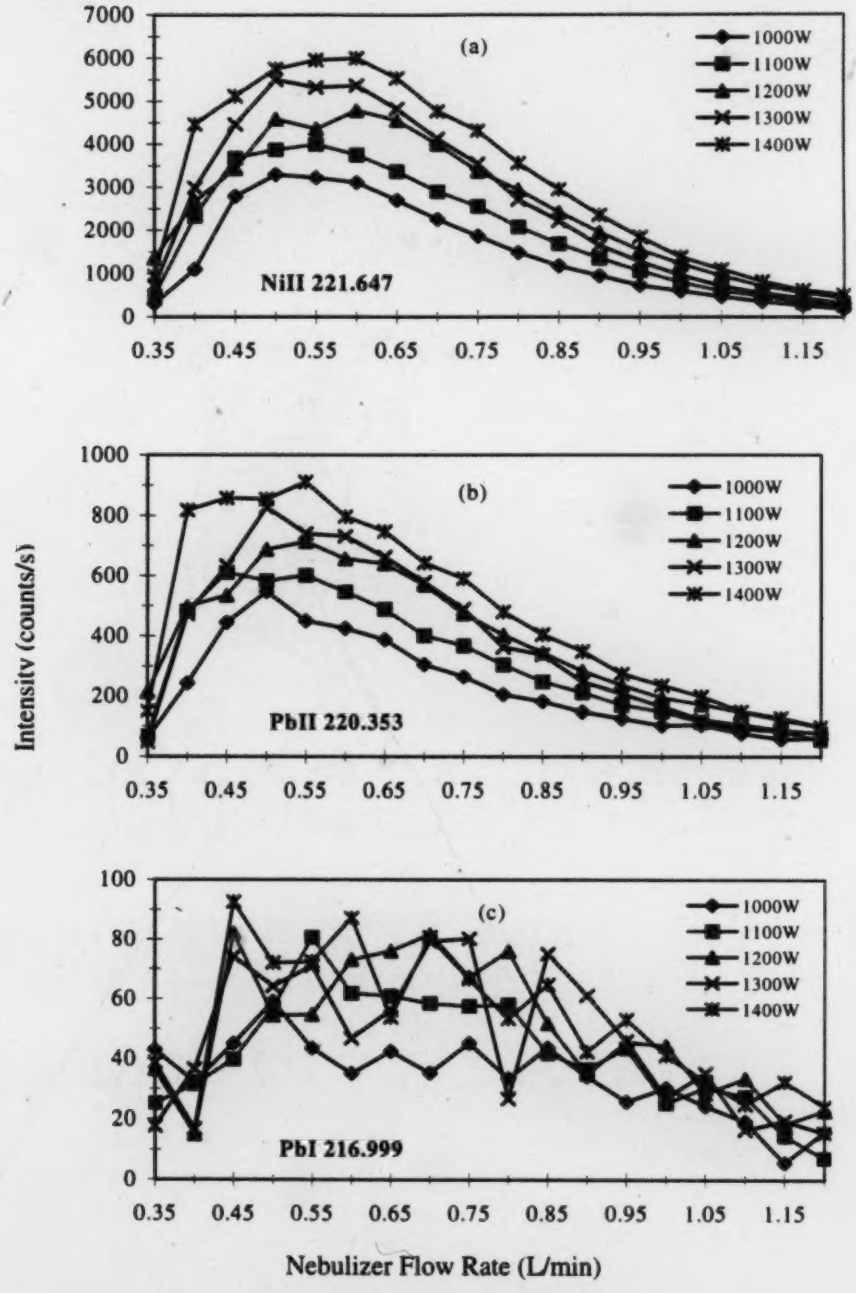

Figure 3.9 Intensity vs Nebulizer Flow Rate Plots for Ni (a) and Pb (b, c) at different Power.

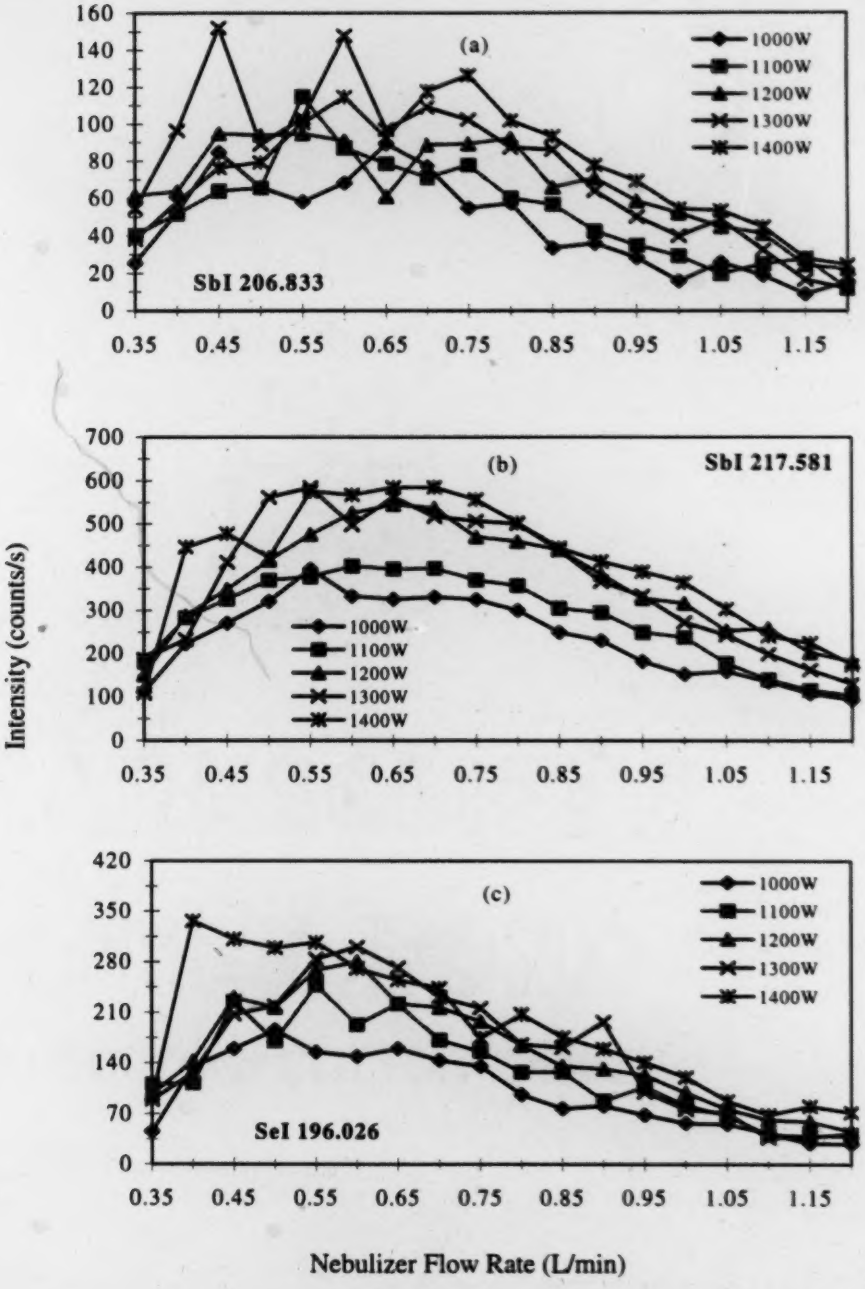

Figure 3.10 Intensity vs Nebulizer Flow Rate Plots for Sb (a, b) and Se (c) at different Power.

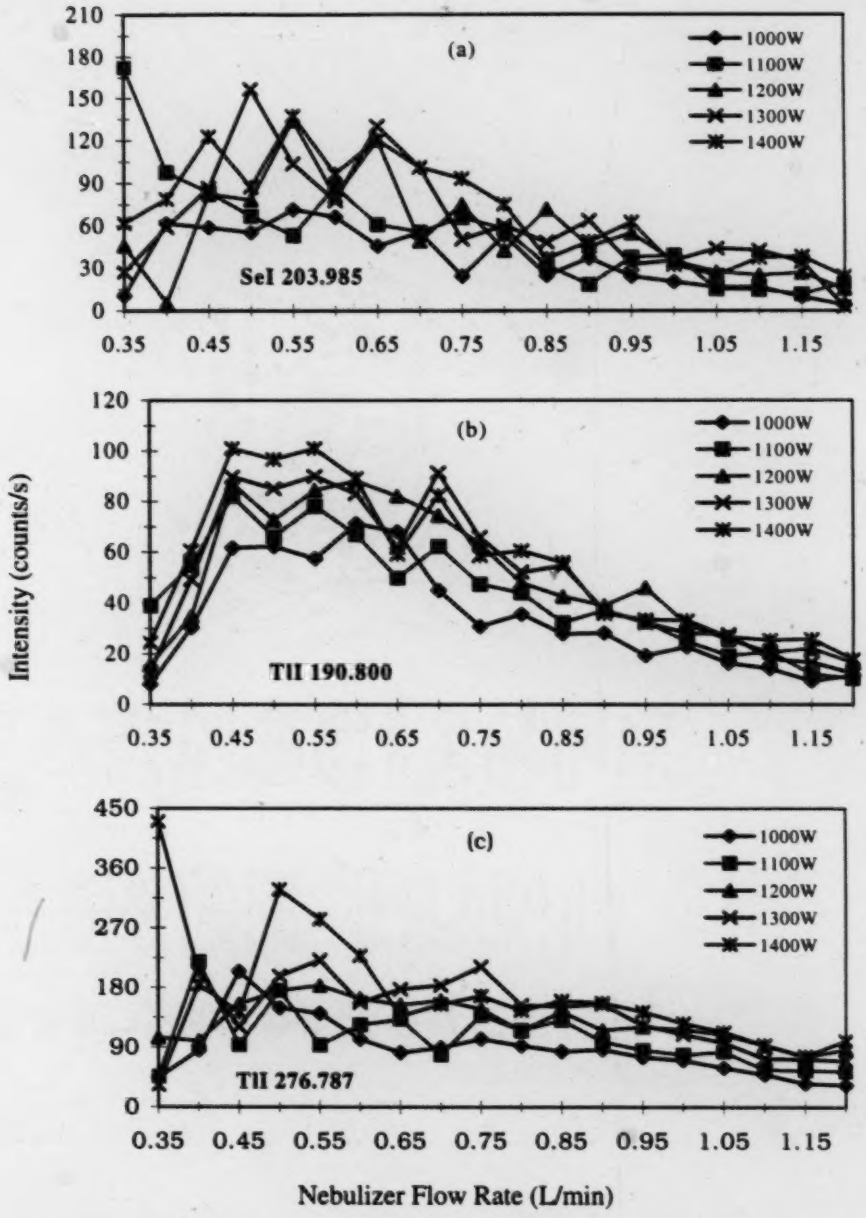

Figure 3.11 Intensity vs Nebulizer Flow Rate Plots for Se (a) and Tl (b, c) at different Power.

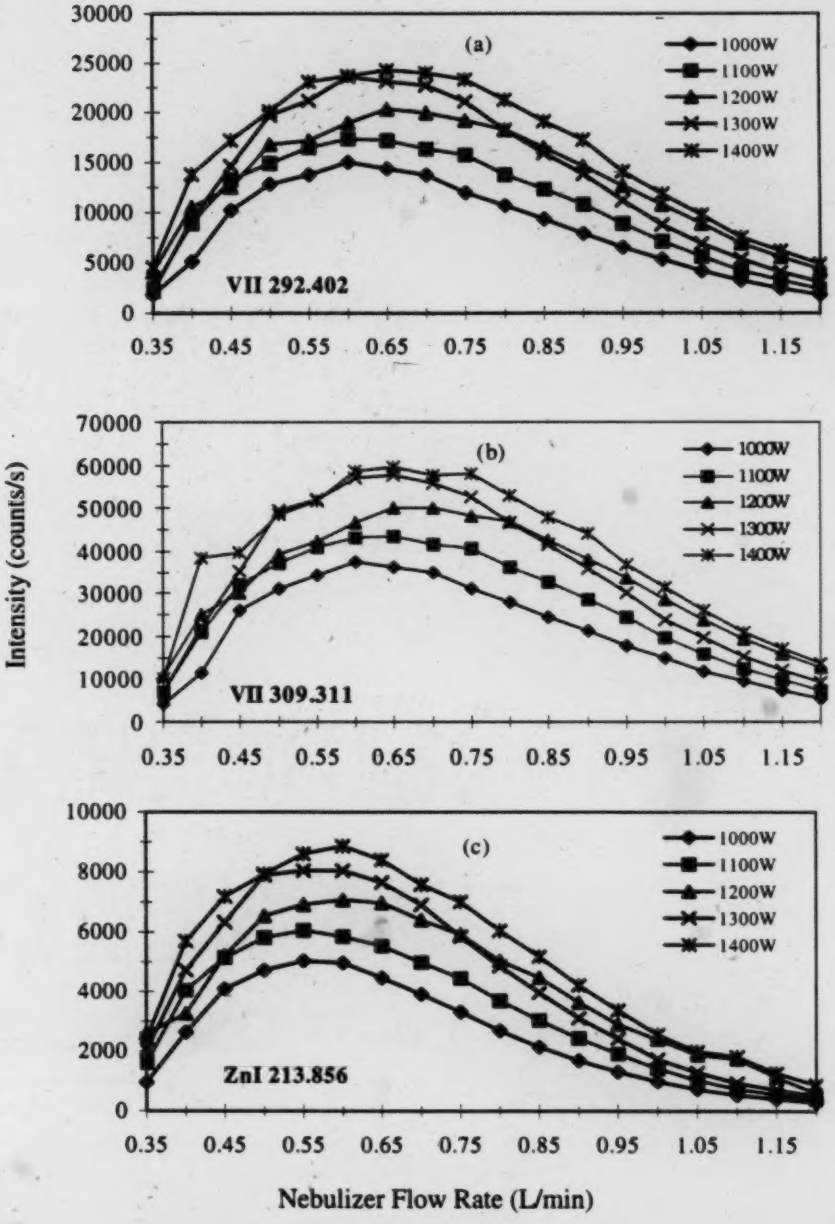

Figure 3.12 Intensity vs Nebulizer Flow Rate Plots for V (a, b) and Zn (c) at different Power.

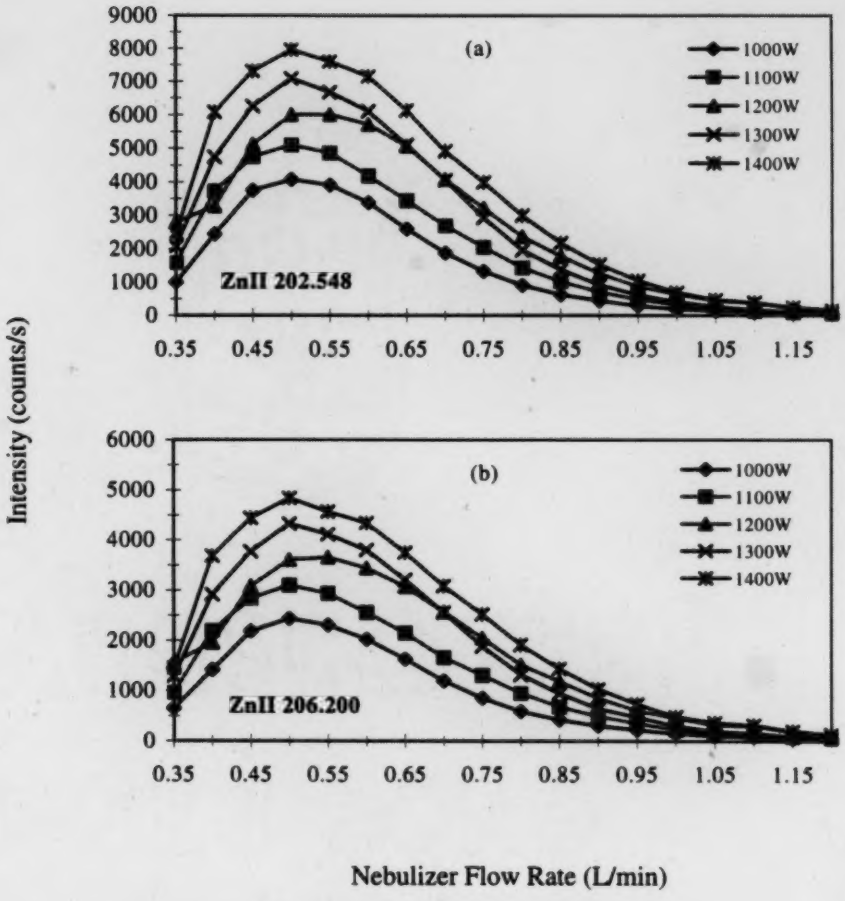

Figure 3.13 Intensity vs Nebulizer Flow Rate Plots for Zn (a, b) at different Power.

there is a steep signal drop when the nebulizer flow rate is altered from the optimum flow.

The position of this maximum signal intensity does not vary significantly from one element to another element although plots for CuI 324.754 nm gives a maximum at higher flow rates compared to other plots. Thus at all the powers tested, the elements studied have a signal maximum closed to 0.60 l/min except for CuI 324.754 nm where the maximum is close to 0.90 l/min.

The count for each element goes through a maximum indicating that at a fixed plasma power, there is an optimum flow rate at which the count and sensitivity is a maximum. This implies that a single set of conditions can be used for quantitative analysis of many elements with little or no sensitivity loss.

The plots of signal intensity vs nebulizer flow rate at fixed power (1000 W) for lines of the same element are shown in Figure 3.14-3.18. The values of the maximum intensities are different for ionic and atomic spectral lines. There are normalized plots of signal intensity vs nebulizer flow rate at 1000 W for CuI 324.754 nm/CuII 224.700 nm, BeI 234.861 nm/BeII 313.042 nm and ZnI 213.856 nm/ZnII 202.548 nm (Figure 3.19). The maximum intensity for three ionic lines is located at a nebulizer flow rate of about 0.50 to 0.55 l/min. The optimum flow rate for atomic lines is shifted to a slightly higher value, about 0.55 to 0.60 l/min, but for CuI 324.754 nm, the maximum is about 0.90 l/min.

The results are similar to that observed by Smith and Horlick [13] and are generally consistent with the trend established by Boumans and his co-workers [1-3] and illustrated extensively by Blades and Horlick [14].

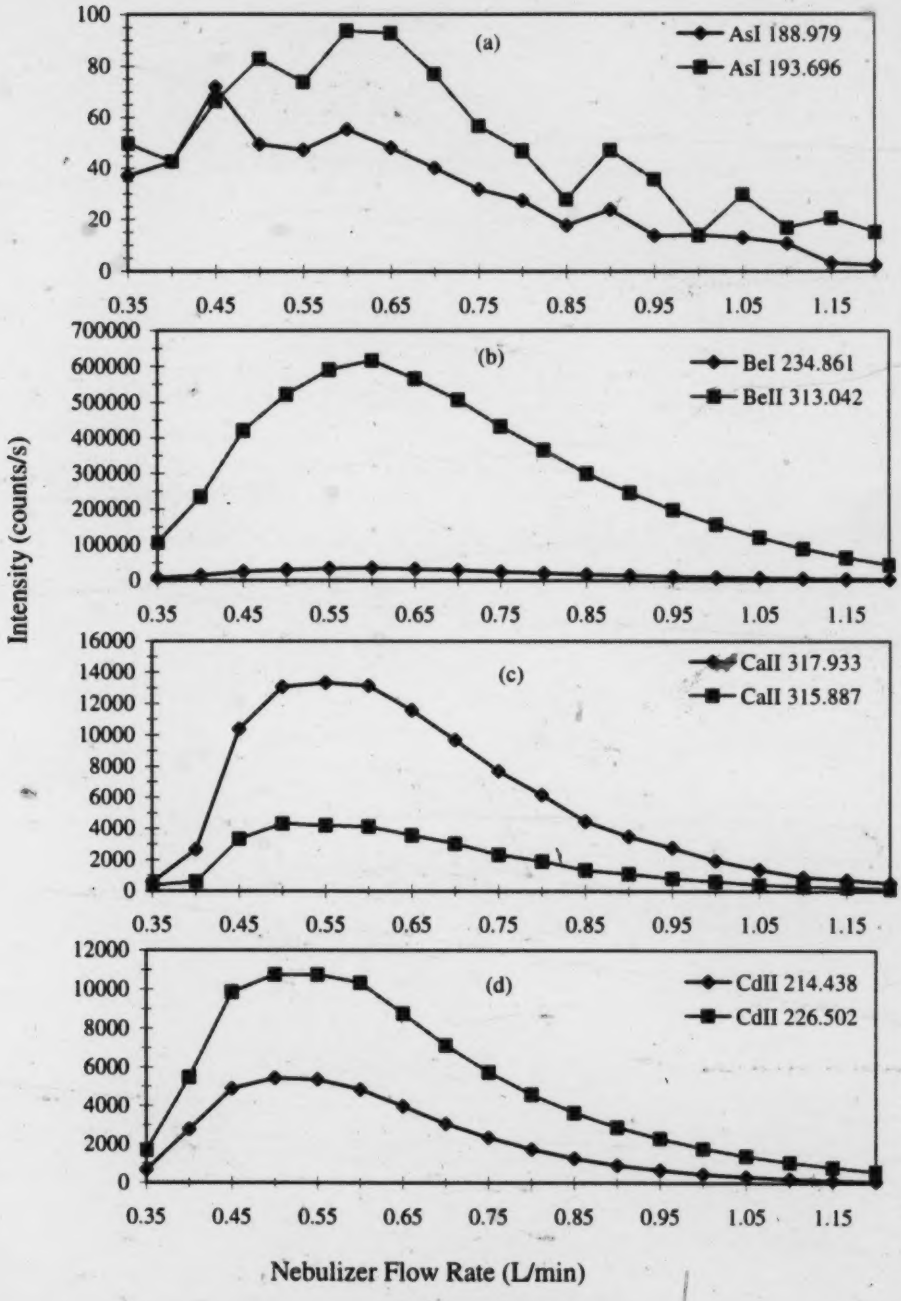

Figure 3.14 Intensity vs Nebulizer Flow Rate Plots for As (a), Be (b), Ca (c) and Cd (d) at 1000 W.

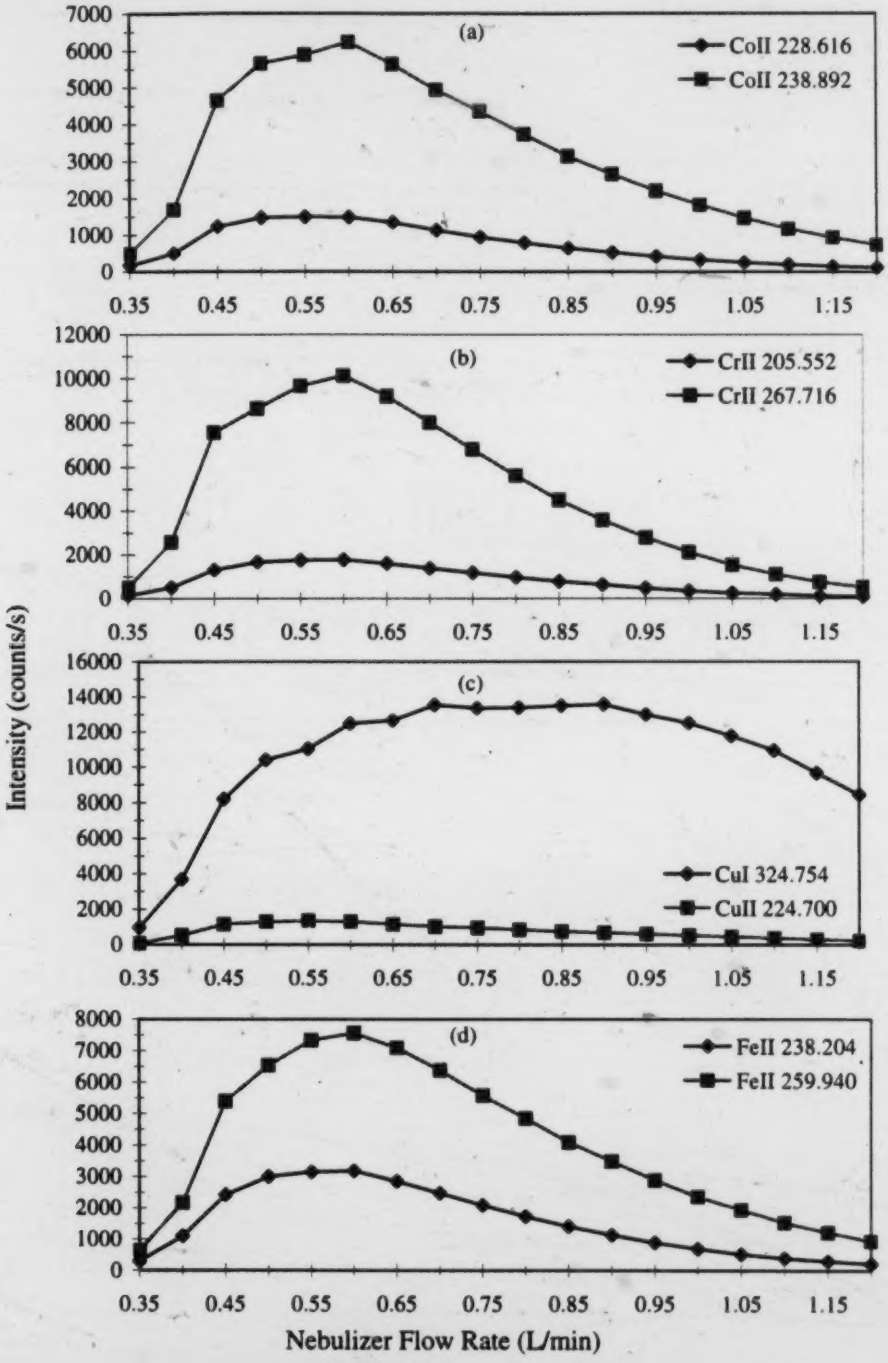

Figure 3.15 Intensity vs Nebulizer Flow Rate Plots for Co (a), Cr (b), Cu (c) and Fe (d) at 1000 W.

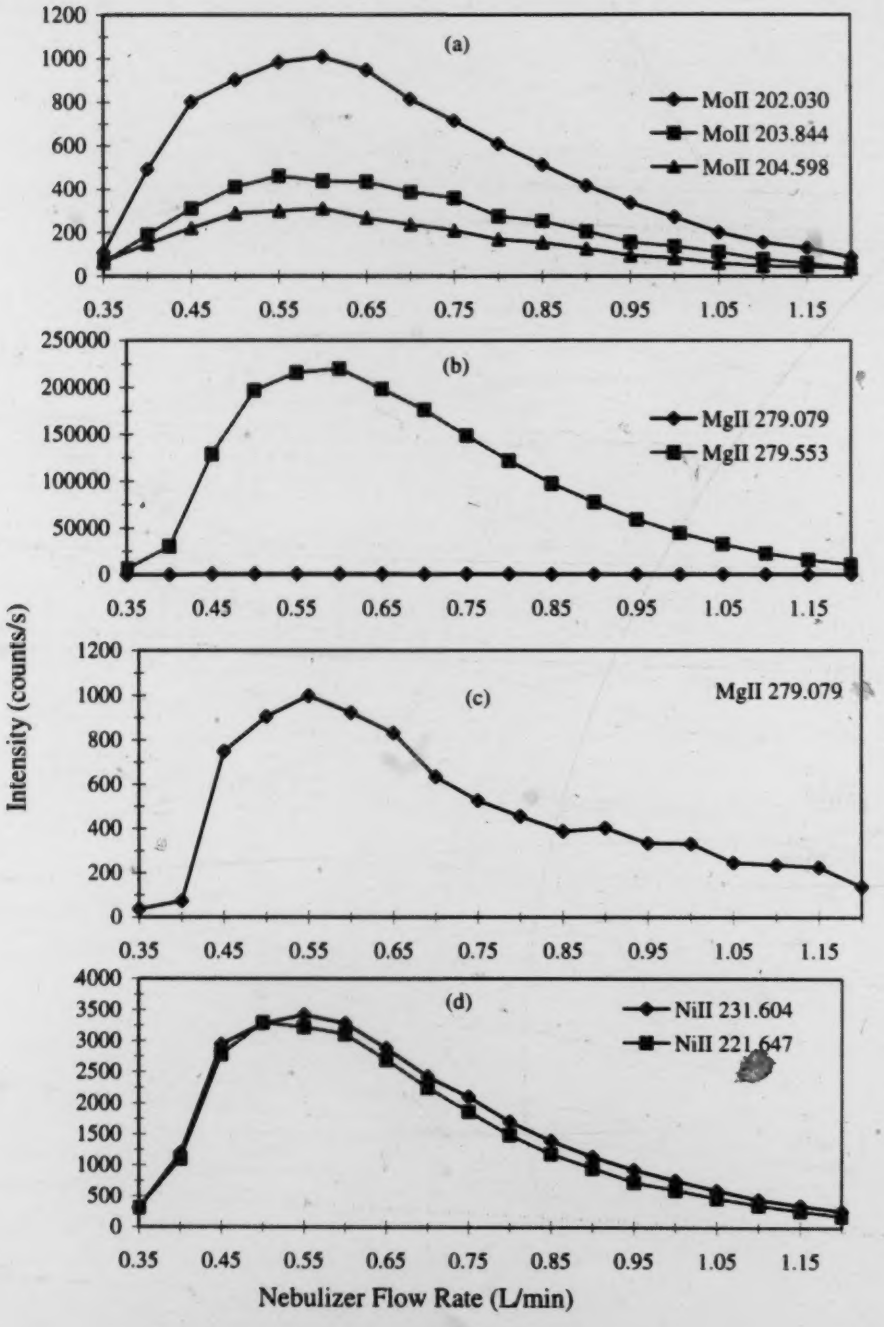

Figure 3.16 Intensity vs Nebulizer Flow Rate Plots for Mo (a), Mg (b, c) and Ni (d) at 1000 W.

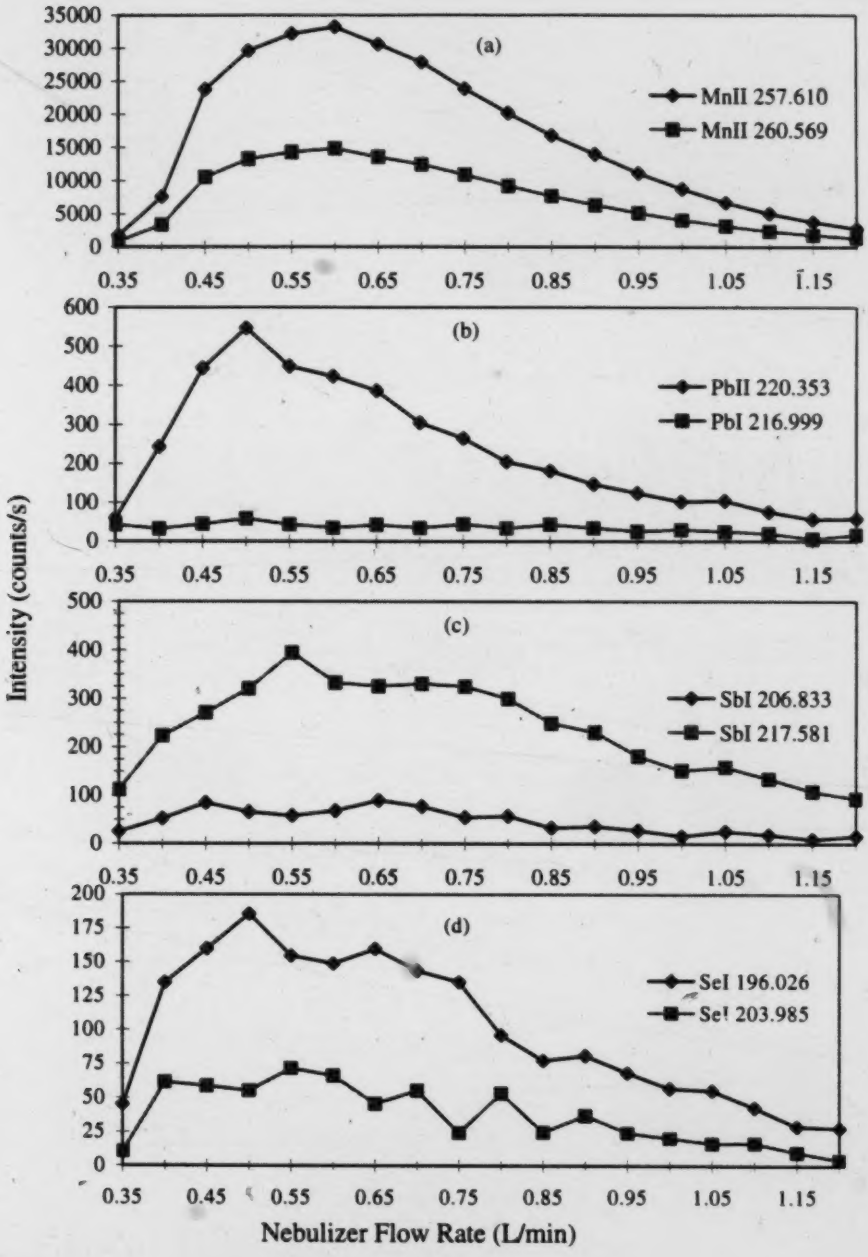

Figure 3.17 Intensity vs Nebulizer Flow Rate Plots for Mn (a), Pb (b), Sb (c) and Se (d) at 1000 W.

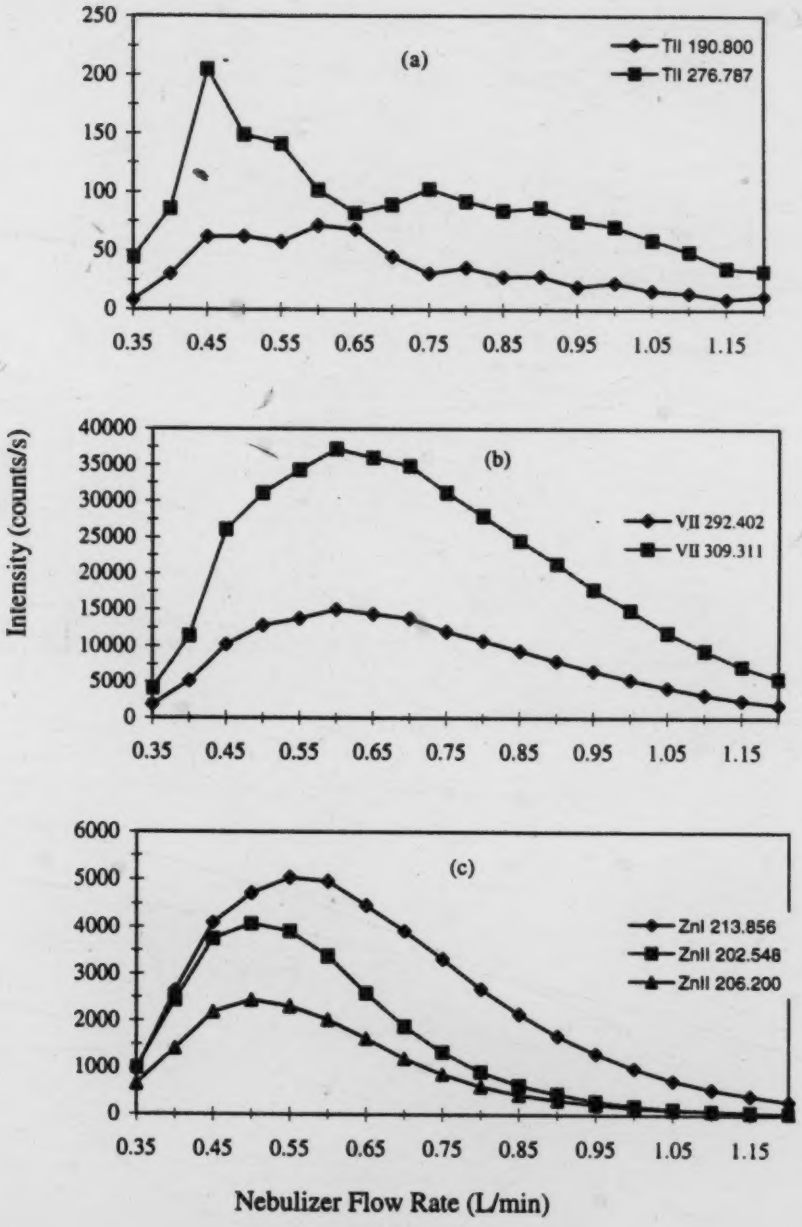

Figure 3.18 Intensity vs Nebulizer Flow Rate Plots for Tl (a), V (b) and Zn (c) at 1000 W.

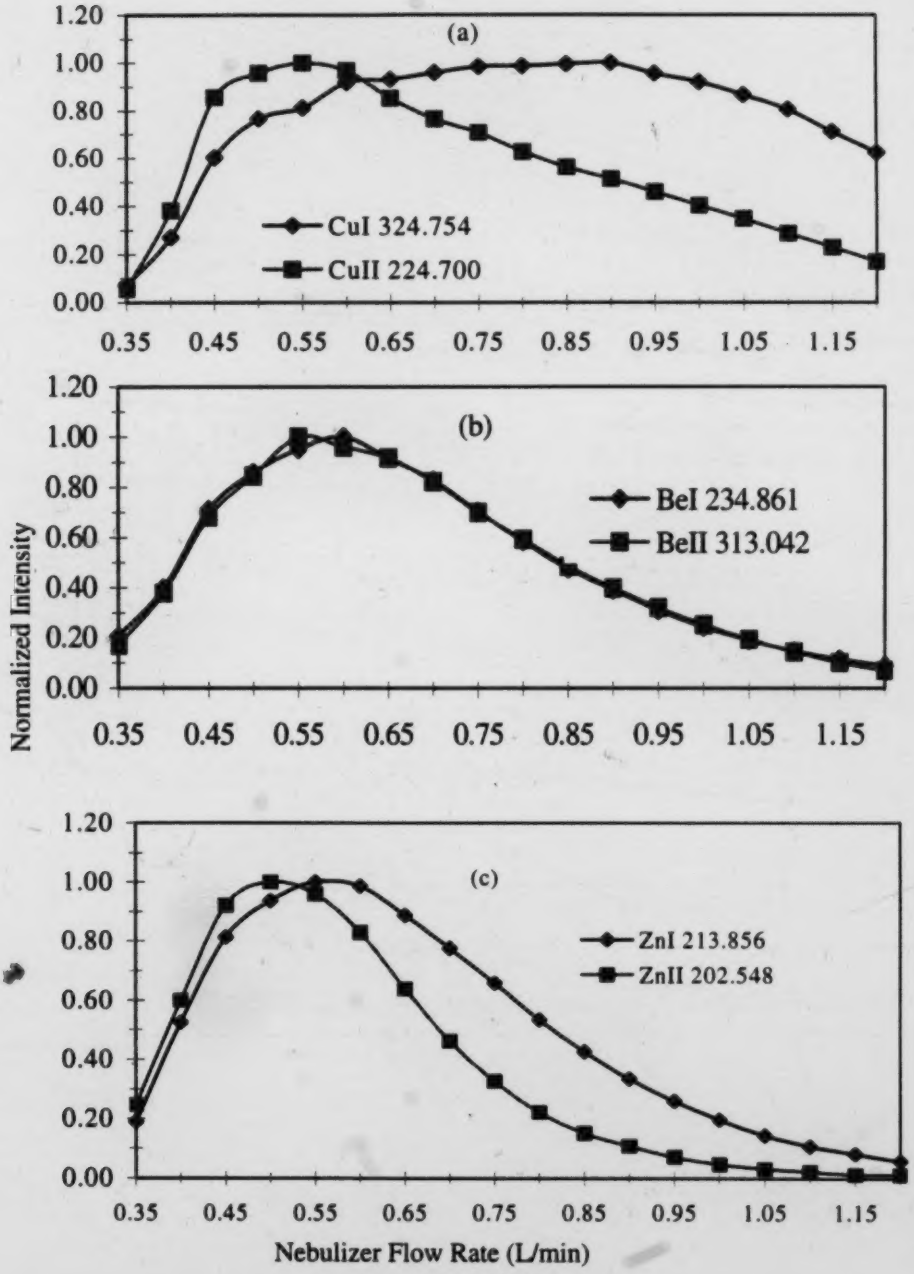

Figure 3.19 Normalized Intensity vs Nebulizer Flow Rate Plots for Cu (a), Be (b) and Zn (c) at 1000 W.

Boumans used the term hard and soft lines to distinguish these two types of lines. Atomic lines of elements of low to medium first ionization potential (Li I, Ba I, Mn I) and ionic lines of elements of low second ionization potential (Ba II) are known as soft lines. And atomic lines of elements of high first ionization potential (Cd I, Zn I) and ionic lines of elements of high second ionization potential (Cd II, Zn II) are known as hard lines. The soft lines show a decrease in intensity with an increase in power and the hard lines show an increase in intensity with an increase in power.

The lower nebulizer flow rate maximum for the ionic lines reflect a hotter more energetic plasma while the less energy atomic lines have their maximum signal level in a cooler plasma which is created with slightly higher flow rate. The rather large difference seen in the case of Cu reflects a large difference in excitation energy for these two lines (see Figure 3.19).

Wavelengths, excitation potentials, and ionization potentials for the elements studied in this chapter are summered in Table 3.2. From Table 3.2, It can be seen that the excitation potential for CuI 324.754 nm is only 3.82 ev, it is much smaller compared with that for BeI 234.861 nm (5.28 ev) and ZnI 213.856 nm (5.80 ev). So the maximum intensity for CuI 324.754 nm is located at higher nebulizer flow rate.

3.2.2 Effect of RF Power on Analyte Signals

Over the range tested (1000 to 1400W) power had a modest effect on signal intensity (see Figure 3.20 to 3.24). Generally, the signal intensity increased with an increase in plasma power, but typically not by more than a factor of two for this power range.

Table 3.2 Wavelengths, Excitation Potentials, and First Ionization Potentials for the Elements Studied in this Chapter

Element	Line (nm)	EP (eV)	IP (eV)
AsI	188.979	6.56	
AsI	193.696	6.40	
BeI	234.861	5.28	
BeII	313.042	3.96	9.32
CaII	317.933	7.05	6.11
CaII	315.887	7.05	6.11
CdII	214.438	5.78	8.99
CdII	226.502	5.47	8.99
CoII	228.616	5.84	7.86
CoII	238.892	5.60	7.86
CrII	205.552	6.03	6.76
CrII	267.716	6.18	6.76
CuI	324.754	3.82	
CuII	224.700	8.23	7.72
FeII	238.204	5.20	7.87
FeII	259.940	4.77	7.87
MgII	279.079	8.86	7.64
MgII	279.553	4.43	7.64
MnII	257.610	4.81	7.43
MnII	260.569	4.75	7.43
MoII	202.030	6.13	7.10
MoII	203.844	6.08	7.10
MoII	204.598	6.06	7.10
NiII	231.604	6.38	7.63
NiII	221.647	6.63	7.63
PbII	220.353	7.37	7.42
PbI	216.999	5.71	
SbI	206.833	5.98	
SbI	217.581	5.69	
VII	292.402	4.63	6.74
VII	309.311	4.40	6.74
ZnI	213.856	5.80	
ZnII	202.548	6.12	9.39
ZnII	206.200	6.01	9.39

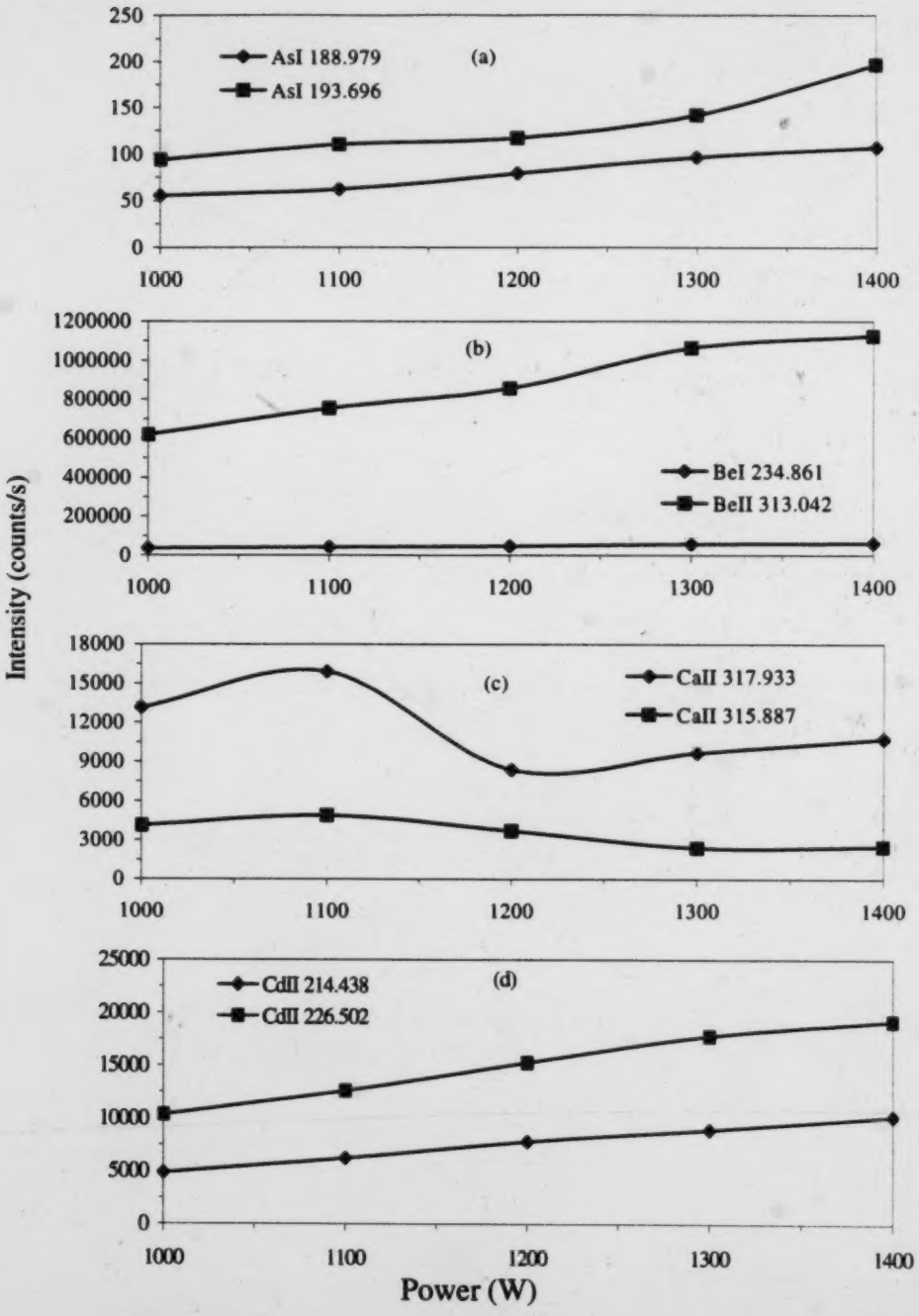

Figure 3.20 Intensity vs Power Plots for As (a), Be (b), Ca (c) and Cd (d).

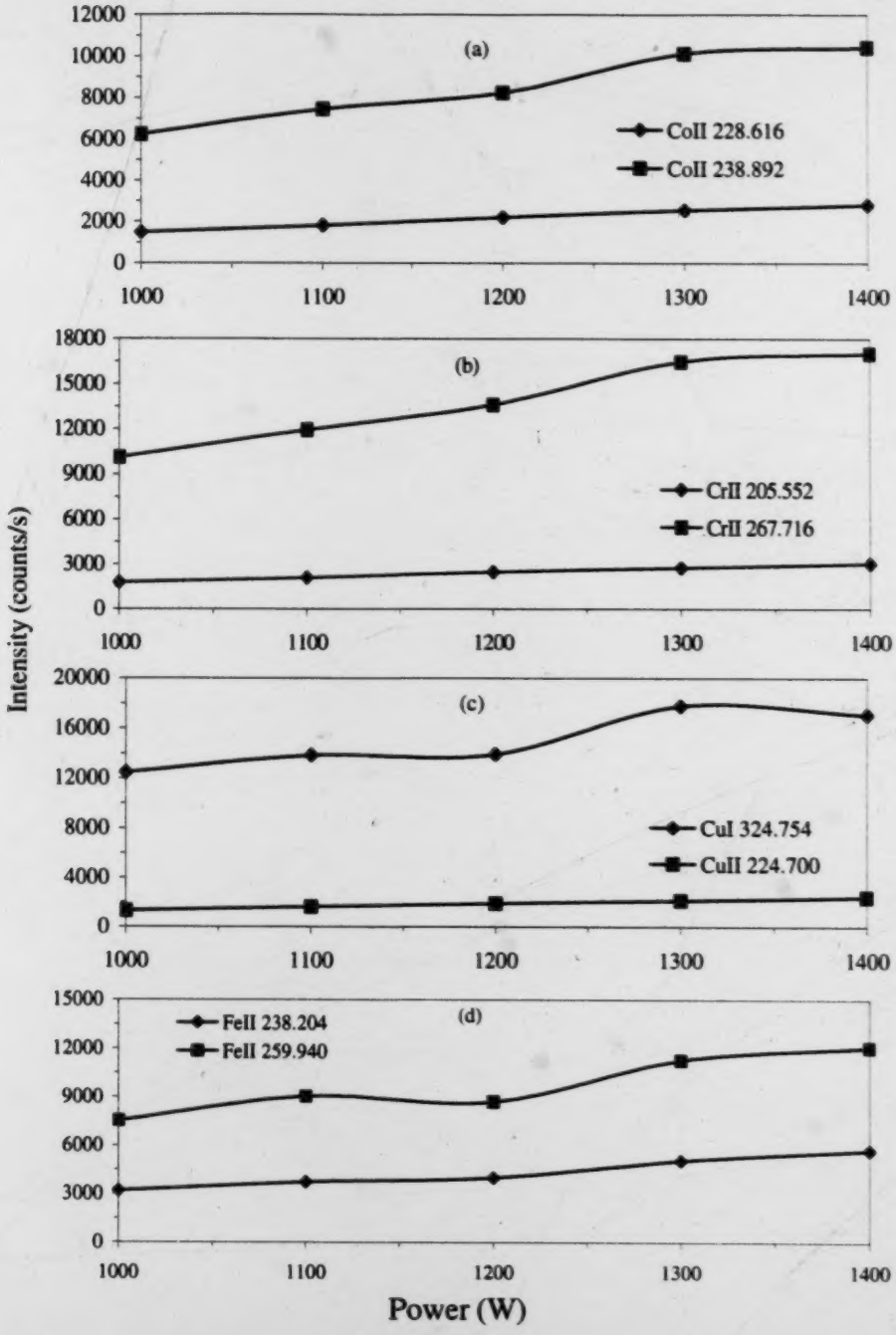

Figure 3.21 Intensity vs Power Plots for Co (a), Cr (b), Cu (c) and Fe (d).

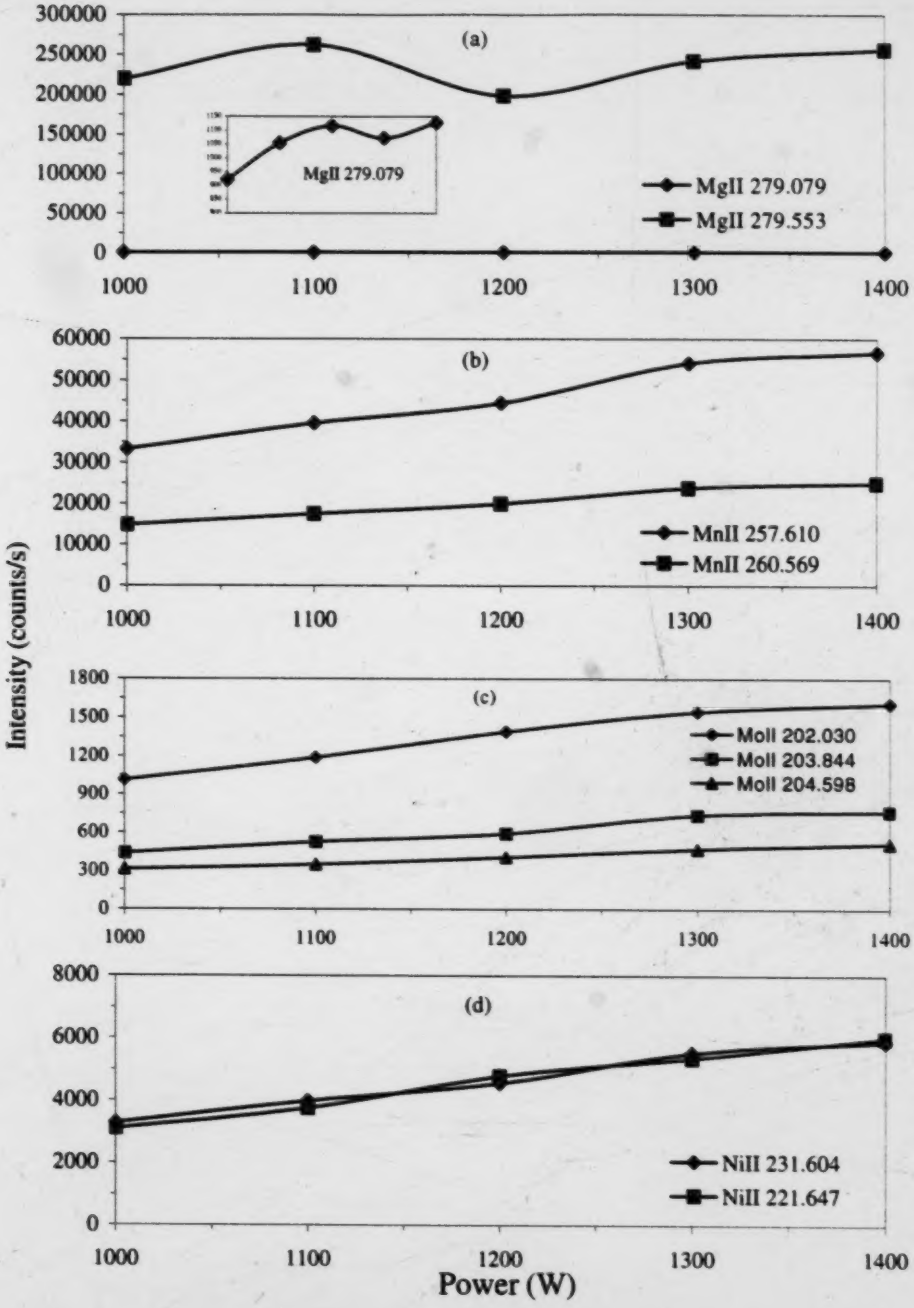

Figure 3.22 Intensity vs Power Plots for Mg (a), Mn (b), Mo (c) and Ni (d).

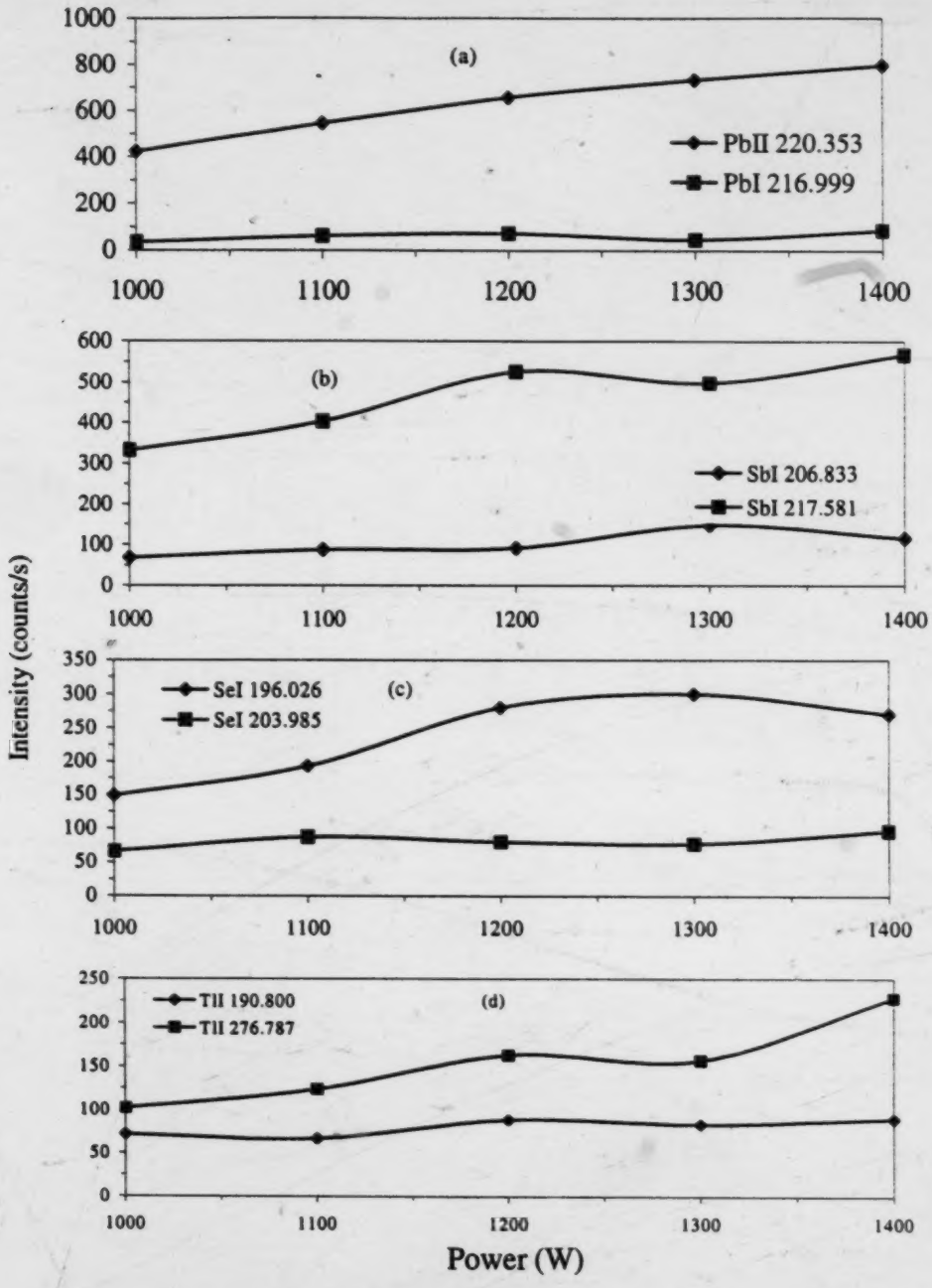

Figure 3.23 Intensity vs Power Plots for Pb (a), Sb (b), Se (c) and Tl (d).

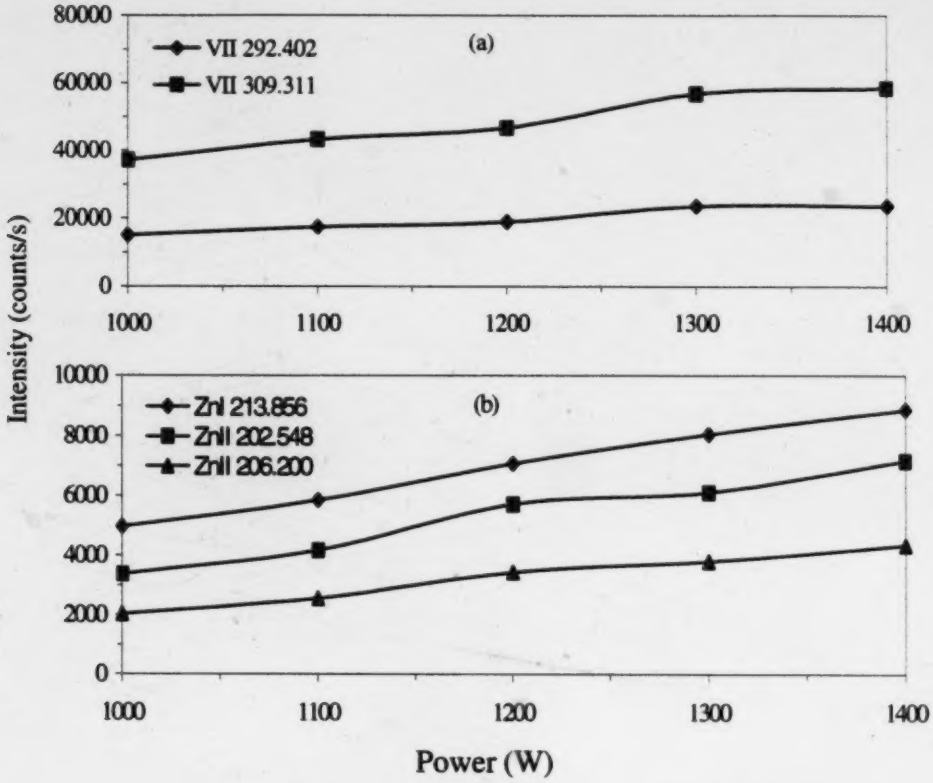

Figure 3.24 Intensity vs Power Plots for V (a) and Zn (b).

3.2.3 Ca and Mg Interference and K Matrix Effect on Analyte Signals (with Xinbang Feng)

The sample matrix, in addition to introducing background spectral features also may induce changes in the analyte signal intensity. Matrix effects are always a concern in inductively coupled plasma atomic emission spectrometry (ICP-AES) and an area of intense investigation, because some serious matrix effects have been observed.

Usually matrix effects are caused by a high concentration of a concomitant and Ca, Mg and K are common major constituent elements in samples. Matrix effects in ICP-AES are caused by changes in excitation conditions and/or species distribution in the plasma [15] or may be simply related to spectral interference.

The experiments were carried out at a RF power of 1100 W, auxiliary flow rate at 0.5 l/min, plasma flow rate at 15.0 l/min and nebulizer flow rate at 0.6 l/min. First calibration curves were obtained for the elements studied. Then 10 ppm, 100 ppm, and 1000 ppm solutions of Ca and Mg (single element) were "analyzed" for the tested elements. The signal intensity reported is corrected signal intensity (blank subtracted with background correction). The results for the Ca and Mg interference studies are shown in Table 3.3 and Table 3.4 where both signal level and equivalent ppm are presented.

There is almost no interference indicated for the elements studied except for the effect of Mg on MnI 279.482nm and Ca on SI (sulfur) 180.669nm.

Table 3.3 Interference of Ca on Analyte Signal.

Elements Lines Tested	10 ppm Ca	100 ppm Ca	1000 ppm Ca
SI 180.669	**27.4(0.175 ppm)**	**162.6(2.89 ppm)**	**1374.3(27.2 ppm)**
ZnII 202.548	54.7(0.013 ppm)	324.1(0.044 ppm)	241.5(0.034 ppm)
ZnI 213.856	567.4(0.021 ppm)	1345.6(0.088 ppm)	1874.4(0.134 ppm)
CdII 214.438	84.0(-0.001 ppm)	92.2(0.000 ppm)	48.8(-0.004 ppm)
CdI 228.802	36.8(-0.005 ppm)	43.3(-0.002 ppm)	52.9(0.002 ppm)
CuII 224.700	37.5(0.002 ppm)	120.5(0.026 ppm)	134.8(0.030 ppm)
CuI 324.754	4709.6(0.000ppm)	7118.0(0.024 ppm)	6896.0(0.022 ppm)
FeII 238.204	97.0(0.008 ppm)	98.4(0.009 ppm)	128.8(0.016 ppm)
MnII 257.610	-33.6(0.000 ppm)	122.4(0.002 ppm)	-36.4(0.000 ppm)
MnI 279.482	6605.4(0.003 ppm)	8413.8(0.004 ppm)	22972.5(0.014 ppm)
MgII 279.079	-84.9(-0.007 ppm)	-52.1(-0.001 ppm)	-66.9(-0.004 ppm)
MgI 285.213	1440.8(0.003 ppm)	1658.8(0.004 ppm)	3913.5(0.017 ppm)
NaI 589.592	8060.9(0.012 ppm)	6125.8(0.006 ppm)	15685.7(0.036 ppm)
KI 766.491	2013.8(0.001 ppm)	1715.1(-0.005 ppm)	2277.8(0.005 ppm)

Table 3.4 Interference of Mg on Analyte Signal.

Elements Lines Tested	10 ppm Mg	100 ppm Mg	1000 ppm Mg
MnI 279.482	**12899933.4(8.90 ppm)**	**Saturated**	**Saturated**
SI 180.669	**-22.7(-0.831 ppm)**	**-266.9(-5.74 ppm)**	**-783.2(-16.1 ppm)**
ZnII 202.548	-57.0(0.001 ppm)	46.1(0.012 ppm)	-3431.5(-0.382 ppm)
ZnI 213.856	390.7(0.006 ppm)	1023.8(0.060 ppm)	803.5(0.041 ppm)
CdII 214.438	72.8(-0.002 ppm)	18.9(-0.007 ppm)	-15.3(-0.010 ppm)
CdI 228.802	45.3(-0.001 ppm)	48.6(0.000 ppm)	57.3(0.004 ppm)
CuII 224.700	47.1(0.005 ppm)	137.5(0.031 ppm)	61.2(0.009 ppm)
CuI 324.754	4539.4(-0.001 ppm)	7088.1(0.024 ppm)	4298.7(-0.004 ppm)
FeII 238.204	102.4(0.010 ppm)	103.8(0.010 ppm)	218.8(0.036 ppm)
MnII 257.610	6.9(0.001 ppm)	98.5(0.002 ppm)	1701.7(0.021 ppm)
NaI 589.592	7521.8(0.011 ppm)	15112.4(0.034 ppm)	21163.6(0.053 ppm)
KI 766.491	1781.1(-0.003 ppm)	3461.6(0.026 ppm)	3425.4(0.025 ppm)

Mg has an intense emission line at a 279.553nm, and the effect is huge, 10 ppm Mg appears as 8.90 ppm Mn and it causes the MnI 279.482nm channel to saturate at 100 ppm. It is better to avoid the use of the MnI 279.482nm wavelength when Mg concentration is high in solution.

Ca has an emission wavelength at 180.674nm. So Ca has an effect on S 180.669nm wavelength. The two lines almost overlap (Figure 3.25a). There are two spectra inside the sulfur window, one is 10.0 ppm sulfur standard (without Ca) and the other one is 100.0 ppm pure Ca solution. Although the effect of Ca on SI 180.669nm is not as severe as Mg on MnI 279.482nm, 100.0 ppm Ca is equal to 2.89 ppm S. So if the concentration of Ca is high in solution, a correction will be necessary for S measurement.

Mg has a negative effect on SI 180.669nm. This is probably due to the background correction points selected are not good. Generally, background correction points are set near the analyte peak on part of the spectrum that does not contain peaks from interfering emission lines. See Figure 3.25a for details. BG_1 and BG_2 are two background correction points, and BG is the resultant background correction. BG will be subtracted from the peak intensity to give an intensity value corrected for background influences.

There is a Mg wavelength at 180.075 nm, as concentration of Mg increases, the signal intensity of Mg 180.075nm increases. If the background correction points are just sitting on the peak, overcorrecting will happen (Figure 3.25b). BG_1 is just sitting on the peak of interfering emission lines (Mg 180.075). So it is better to use just one point background correction or no background correction points at all if the concentration of Mg is high when determining S.

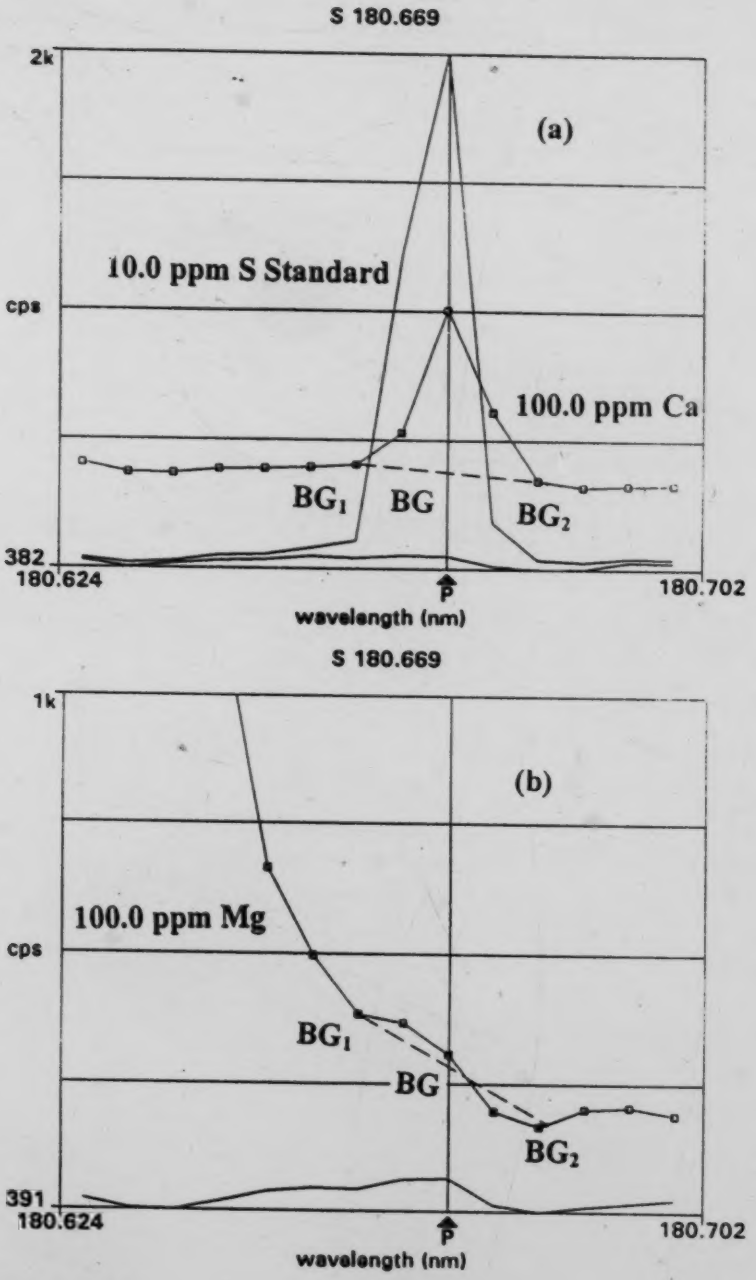

Figure 3.25

Mg and Ca Interference on SI 180.669 nm. (a) is Ca Interference on Sulfur. (b) is Mg Interference on Sulfur.

The results of the K matrix effect on Cu, Cd, Mg and Na are shown in Figures 3.26-3.29. All of the figures represent the emission intensity of elements studied here without and with the presence of K. The concentrations of Cu, Cd, and Mg are 2.0, 6.0 and 10.0 ppm, the concentrations of Na are 10.0, 20.0, and 40.0 ppm.

The effect on atomic and ionic lines is similar (Figure 3.26-3.28), but the effect is larger for atomic lines. For atomic lines, the intensity is almost double comparing 10,000 ppm K with 0 ppm K. For ionic lines, the intensity does not increase that much.

The reason of such an effect is probably due to either an increase in the amount of analyte transferred to the plasma, or traditional easily ionized element effect due to the presence of K. The clear meaning is that "end-on" plasma intensities can be significantly altered by an easily ionized element such as K.

The analyte emission passes through cooled tail plume zone of plasma for end-on viewing, although there is sheer gas to cut off the plume zone. Easily ionized element presented in the sample may affect the performance of analyte signal. When easily ionized elements, such as K, present in the sample, the population of electrons will be high. So it will cause equation (2) shift to left (A is analyte), the concentration of neutral speciation of analyte will increase. So the intensity of atomic lines will increase.

$$K = K^+ + e \quad (1)$$

$$A = A^+ + e \quad (2)$$

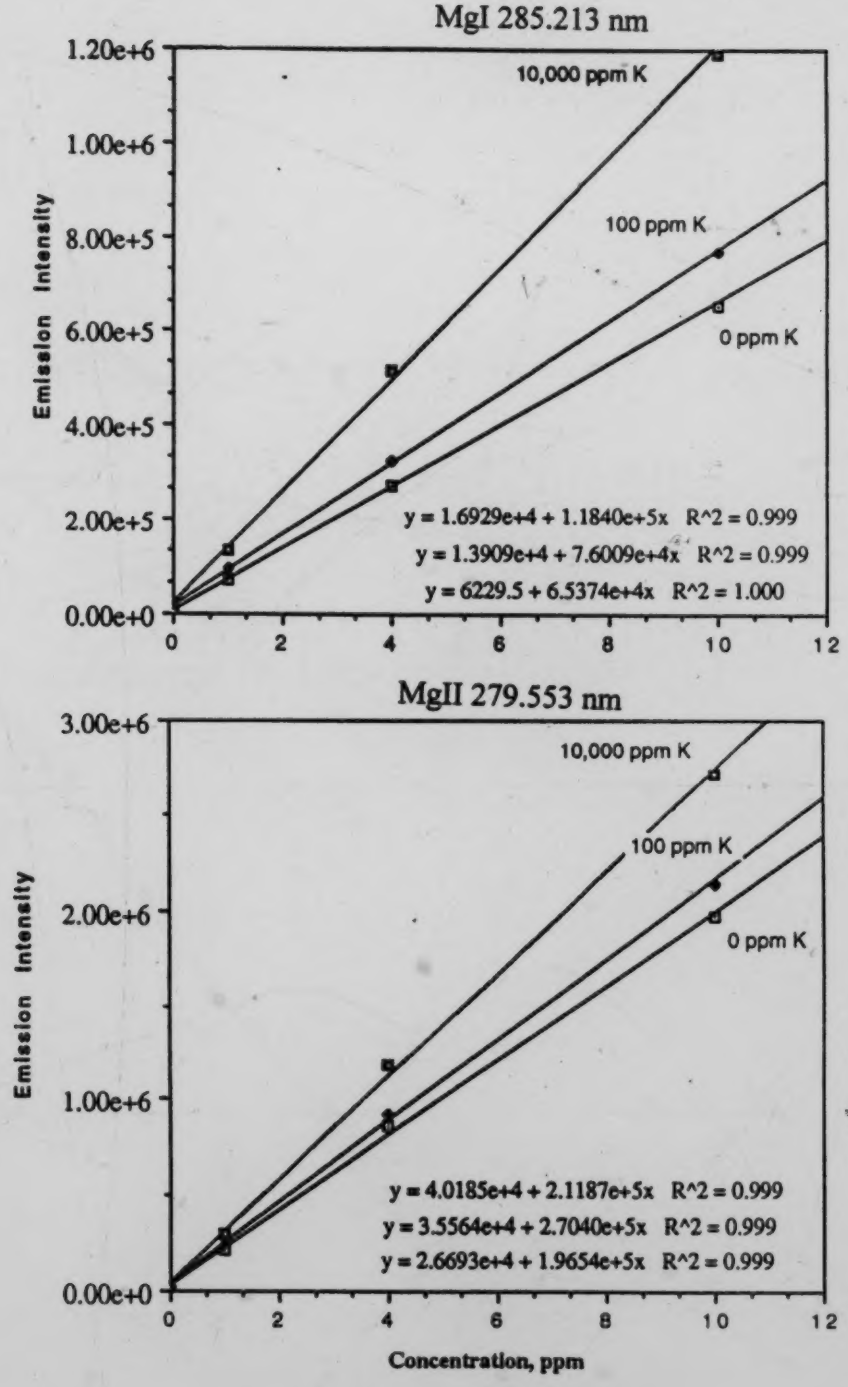

Figure 3.26 K Matrix Effects on Mg.

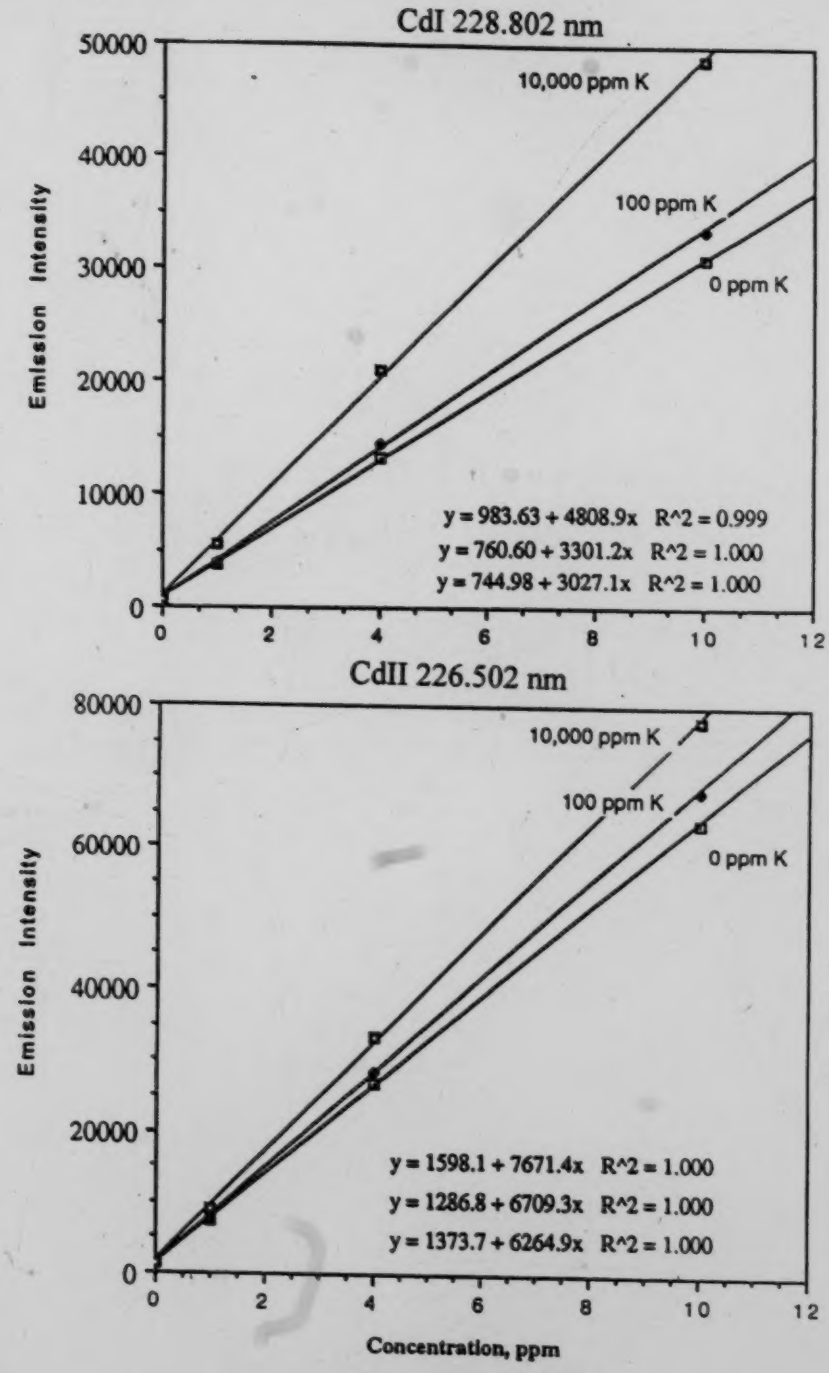

Figure 3.27 K Matrix Effects on Cd.

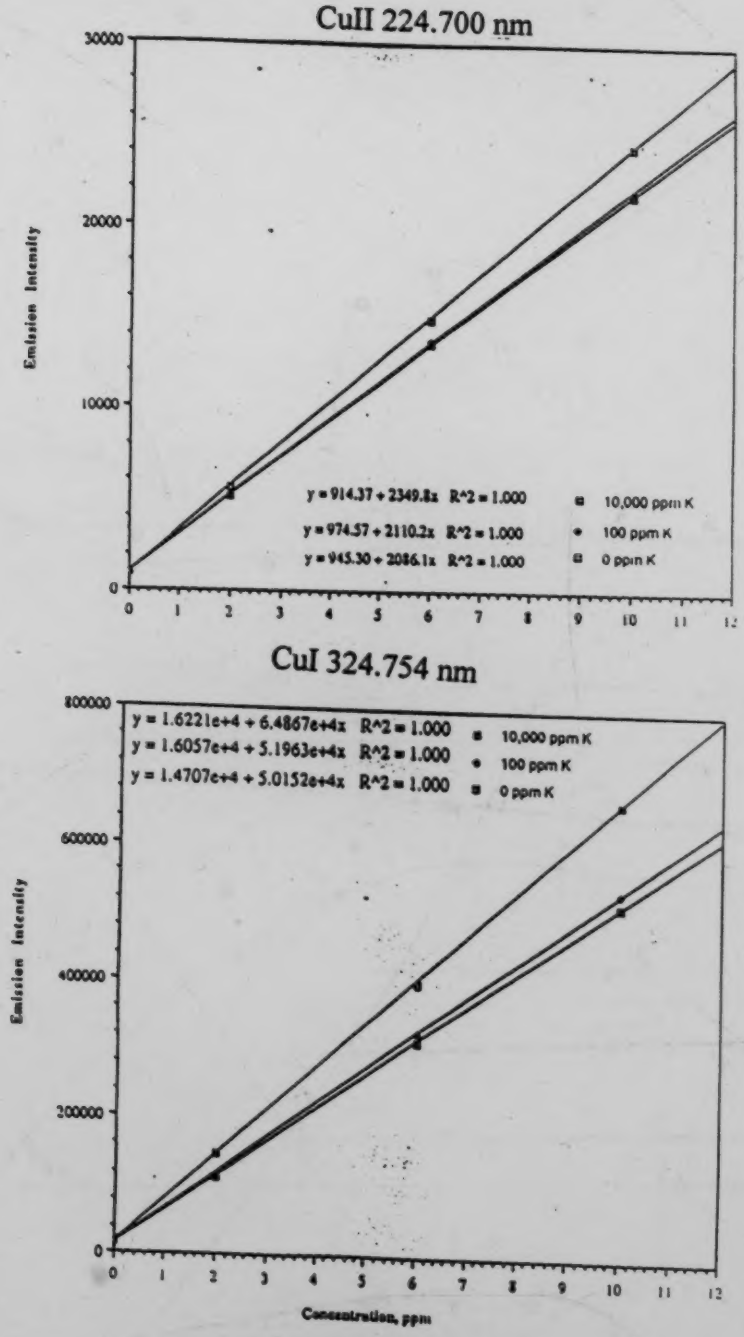

Figure 3.28 K Matrix Effects on Cu.

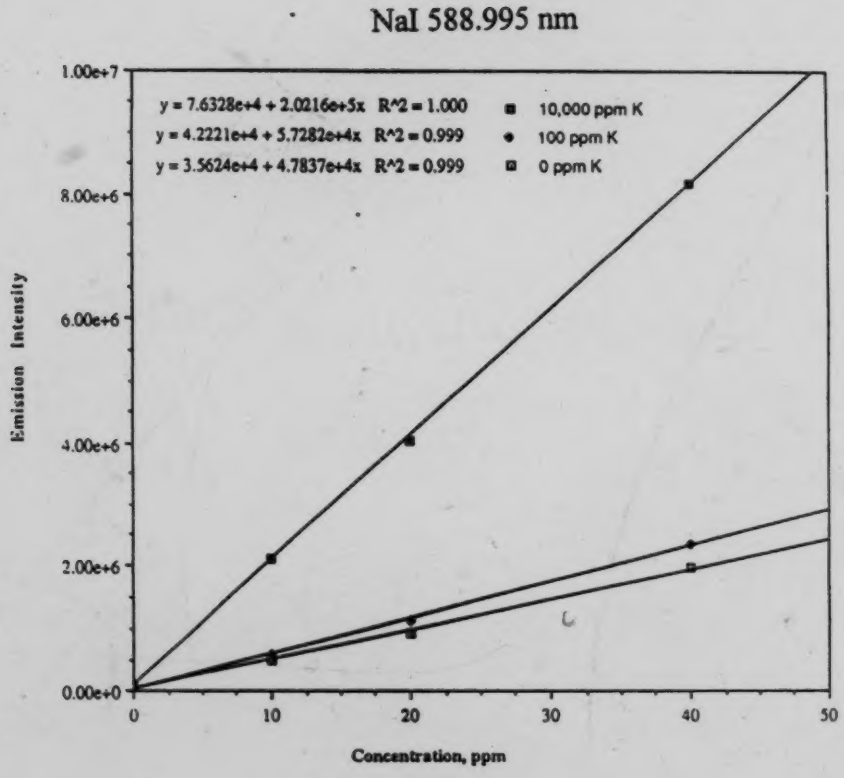

Figure 3.29 K Matrix Effects on Na.

3.2.4 The Analysis of NIST SRM 88a (Dolomitic Limestone) and Real Rock Samples

Spex industries single element standard solutions and analytical reagent grade HCl were used to prepare the following solutions for ICP-AES:

A. 10.0 ppm Fe, Mn, Al, Sr, Na, and K

B. 2% HCl

The calibration standard solutions of Fe, Mn, Al, Sr, Na, and K with concentrations ranging from 0.010 to 5.000 ppm were then prepared by appropriate dilutions. The calibration standard solutions of Ca and Mg with concentrations ranging from 10.0 to 200.0 ppm for Ca and 12.5 to 250.0 ppm for Mg were prepared by dilutions from 1000 ppm stock solutions. A solution of 2% HCl was used as the blank. All solutions used for calibration are shown in Table 3.5.

About 0.1g samples of SRM88a and rocks were digested with 10 ml concentrated HCl on a hotplate, evaporated to almost dry, then transferred to a 100 ml volumetric flask.

Table 3.5 Calibration Standards Used in This Section (ppm).

Ca 317.933 nm	0.0	10.00	50.00	100.0	200.0
Mg 285.213 nm	0.0	12.50	62.50	125.0	250.0
Fe 238.204 nm	0.0	0.010	0.100	1.000	5.000
Mn 257.610 nm	0.0	0.010	0.100	1.000	5.000
Sr 407.771 nm	0.0	0.010	0.100	1.000	5.000
Na 588.995 nm	0.0	0.010	0.100	1.000	5.000
K 776.491 nm	0.0	0.010	0.100	1.000	5.000

The data were obtained at RF power 1100 W, auxiliary flow rate at 0.5 l/min, plasma flow rate at 15 l/min and nebulizer flow rate at 0.7 l/min. All intensity data acquired were an average of six repetitive measurements. A typical relative standard deviation was less than 0.5% (most of them between 0.2% and 0.3%) for Ca and Mg measurements, less than 1.0% for Fe, Mn and Sr measurements and somewhere between 1.0 % to 10.0% for Al, Na and K measurements.

The ICP-AES analytical results of real rock samples (British Columbia dolomite) and SRM 88a are shown in Table 3.6. The results obtained by ICP-AES for major elements Ca and Mg in SRM88a are very closed to the certified value.

There are no certified values for the minor elements tested here, so ICP-MS result (provided by Xinbang Feng) was used to verify Mn and Sr in some samples. The analytical results obtained for both ICP-MS and ICP-AES are tabulated together in Table 3.7.

The results obtained for ICP-AES and ICP-MS shows very clearly the agreement between the two methods. The disagreement is within 10% for most samples, and it is about 15 to 20% for the others. In the absence of interference, the concentration obtained by one method should be close to concentration values obtained using other techniques.

Magnesium and calcium are shown to be present at a high concentration (this is what we expected this from rock sample). The high concentration of Mg affects the measurement of Mn 279.482nm wavelength as discussed in section 3.2.3, so I used Mn 257.610nm instead of Mn 279.482nm to avoid Mg interference. The calcium concentration does not show a wide variation. But magnesium does shows a wide variation.

Table 3.6 Analytical Results of ICP-AES.

Sample	Mg285.213 ppm	Ca317.933 ppm	Fe238.204 ppm	Mn257.610 ppm	Al309.271 ppm	Sr407.771 ppm	Na588.995 ppm	K776.491 ppm
88a	**121.62**	**215.30**	**1.659**	**0.203**	**0.806**	**0.040**	**0.207**	**0.390**
Certified	**128.4**	**215.50**	**n/a**	**n/a**	**n/a**	**n/a**	**n/a**	**n/a**
41s			0.492	0.084	0.529	0.040	0.106	0.083
47s			4.029	0.307	1.978	0.317	0.107	0.916
49			1.463	0.117	0.528	0.063	0.080	<DL
49s	22.26	360.18	1.470	0.119	0.555	0.064	0.075	<DL
50	1.83	278.06	0.193	0.043	0.574	0.124	0.057	<DL
52	99.94	287.56	3.764	0.220	0.881	0.089	0.083	0.091
53s	124.34	225.34	0.883	0.102	0.870	0.091	0.081	0.075
54s	180.15	413.82	1.019	0.165	1.205	0.101	0.468	0.449
55	128.48	233.94	1.029	0.130	0.885	0.055	0.161	0.054
56s	125.98	228.45	0.968	0.114	0.911	0.065	0.103	0.162
57	114.78	240.46	5.463	0.224	1.263	0.057	0.080	0.353
58	48.48	323.35	4.553	0.112	0.657	0.172	0.067	<DL
59	101.66	167.57						
59s			0.552	0.070	0.748	0.038	0.066	0.003
60	125.68	234.30	1.038	0.136	0.949	0.077	0.402	0.038
61	132.59	243.37	1.645	0.146	0.911	0.058	0.270	0.081
63s	142.35	271.42	1.223	0.131	0.949	0.052	0.063	0.009
64s	108.68	191.10	0.682	0.085	0.991	0.057	0.059	0.262
65	93.24	254.33	3.940	0.200	0.930	0.083	0.071	0.118
66s	101.81	173.18	0.796	0.073	0.813	0.076	0.067	0.034
67	109.07	183.21	0.603	0.080	0.897	0.043	0.070	0.156
68	123.60	219.22	1.431	0.172	0.913	0.035	0.064	0.066
69	105.38	178.70	0.589	0.075	0.985	0.038	0.063	0.137
70	116.22	199.76	0.317	0.076	0.505	0.046	0.137	0.113
71	120.01	208.94	0.686	0.099	0.498	0.041	0.129	0.052
72	-0.91	441.34	0.984	0.601	0.370	0.224	0.092	<DL
73	82.58	324.87	0.084	0.071	0.565	0.124	0.095	<DL
74	116.37	205.36	0.458	0.071	0.678	0.057	0.094	0.027
75	125.89	225.60	1.058	0.107	0.680	0.050	0.089	<DL
76	121.96	221.31	0.770	0.088	0.728	0.080	0.085	0.024
77	120.06	221.30	3.593	0.267	1.018	0.066	0.076	0.076
78	122.55	223.04	1.630	0.168	0.811	0.067	0.406	0.069
79	122.65	221.18	0.662	0.084	1.203	0.073	0.199	0.664
80	129.29	260.76	1.112	0.130	0.997	0.106	0.275	0.391
81	103.45	280.03	1.192	0.157	0.708	0.129	0.084	0.025
82s	120.97	222.54	1.621	0.210	1.241	0.073	0.051	0.035
83s	102.01	174.00	0.765	0.093	0.770	0.047	0.307	0.156
84s	123.60	219.27	0.815	0.104	0.836	0.051	0.202	0.145
85s	115.83	206.42	1.338	0.098	0.950	0.082	0.234	0.294
86s	58.02	97.29	3.772	0.115	0.691	0.049	0.310	0.105
87s	118.03	219.80	0.331	0.101	0.924	0.067	0.071	<DL
88s	128.74	230.02	0.764	0.102	1.067	0.051	0.085	0.132
89s	123.03	215.90	0.519	0.107	1.130	0.055	0.304	0.185
90s	79.37	126.86	0.853	0.097	1.146	0.035	0.041	-0.036
91	120.97	217.28	3.764	0.136	1.201	0.067	0.172	0.434
93	18.25	464.73	0.318	0.081	1.306	0.276	0.033	<DL
95s	28.25	400.15	0.181	0.103	0.882	0.330	0.072	<DL
96s	2.15	430.00	0.653	0.098	0.595	0.074	0.070	<DL
98	7.59	367.59	1.108	0.361	1.057	0.347	0.217	0.144
99	0.90	427.44	0.049	0.083	0.558	0.151	0.062	<DL
100s	104.92	266.45	0.208	0.034	0.580	0.806	0.358	0.071
101s	60.01	356.10	0.857	0.055	0.474	0.208	0.456	0.077
102s	0.45	416.63	0.732	0.051	0.835	0.277	0.145	0.137

Table 3.6 Analytical Results of ICP-AES.

103s	60.44	322.55	0.206	0.027	0.583	0.135	1.195	0.107
104s	120.31	214.76	0.540	0.110	0.784	0.097	0.153	0.045
105s	121.93	217.38	0.472	0.107	0.704	0.098	0.123	0.061
106s	112.67	191.81	0.458	0.092	0.752	0.036	1.124	0.127
107s	120.27	210.13	0.527	0.101	0.789	0.038	0.305	0.021
108t	121.31	211.61	0.662	0.113	1.272	0.029	0.048	0.019
109t	123.13	216.00	0.731	0.119	1.332	0.025	0.034	<DL
110s	122.40	216.19	1.141	0.150	1.388	0.032	5.137	0.252
111s	115.90	202.01	1.098	0.135	1.464	0.038	2.026	0.233
112s	123.74	216.55	0.576	0.103	1.404	0.037	1.089	0.180
113s	123.10	215.55	0.626	0.103	1.375	0.037	0.222	0.055
114s	131.09	241.06	0.874	0.136	1.462	0.041	0.253	0.071
115s	121.46	231.15	0.784	0.124	1.453	0.108	0.220	0.058
116s	1.30	350.89	0.391	0.038	1.485	0.373	0.030	<DL
117s	121.37	210.68	0.642	0.092	1.512	0.052	0.025	0.054
118	122.74	220.46	0.897	0.105	0.840	0.057	0.082	0.105
119s	124.72	227.78	0.715	0.105	0.852	0.067	0.082	0.075
122			0.025	0.005	0.389	0.000	0.054	<DL
123	11.72	336.30	1.664	0.178	1.590	0.180	0.172	0.376
124	118.82	221.47	0.354	0.105	1.711	0.067	0.011	<DL
125	117.95	203.53	0.347	0.079	1.025	0.049	0.075	0.093
126	123.91	219.29	0.914	0.124	1.122	0.041	0.069	0.018
127	126.45	229.14	0.987	0.140	1.163	0.069	0.068	0.096
128	109.27	187.75	0.542	0.077	1.655	0.069	0.023	0.177
129	100.26	170.44	3.060	0.107	1.662	0.053	0.024	0.329
130	117.85	204.08	1.352	0.119	1.609	0.048	0.190	0.075
131	173.13	378.92	0.874	0.160	1.938	0.094	0.717	0.440
132	<DL	171.58	0.506	0.046	1.292	0.056	0.009	<DL
133	121.43	212.35	0.464	0.092	1.627	0.053	0.031	0.065

DL: Detection Limit

Table 3.7 Analytical Results of ICP-AES and ICP-MS.

Sample	Mn (MS) ppm	Mn257.610 (AES) ppm	Sr (MS) ppm	Sr407.771 (AES) ppm
88a	**0.212**	**0.203**	**0.041**	**0.040**
50	0.045	0.043	0.125	0.124
64s	0.097	0.085	0.063	0.057
82s	0.236	0.210	0.076	0.073
88s	0.110	0.102	0.052	0.051
89s	0.124	0.107	0.062	0.055
90s	0.121	0.097	0.041	0.035
93	0.083	0.081	0.277	0.276
108t	0.143	0.113	0.036	0.029
109t	0.149	0.119	0.031	0.025
110s	0.187	0.150	0.038	0.032
111s	0.161	0.135	0.042	0.038
112s	0.119	0.103	0.041	0.037
113s	0.105	0.103	0.038	0.037
114s	0.162	0.136	0.047	0.041
115s	0.146	0.124	0.125	0.108
116s	0.039	0.038	0.377	0.373
117s	0.097	0.092	0.053	0.052
123	0.180	0.178	0.172	0.180
124	0.105	0.105	0.064	0.067
128	0.077	0.077	0.067	0.069
129	0.111	0.107	0.051	0.053
130	0.114	0.119	0.046	0.048
131	0.157	0.160	0.091	0.094
132	0.043	0.046	0.054	0.056
133	0.091	0.092	0.051	0.053

REFERENCES

1. P. W. J. M. Boumans and F. J. Deboer, *Spectrochim. Acta* **27B,** 391 (1972).
2. P. W. J. M. Boumans and F. J. Deboer, *Spectrochim. Acta* **30B,** 309 (1975).
3. P. W. J. M. Boumans and F. J. Deboer, *Spectrochim. Acta* **31B,** 355 (1975).
4. S. Berman and J. W. McLaren, *Appl. Spectrosc.* **32**, 372 (1978).
5. F. E. Lichte and S. R. Koirtyohann, *FACSS Meeting*, Philadelphia, PA (1976), **paper No. 26**.
6. D. R. Demers, *Appl. Spectrosc.*, **36**, 584 (1979).
7. J. C. Ivaldi and J. F. Tyson, *Spectrochim. Acta* **50B,** 1207 (1995).
8. J. W. Milburn, *At. Spectrosc.* **17,** 9 (1996).
9. C. Dubuisson, E. Poussel and J-M. Mermet, *J. Anal. At. Spectrom.* **12,** 281 (1997).
10. L. Soudier and J-M. Mermet, *Appl. Spectrosc.* **49**, 1478 (1995).
11. C. Rivier and J-M. Mermet, *Appl. Spectrosc.* **50**, 959 (1996).
12. Lynda Margaret Harris Faires, *Fourier Transform and Polychromator Studies of the Inductively Coupled Plasma,* Los Alamos National Laboratory, Los Alamos, New Mexico.
13. D. L. Smith, M. Sc. Thesis, University of Alberta (1994).
14. M. W. Blades and G. Horlick, *Spectrochim. Acta* **36B,** 861 (1981).
15. K. Lepla, M. A. Vaughan and G. Horlick, *Spectrochim. Acta* **46B,** 967 (1991).

16. M. H. Abdallah, R. Diemiaszonek, J. J. Jarosz, J. M. Mermet, J. Robin, and C. Trassy, *Anal. Chim. Acta,* **84,** 271 (1976).

17. C. D. Skinner and E. D. Salin, *J. Anal. At. Spectrom.* **12,** 725 (1997).

CHAPTER 4

DIRECT SAMPLE INSERTION MEASUREMENTS

4.1 Introduction

Pneumatic nebulization of solution samples is the most popular means of sample introduction into the inductively coupled plasma (ICP). However, in spite of its wide applicability, there are several shortcomings associated with this kind of sample introduction method. Included in these are: poor nebulization efficiency, blockage at high salt concentrations, the requirement for solution samples and volumes greater than 1ml and drift [1-3].

In order to overcome or eliminate some of those shortcomings, a number of researchers have demonstrated the feasibility of more direct sample introduction methods for the ICP [1-5], including fluidized bed atomization; slurry atomization; electrothermal vaporization; arc and spark atomization; laser ablation and direct sample insertion via graphite cups or wire-loops. These methods have been reviewed by McLeod, Routh and Tikkanen [6]. In most instances the generated aerosol has been transported to the plasma in a stream of carrier gas [7].

For a number of years in the laboratory we have been developing a technique known as Direct Sample Insertion (DSI) [1, 8-14]. In this system a sample is placed into a probe and the probe is then inserted into the plasma. In most systems the probe is a graphite cup which is inserted axially into the central channel of the plasma from below the discharge. Some of

the features of DSI include: the direct analysis of various sample forms including solutions, solution residues, slurries, powders and solids; high efficiency, in that 100% of the sample enters the plasma; the ability to handle small amounts (a few μl or mg) of sample, and the ability to process the sample through dry, ash and vaporization *in situ*. Limitations attributed to DSI include a low vaporization temperature (about 2000 K) [15-18], which results in selective volatilization, an inability to vaporize refractory materials and carbide formation [6]. Karanassios and Horlick [19] presented an extensive review of DSI devices and they have built and characterized a DSI system for ICP-AES [1, 13, 14] and ICP-MS [20-22].

The study described here involves the direct insertion of sample solution residues into a continuously running argon ICP using an axial graphite rod on to which the sample is applied with a micropipette.

The instrument employed was the Optima 3000XL (Perkin-Elmer) with an axial viewed torch (see Tables 2.1, 2.2 for details). The insertion device consisted simply of a standard 38.1 mm graphite rod, diameter 4.57 mm (see Table 2.2), attached to a quartz rod. Details of the system were described in Chapter 2 (Figure 2.4 and Table 2.2).

The plasma operating conditions are summarized in Table 4.1. Those operating parameters were used for the experiments in this chapter. The reason that 1100W plasma power was selected is that the Optima 3000XL couldn't sustain a stable discharge upon sample insertion at higher plasma power. The instrument itself automatically adjusted the plasma power to a level between 1100W and 1200W even if a higher plasma power was selected.

Table 4.1 Plasma Operating Parameters Used in This Chapter

Plasma power	1100 W for most measurement
Gas flow rate	
plasma flow rate	15 l/min
auxiliary flow rate	0.5 l/min
Nebulizer flow rate	0.6 l/min for most measurement

The DSI device (Stepper motor and probe driving mechanism) is that described by Karanassios and Horlick [20]. Figure 4.1 is a three dimensional view of the DSI device (not to scale).

The software that controls the stepper motor was rewritten by Lishi Ying, providing full range control of the stepper motor. Compared to other driving systems [7-9, 18, 23-28], this computer controlled stepper motor can provide fast insertion, flexible and precise control in speed, timing and position. Fast insertion speed produced sharp signal peaks and better precision for volatile elements, thus improving analytical performance [1].

The synchronization of the start of integration and the start of the sample probe insertion was carried out manually, because there was no communication between the stepper motor and the computer on the Optima 3000XL.

Youbin Shao designed a side door to replace the original one on the instrument. This new door provides the connection between the DSI device and torch. Figure 4.2 shows the diagram of side door used in the DSI experiment.

There are two holes on the door. The first one located at the upper center of the door is for the sample probe to enter the torch. After

This Figure was removed due to copyright.

Figure 4.1

Three-dimensional view of the DSI device (not to scale).

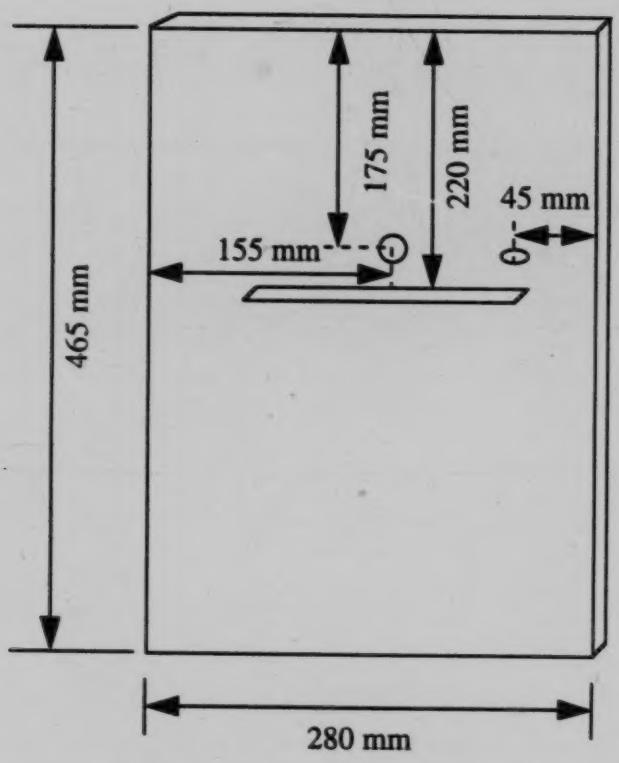

Figure 4.2
The diagram of side door used in this work.

connecting the DSI device onto the door, alignment has to be carried out involving the sample probe, the hole for the sample probe to enter and the torch. Otherwise, the sample probe and/or the supporting quartz rod may break during the insertion. The second hole is smaller than the first one, it allows a cable to pass through it, and the cable is connected with a shutter.

The shutter is just inside the side door, see Figure 4.1 for details. The shutter is used to prevent the inner tube of the torch from being damaged by the plasma while the sample probe is not inside the torch. Although the plasma can be operated with the shutter open (the shutter must be closed during plasma ignition), the discharge physically moves down and rests upon the inner tubes of the torch, thus causing overheating of the torch and then may cause torch melt-down.

The torch is a modified torch with a large central tube that allows the sample probe to enter the plasma. Figure 4.3 is a diagram of modified torch for DSI-ICP-AES. It was found that the relatively large diameter of the central tube of the torch helps to keep the plasma stable, because if the space between the central tube and sample probe is too small, the plasma is extinguished upon rapid insertion of the probe into the plasma. A high outer gas flow rate is also effective in stabilizing the plasma while operating the DSI device [29].

There are several kinds of sample probes used in DSI-ICP [19]. Metal cups and metal wire loops have been used as sample probes [1, 11, 27, 28, 30, 31]. Among different probes, the graphite cup is the most widely used. A diagram of the graphite cup used in this study is shown in Figure 2.4. All graphite rods were pre-burned in the plasma for about 30 seconds to remove impurities.

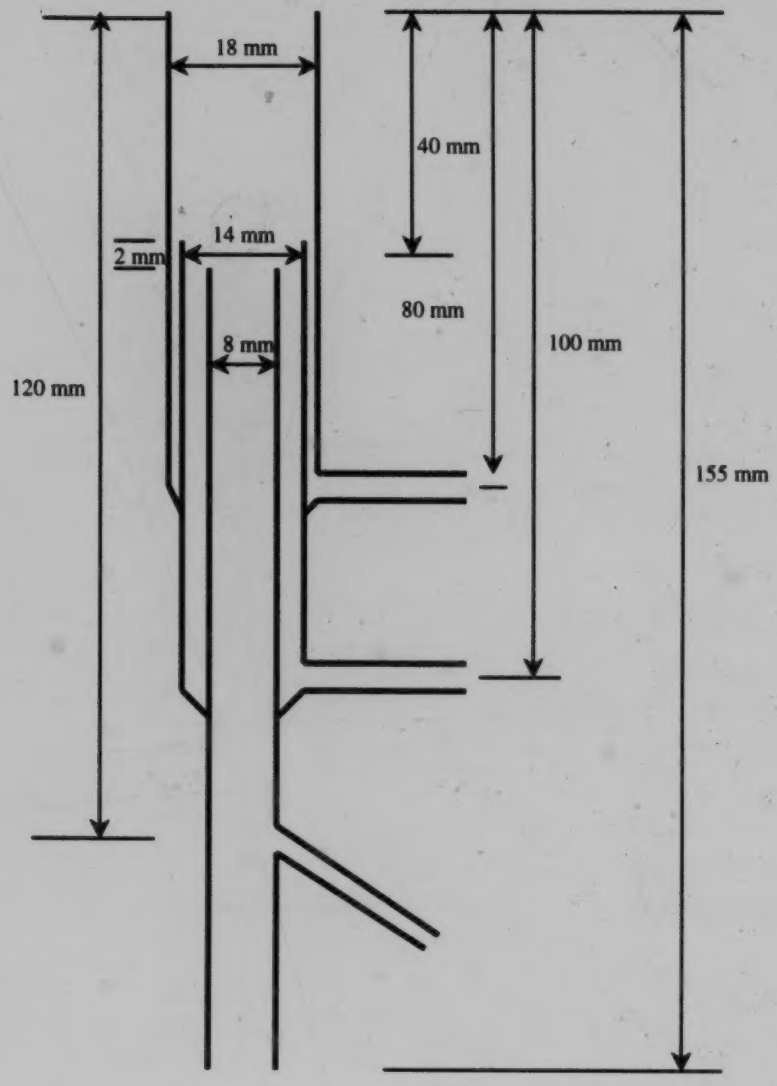

Figure 4.3

Diagram of modified torch for DSI-ICP-AES.

All stock solutions (1000 ppm) were prepared in our laboratory using deionized distilled water. Before insertion, solution samples were dried in an aluminum holder by using an infrared lamp for about two minutes [9]. A heating chamber was used to prevent contamination from the dust in the air while the sample was being dried. A diagram of the heating chamber is shown in Figure 4.4.

The advantages of using DSI for sample introduction are lower detection limits due to improvement in analyte transport efficiency (100% of sample enters the plasma); the ability to analyze small samples (μl of solution sample or mg of powder/solid sample); and the ability to analyze samples high in organic, solids and acids without or with little sample pretreatment. A generic diagram of a DSI device for ICP-AES was shown in Figure 1.2.

4.2 Results

4.2.1 Operating Parameter Studies

A large number of variables affect the measured signal intensity in DSI-ICP-AES. A detailed list of these variables can be found in the papers of Horlick et al [1, 9, 19, 20].

In this section, data on the effects of insertion position of the sample probe, instrument read delay time, ashing time and integration time on the measured signal intensity will be presented. Our goal is to find the relationship between the various parameters studied and their effects on signal intensity.

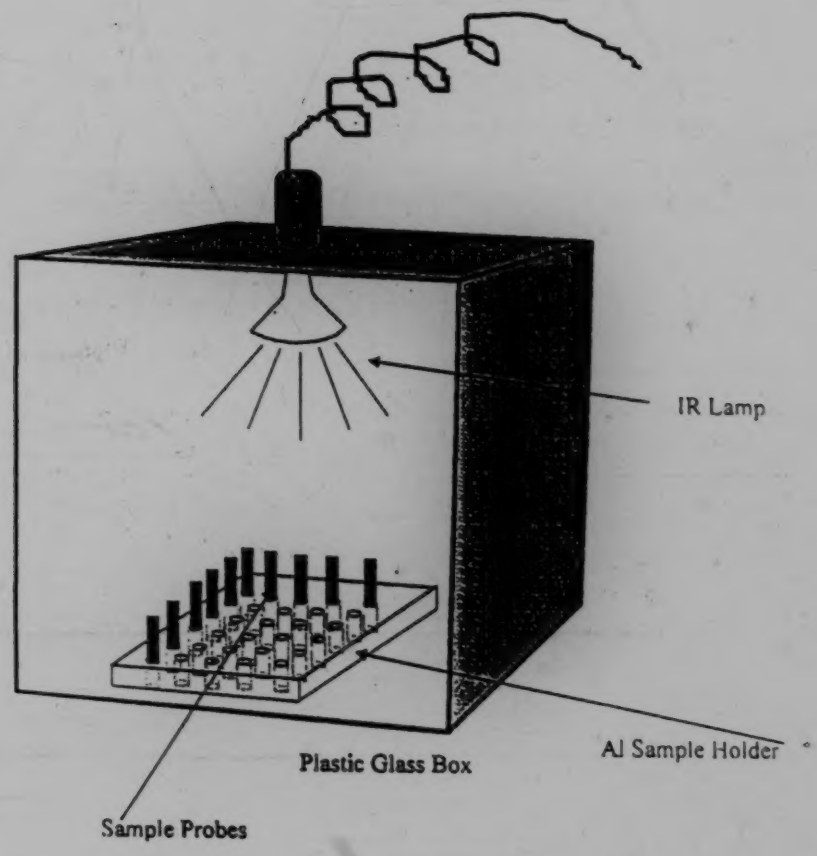

Figure 4.4

Diagram of heating chamber.

In this study, insertion position of the sample probe refers to the final position relative to the front coil of the load coil of the ICP. Typically, the ICP will end up about 2 mm in front of the load coil.

Instrument read delay time is the delay period in seconds between when a Read Key is pressed and the time at which the first signal measurement is begun. This delay is to enable the signal to stabilize. Integration time is the time period over which the detectors will be collecting photons (light) from the plasma during the analysis.

Ashing time is the time period over which the organic contents of sample will be removed under plasma while sample probe stops at ashing position. The dry, ash and atomize cycles used here are analogous to the terms utilized in Graphite Furnace Atomic Absorption Spectrometry. The dry position is well below the plasma to remove water content from sample. Because an IR lamp was used to dry sample in this study, the dry cycle was not used. Ashing position is also below the plasma, but very close, to remove the organic contents of sample. Although the samples used in this study are only solution residues, the ash cycle was used to observe the effect of the plasma on sample during ash cycle. The atomic position is same as final position of the sample probe. See Figure 4.5 for the time relationship.

A 0.1 ppm multielement stock solution of As, Be, Ca, Cd, Co, Cr, Cu, Fe, Mg, Mn, Mo, Ni, Pb, Sb, Se, Tl, V, and Zn was used in the experiment and data were collected at optimized operating conditions.

DSI has the ability to process the sample through dry, ash and atomic cycle *in situ* [12]. The sample is placed into a graphite cup, which is subsequently introduced into the plasma. By positioning the sample carrying cup at positions successively closer to the plasma, drying and ashing can be

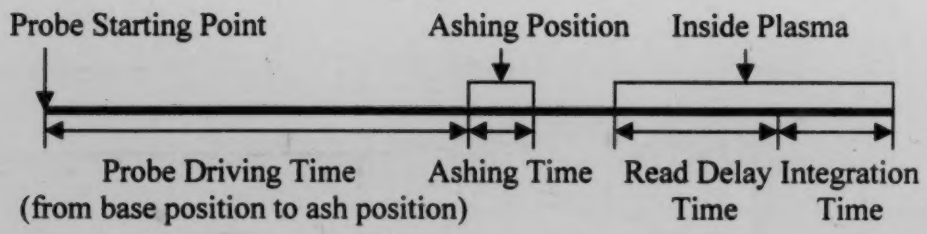

Figure 4.5 Diagram of Time Relationship used in Chapter 4.

achieved prior to sample vaporization inside plasma. Habib and Salin [32] found there were no sample losses during sample ashing for Pb, Cd and As for side-on viewing plasma, but for Zn and P, there was a little loss with increased ashing time in their set up and operating conditions. However, the results obtained here show a significant loss of sample during sample ashing for end-on viewing plasma.

There are sample losses during ashing for Pb, Cd and Zn. The shorter the ashing time, the higher the analyte signal intensity. The results summarized in Table 4.2 were obtained for 1.0 ppm Pb solution residue at different ashing times. The operating conditions are as follow: instrument read delay time is 5 seconds, integration time is 1 second, and final position of sample probe is about 2 mm past the load coil.

The results in Table 4.2 show that the analyte signal at 0 second ashing time is about 3 times better than that at 5 seconds ashing time for Pb.

The position of the DSI probe in the plasma has a great effect on the analyte signal [1, 7, 9, 19, 25, 27]. The sample cup insertion position is set so that, when it is fully inserted, the top of the cup is about 2 mm past the load coil. The position of the cup is measured relative to the front of the load coil.

Table 4.2 Optimization of Sample Ashing Time.

Ashing time	Pb220.353 (counts/s)
0 s	10937.4
1 s	10015.6
2 s	9236.2
3 s	7064.6
4 s	4976.4
5 s	3157.3

Note: sample concentration is 1.0 ppm, read delay is 5 seconds, integration time is 1 second, position of sample probe is 2 mm past the load coil.

The Pb wavelength showed maximum signal for an insertion position at about 2 mm past the load coil (see Table 4.3a for details). A final probe position in the plasma of about 2 mm past the front load coil was chosen for Pb.

Unfortunately it seems that the maximum signal is at about 3 mm before the front of the load coil for Cd and about 8 mm before the front of the load coil for Zn (Table 4.3b).

Table 4.3 Optimization of Insertion Position of Sample Probe.

(a)

Probe Position	Pb220.353 (counts/s)
-3 mm	8234.4
0 mm	15429.6
2 mm	16465.5
4 mm	14828.2
5 mm	13621.1
10 mm	5798.0

(b)

Probe Position	Cd214.438 (counts/s)	Zn202.548 (counts/s)
-8 mm	64302.2	14189.2
-5 mm	64543.0	11601.5
-3 mm	Saturated	10706.9
-1 mm	44469.3	8558.0
0 mm	53310.3	4429.9
2 mm	17103.3	2333.2

Note: sample concentration is 1.0 ppm, read delay is 3 seconds, integration time is 1 second, and there is no ashing time.
"-": sample probe is before the front of load coil.

Shao and Horlick [9] observed that volatile elements vaporize in a short period of time, about 2 to 10 seconds, and less volatile elements, Cr for example, may take up to a minute to vaporize. According to the time for peak emission, the sequence of volatilization is Cd (3 s), Zn (4 s), and Pb (6 s) for the operating conditions used here. The concentration of Cd, Zn and Pb is 1.0 ppm, integration time is 1.0 second, the final position of sample probe is about 2 mm past the front of the load coil and there is no ashing time as stated above.

Although the Optima 3000XL can be set to have multiple integration times for different elements with a steady state pneumatic nebulization sample introduction system, it can only be set to have one common integration time for all elements for direct sample insertion sample introduction system, because of the transient nature of the signal.

Data for the analyte signal intensity at different integration times and instrument read delay times with aqueous solution residues are summarized in Table 4.4a – 4.4c. Note that a single common integration time (1 second) can be used for Pb, Cd, and Zn in this sample introduction system with little sensitivity loss. However, there is no optimal read delay time, so two sets of operating conditions were used throughout this chapter. For Pb, a 6 second read delay time was selected. For Cd and Zn, a 3 second read delay time was selected. All the other operating conditions for Pb, Zn and Cd are as follow: integration time is 1 second, there is no ashing time, and the final position of sample probe is 2 mm past the front of the load coil (see Table 4.1 for plasma conditions).

Table 4.4 Optimization of Integration Time and Read Delay Time.

Pb 220.353 nm

(a) counts/s

IT	1 s Read Delay	2 s Read Delay	3 s Read Delay	4 s Read Delay	5 s Read Delay	6 s Read Delay
1 s	57.9	156.2	1312.3	4992.9	10937.4	**15778.0**
2 s	95.7	182.7	3985.8	12008.3	16592.4	15010.9
3 s	193.7	3127.0	6430.3	10389.2	14206.1	10150.3
4 s	2026.4	3776.8	6658.4	12108.4	12234.0	8224.0
5 s	3448.8	6150.4	8107.4	9442.8	10214.3	7430.7

Cd 214.438 nm

(b) counts/s

IT	1 s Read Delay	2 s Read Delay	3 s Read Delay	4 s Read Delay	5 s Read Delay	6 s Read Delay
1 s	13872.3	21022.1	**37243.3**	22333.2	4013.5	485.9
2 s	9104.9	21809.8	36088.2	9010.0	576.4	127.7
3 s	12457.8	24506.0	18570.0	12188.0	1494.8	101.9
4 s	21901.8	S	18215.7	5947.7	1040.0	40.9
5 s	S	18254.0	14247.3	8222.3	1205.5	130.3

Zn 202.548 nm

(c) counts/s

IT	1 s Read Delay	2 s Read Delay	3 s Read Delay	4 s Read Delay	5 s Read Delay	6 s Read Delay
1 s	944.8	2643.5	**19298.0**	22176.5	17550.9	1893.5
2 s	1440.6	4706.5	24872.4	18778.8	3994.1	746.9
3 s	2626.0	14902.6	17456.9	15537.0	7306.7	547.8
4 s	12422.5	15634.4	13861.3	10423.1	5949.1	453.3
5 s	11825.4	12013.1	10830.3	9458.7	5122.8	704.1

Note: There is no ashing time and the concentration is 1.0 ppm.
IT: integration time. S: saturated.

A pre-burned graphite cup with DI water residue was used as blank. There are no big changes for blank signal intensities as integration time and instrument read delay time changes. The blank intensity of Pb, Cd and Zn are shown in Table 4.5.

Table 4.5 Blank Intensity of Pb, Cd and Zn.

Elements	Pb 220.353	Cd 214.438	Zn 202.548
Blank Intensity (counts/sec)	166.2	68.4	18.7

Note: integration time is one second, instrument read delay time is three seconds for Cd and Zn, and six second for Pb.

4.2.2 Figure of Merit

Precision data for solution sample residues (10 µl, 1.0 ppm) are presented in Table 4.6 at optimized operating conditions for Pb as stated above. The precision for Pb is better than that for Cd and Zn. The operating conditions used here are optimized for Pb, the sensitivity losses for Cd and Zn perhaps make them somehow less reproducible. The effect of insertion position can also influence the analyte signal intensity as stated above.

Table 4.6 Reproducibility of Pb, Cd, and Zn (10 µl, 1.0 ppm).

	Cd 214.438	Pb 220.353	Zn 202.548
1	4956.5	10266.3	16663.2
2	1914.3	13633.6	10928.1
3	1437.5	14511.4	7314.4
4	3315.9	13046.6	16083.2
5	2572.9	13936.7	13960.6
6	1622.6	16957.2	8740.5
7	1270.4	15475.4	6865.2
8	2333.3	14653.4	12352.8
9	1325.2	16817.1	6878.9
10	1696.5	14986.6	8892.1
11	1368.7	15029.6	7209.9
Std	1120.6	1843.92	3711.0
Average	2100	14500	10500
RSD%	52	13	35

Experimental results shown in Table 4.3 indicate that there is 10% signal change with a 2.5-mm difference in insertion position.

The detection limits (3σ of the background) for some elements are listed in Table 4.7. The detection limits were determined by measuring eleven repeat water blank runs. The detection limits are calculated from following equation:

$$D.L.\ (pg) = 3\ (SD)_B/S \qquad (3)$$

Where $(SD)_B$ is the standard deviation of the peak area intensities of 11 blank sample cups integrated for the same intervals as the sample, S is the sensitivities from the calibration curves, i.e., peak area intensity/pg.

Table 4.7 Detection Limits for Solution Residue of Pb, Cd, and Zn (10 μl sample).

Elements + Wavelengths	DL (pg)
Cd 214.438 nm	11
Cd (II) 226.502 nm	12
Pb (II) 220.353 nm	25
Pb (I) 216.999 nm	72
Pb 261.418 nm	32
Pb 283.306 nm	42
Pb 224.688 nm	490
Zn (II) 202.548 nm	20
Zn 206.200 nm	28

The detection limits are comparable to those values described in reference 19 and 29. For Pb 224.688 nm, the DL is high.

The calibration curves for solution residue samples are shown in Figures 4.6 to 4.8. The linearity for the elements tested was acceptable. The concentration of analyte in the standard solutions ranged from 0.001 ppm to

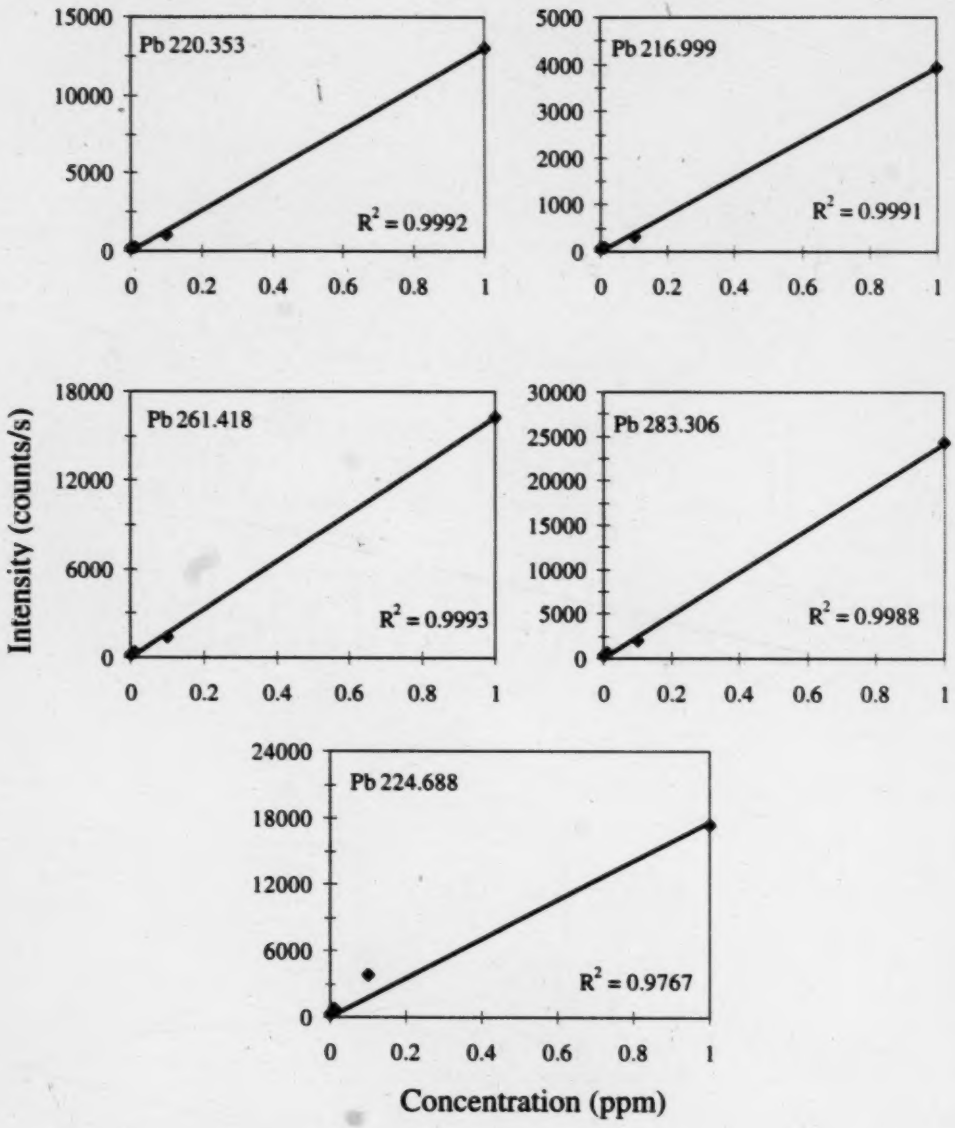

Figure 4.6

Calibration curves of Pb solution residue.

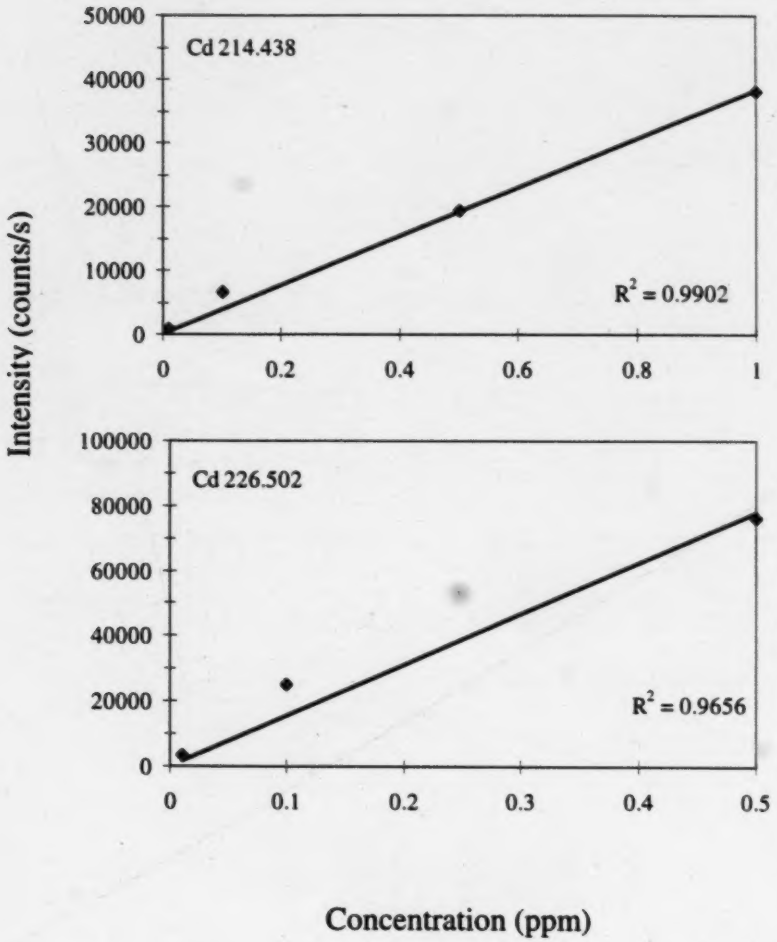

Figure 4.7

Calibration curves of Cd solution residue.

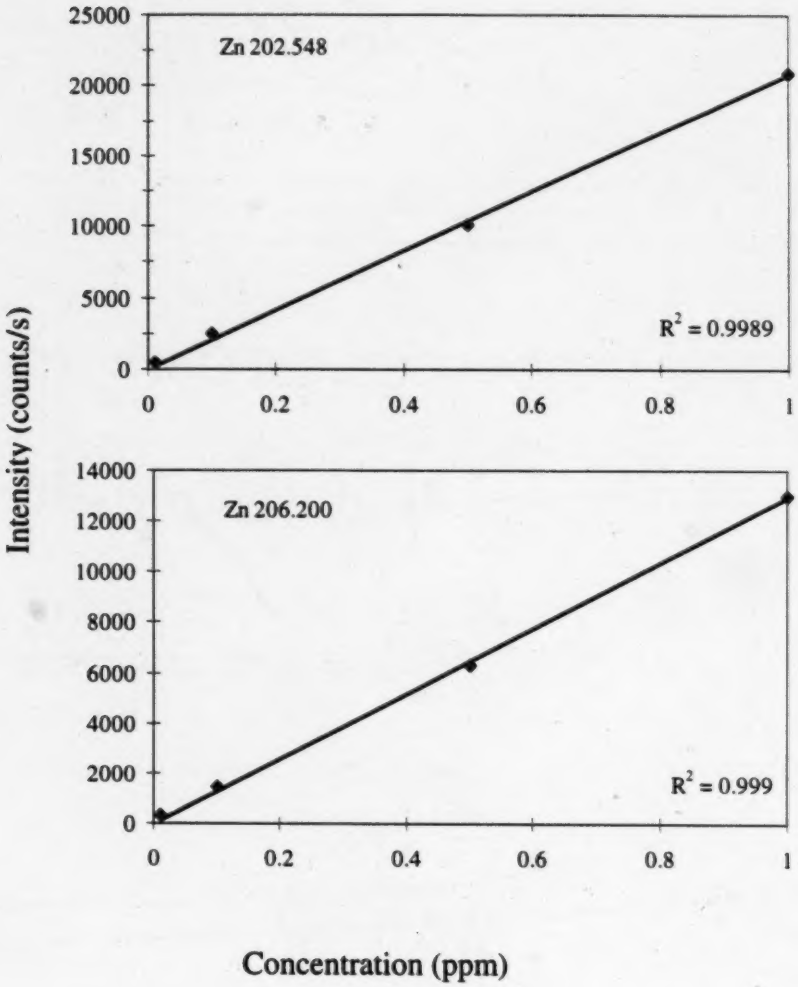

Figure 4.8

Calibration curves of Zn solution residue.

1.0 ppm for Pb, Zn and Cd 214.438nm wavelength and 0.001 ppm to 0.5 ppm for Cd 226.502nm. No satisfactory results were obtained for log-log plot of the elements studied here.

4.3 Introduction of Oxygen into the Plasma

4.3.1 Introduction

The advantages of direct sample insertion (DSI) include: the direct analysis of various sample forms including solutions, solution residues, slurries, powders and solids; high efficiency, one hundred percent of the sample enters the plasma; the ability to handle small amounts (a few µl or mg) of samples; and the ability to process the sample through dry, ash and vaporization cycles *in situ.* Limitations of DSI include a low vaporization temperature (~ 2000 K), which results in selective volatilization, an inability to vaporize refractory materials and carbide formation.

Chemical modification of the sample has been used to overcome some of these limitations [12]. However, chemical modifiers can introduce contaminants and may interfere with the stable operation of the plasma because of vapor generation. In addition, powdered chemical modifiers cannot be effectively added to chip form samples, solids or oils.

Another approach to enhance the volatilization of samples is to modify the plasma. Mixed-gas plasmas have been used to improve the performance of DSI systems [12, 31, 33]. In this section, a short study of mixed gas (Ar-O_2) ICP-AES was performed.

The inductively coupled plasma (ICP) system used is the Perkin-Elmer Optima 3000 XL. The DSI subsystem was described earlier in this thesis and chapter.

Two Matheson Rotameters (Matheson, East Rutherford, N. J.) were used to mix argon and oxygen gases prior to introducing the coolant gas into the plasma discharge. Matheson model 605 (Ar) and 603 (O_2) flow tubes were used to mix the plasma gases for the coolant stream. The plasma was first ignited using pure argon and then oxygen was gradually introduced into the coolant gas flow, otherwise, the plasma could not be ignited. We used 90% argon and 10% oxygen as the coolant gas. If the content of oxygen higher, the plasma shut down.

The plasma volume was reduced considerably when oxygen was introduced into the argon discharge, and the plasma was quite unstable. The reason for this volume reduction has been described in terms of the thermal pinch effect [34]. Since argon and most gases have different thermal conductivities in the plasma, introducing oxygen or any foreign gases into the Ar-ICPs will change the thermal conductivity characteristics of the plasmas. In the 7000K plasma, oxygen has a better thermal conductivity than that of argon.

The purpose of the cooling gas is to prevent melt down of the external quartz tube, therefore, introducing oxygen into the cooling gas flow provides better cooling than that of argon. So the outer surface of the mixed gas plasma becomes cooler and hence has less electrical conductivity. The plasma then has a smaller volume than that of the pure argon plasma as a consequence of the thermal pinch effect.

4.3.2 Results

The operating conditions are shown in Table 4.1. The only difference is that mixed gases were used here for the plasma gas instead of pure argon. The detection limits obtained here are calculated from a single insertion of 10.0 µl, 0.1 ppm solution sample. The detection limits for some elements are listed in Table 4.8. The detection limits were based on a signal level of 3 times standard deviation of baseline. The detection limits are calculated from following equation:

$$\text{D.L. (pg)} = 3\,(SD)_B/S \qquad (3)$$

Where $(SD)_B$ is the standard deviation of the baseline, S is the peak area intensity/pg. The detection limits of those elements measured by normal DSI-ICP-AES also summarized in Table 4.8.

The results show that there is no big difference between mixed-gas DSI-ICP-AES and normal DSI-ICP-AES for Au (II) 208.209 nm, Ga (I) 294.364 nm, In (I) 325.609 nm, Mg (II) 279.079 nm, Si (I) 212.412 nm, Si (I) 251.611 nm, Sn (I) 235.484 nm and Zn (II) 202.548 nm. But for Au (I) 242.795 nm, Co (II) 228.616 nm, Cr (I) 357.869 nm, Cr (II) 267.716 nm, Fe (II) 273.955 nm, Se (I) 196.026 nm and Yb (II) 328.937 nm, the detection limits are about 5 to 10 times better for mixed-gas DSI than that of normal DSI. Note that there is no emission at all for Se (I) 196.026 nm and Yb (II) 328.937 nm at normal DSI operating conditions.

Table 4.8 Detection Limits for Solution Residue Sample (10 μl, mixed-gases).

Elements + Wavelengths	DL (pg) mixed gases	DL (pg) pure argon
Au (I) 242.795 nm	16	142
Au (II) 208.209 nm	83	92
Co (II) 228.616 nm	15	88
Cr (I) 357.869 nm	60	351
Cr (II) 267.716 nm	3	24
Fe (II) 273.955 nm	10	94
Ga (I) 294.364 nm	27	28
In (I) 325.609 nm	31	46
Mg (II) 279.079 nm	27	37
Se (I) 196.026 nm	210	N/A
Sn (I) 235.484 nm	250	588
Si (I) 212.412 nm	15	22
Si (I) 251.611 nm	23	32
Yb (II) 328.937 nm	40	N/A
Zn (II) 202.548 nm	13	34

Two spectra of Au (I) 242.795 nm are shown in Figure 4.9. Fig. 4.9a is the spectrum obtained with normal DSI and Fig. 4.9b is the one obtained with mixed gas DSI.

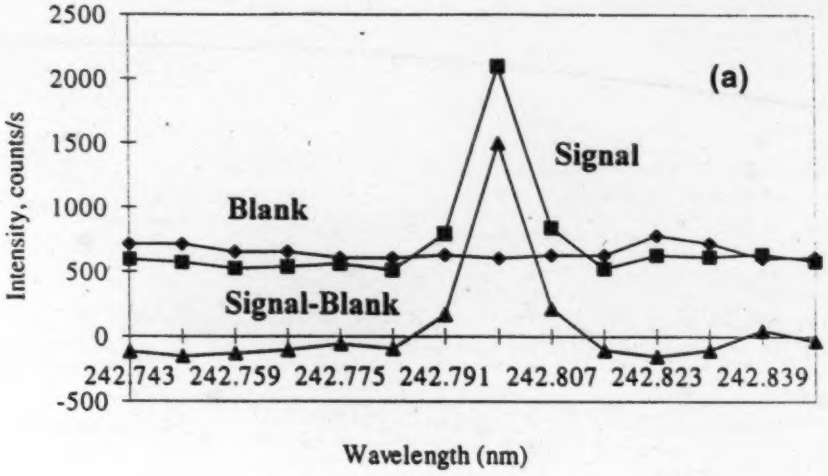

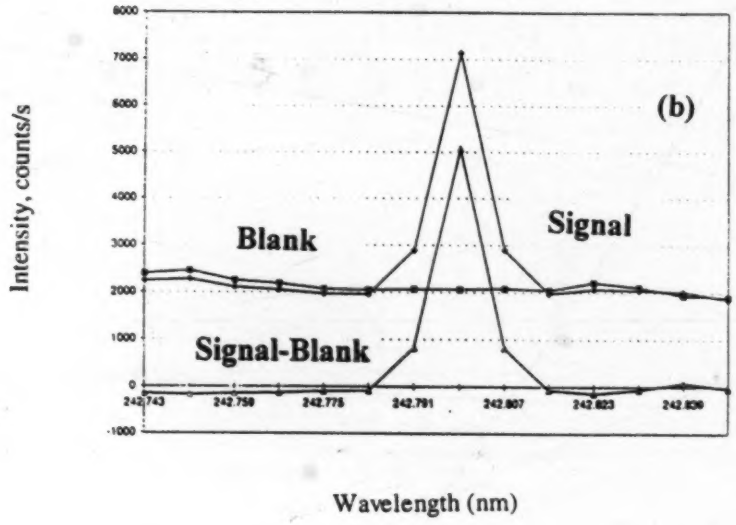

Figure 4.9

Spectra of Au (I) 242.795 nm. (a) is the spectrum obtained with normal DSI operation conditions. (b) is the one with mixed gas DSI.

4.4 Conclusions

In this chapter of the thesis, the operating parameters insertion position of sample probe in plasma, ashing time and integration time were studied. The results show that there are intensity lose for easy ionized elements (Pb, Zn, Cd etc.) during ashing.

The detection limits in pg range are obtained in DSI-ICP-AES. The reproducibility of Pb was also carried out and the RSD% is about 10% for most Pb wavelength in the optimized operating condition for Pb. The dynamic range is 0.001 to 1.0 ppm for Pb and 0.01 to 1.0 ppm for both Zn and Cd.

A short study of mixed gas DSI-ICP-AES was carried out, an Ar-O_2 mixed gas was found to be useful in enhancing sensitivities of nonvolatile and carbide forming elements. Detection limits for all the elements but Se and Sn were in the range of pg, while Se and Sn were in the subnanogram level.

REFERENCES

1. V. Karanassios, G. Horlick and M. Abdullah, *Spectrochim. Acta* **45B,** 105 (1990).
2. R. F. Browner and A. W. Boorn, *Anal. Chem.* **56,** 787A (1984).
3. R. F. Browner and A. W. Boorn, *Anal. Chem.* **56,** 875A (1984).
4. J. C. Van Loon, *Anal. Chem.* **52,** 955A (1980).
5. H. Matusiewicz, *J. Anal. At. Spectrom.* **1,** 171 (1986).
6. C. W. MeLeod, M. W. Routh and M. W. Tikkanen, Introduction of solids into plasmas, in: *Inductively Coupled Plasmas in Analytical Atomic Spectroscopy,* Eds. A. Montaser and G. W. Golightly, 721, VCH Publishers, Inc. (1992).
7. G. F. Firkbright and S. J. Walton, *Analyst* **107**, 276 (1982).
8. E. D. Salin and G. Horlick, *Anal. Chem.* **51,** 2284 (1979).
9. Y. B. Shao and G. Horlick, *Appl. Spectrosc.* **40**, 386 (1986).
10. W. T. Chan and G. Horlick, *Appl. Spectrosc.* **44**, 380 (1990).
11. W. T. Chan and G. Horlick, *Appl. Spectrosc.* **44**, 525 (1990).
12. X. R. Liu and G. Horlick, *J. Anal. At. Spectrom.* **9,** 833 (1994).
13. V. Karanassios and G. Horlick, *Spectrochim. Acta* **45B,** 85 (1990).
14. V. Karanassios, M. Abdullah and G. Horlick, *Spectrochim. Acta* **45B,** 119 (1990).
15. E. R. Prack and G. J. Bastiaans, *Anal. Chem.* **55,** 1654 (1983).
16. N. W. Barnett, M. J. Cope, G. F. Firkbright and A. A. H. Taobi, *Spectrochim. Acta,* **39B,** 343 (1984).

17. A. G. Page, S. V. Godbole, K. H. Madraswala, M. J. Kulkapni, V. S. Mallapurkar and B. D. Joshi, *Spectrochim. Acta,* **39B,** 551 (1984).

18. A. Lorbe and Z. Goldbart, *Analyst,* **110,** 155 (1985).

19. V. Karanassios and G. Horlick, *Spectrochim. Acta Rev.* **13,** 89 (1990).

20. V. Karanassios and G. Horlick, *Spectrochim. Acta* **44B,** 1345 (1989).

21. V. Karanassios and G. Horlick, *Spectrochim. Acta* **44B,** 1361 (1989).

22. V. Karanassios and G. Horlick, *Spectrochim. Acta* **44B,** 1387 (1989).

23. G. F. Firkbright and L.X. Zhang, *Analyst* **107**, 617 (1982).

24. I. B. Brenner, A. Lorbe and Z. Goldbart, *Spectrochim. Acta* **42B,** 219 (1987).

25. G. Zaray, J. A. C. Broekaert and F. Leis, *Spectrochim. Acta* **43B,** 241 (1988).

26. G. Zaray, P. Burba, J. A. C. Broekaert and F. Leis, *Spectrochim. Acta* **43B,** 255 (1988).

27. E. D. Salin and R. L. A. Sing, *Anal. Chem.* **56,** 2596 (1984).

28. D. W. Boomer, M. Powell, R. L. A. Sing and E. D. Salin, *Anal. Chem.* **58,** 975 (1986).

29. X. R. Liu, Ph.D. Thesis, University of Alberta (1994).

30. R. L. A. Sing and E. D. Salin, *Anal. Chem.* **61,** 163 (1989).

31. W. E. Pettit and G. Horlick, *Spectrochim. Acta,* **41B,** 699 (1986).

32. M. M. Habib and E. D. Salin, *Anal. Chem.* **57,** 2055 (1985).

33. D. Sommer and K. Ohls, *Fresenius'Z. Anal. Chem.*, **304**, 97 (1980).

34. E. H. Choot and G. Horlick, *Spectrochim. Acta* **41B,** 889 (1986).

CHAPTER 5

SUMMARY AND FUTURE WORK

The first part of the thesis focuses on the optimizing operating conditions of ICP-AES (Perkin-Elmer, Optima 3000 XL) and successfully utilize this operating conditions to analyze SRM 88a and real rock samples. The results of Mg and Ca show very good agreement with certified values. There are no certified values for Mn, Fe, Sr, Na, K, and Al, so ICP-MS results were obtained for Sr, Mn in real samples, and the most of results show very good agreement between ICP-AES and ICP-MS.

Ca and Mg matrix effect on analyte signals were studied and the results show that there are general effects of Ca and Mg on ZnII 202.548nm, ZnI 213.856nm, CdII 214.438nm, CuII 224.700nm, CdI 228.802nm, FeII 238.204nm, MnII 257.610nm, MnI 279.482nm, CuI 324.754nm, NaI 588.995nm, KI 766.491nm. When concentration of Ca, Mg increases, the matrix effects increase.

In the second part of the thesis, operating parameters of insertion position of sample probe in plasma, ashing time and integration time were studied. The results show that there was an intensity loss of easy ionized elements (Pb, Zn, Cd etc.) during ashing, so there is no ashing time used in this work. The detection limits in pg range obtained in DSI-ICP-AES are comparable with other DSI method [1, 2]. The reproducibility of Pb was also carried out in the optimized operating condition for Pb. The RSD% is about 10% for most Pb wavelength. The calibration curves were obtained

for Pb, Cd and Zn in solution residue (dynamic range is 0.001 to 1.0 ppm for Pb, 0.01 to 1.0 ppm for both Zn and Cd).

The main concern in the direct sample insertion is the incomplete vaporization in the pure argon plasma for non-volatile and carbide forming elements, especially in refractory solid samples. So an argon-oxygen mixed gas ICP was studied to improve the vaporization ability of the DSI-ICP-AES performance [3, 4]. The mixed gas DSI-ICP-AES provided better vaporization ability. The detection limit was then obtained for some non-volatile or hard volatile elements. The detection limit was improved about an order of 5 to 10. Applying DSI-ICP-AES or mixed gas DSI-ICP-AES to analyze different types of real samples is an interesting area and needs more work to be done in the future.

Because of the method of sample introduction into the plasma, the multielement capability of the current system is quite limited. The Optima 3000 XL software does not allow setting of different integration times for simultaneously analysis.

Another weakness of the current system is the manual operation of the control of analysis and step motor. A software to synchronize the control of analysis and the control of the step motor is necessary in the future for more accurate analyses.

The thirdly, the sample change is done manually, an autosampler is needed to be interfaced with the DSI-ICP-AES system.

The DSI-ICP-AES has many advantages [5, 6]. If above shortcomings could be overcomed in the near future, the DSI-ICP-AES will become a powerful, time saving and labor saving technique.

REFERENCES

1. V. Karanassios, G. Horlick and M. Abdullah, *Spectrochim. Acta* **45B,** 105 (1990).

2. R. F. Browner and A. W. Boorn, *Anal. Chem.* **56,** 787A (1984).